


2023

Investigation of Early Complex Formation of Huntingtin Protein With and Without Lipids

Alyssa R. Stonebraker
West Virginia University, as0286@mix.wvu.edu

Follow this and additional works at: <https://researchrepository.wvu.edu/etd>

 Part of the [Analytical Chemistry Commons](#), [Biophysics Commons](#), and the [Physical Chemistry Commons](#)

Recommended Citation

Stonebraker, Alyssa R., "Investigation of Early Complex Formation of Huntingtin Protein With and Without Lipids" (2023). *Graduate Theses, Dissertations, and Problem Reports*. 11962.
<https://researchrepository.wvu.edu/etd/11962>

This Dissertation is protected by copyright and/or related rights. It has been brought to you by the The Research Repository @ WVU with permission from the rights-holder(s). You are free to use this Dissertation in any way that is permitted by the copyright and related rights legislation that applies to your use. For other uses you must obtain permission from the rights-holder(s) directly, unless additional rights are indicated by a Creative Commons license in the record and/ or on the work itself. This Dissertation has been accepted for inclusion in WVU Graduate Theses, Dissertations, and Problem Reports collection by an authorized administrator of The Research Repository @ WVU. For more information, please contact researchrepository@mail.wvu.edu.

Investigation of Early Complex Formation of Huntingtin Protein With and Without Lipids

Alyssa R. Stonebraker

Dissertation Submitted
to the Eberly College of Arts and Science
at West Virginia University

in partial fulfillment of the requirements for the degree of

Doctor of Philosophy
In
Chemistry

Justin Legleiter, Ph.D., Committee Co-Chairperson
Stephen Valentine, Ph.D., Committee Co-Chairperson
Blake Mertz, Ph.D.
Peng Li, Ph.D.
David Smith, Ph.D.

C. Eugene Bennett Department of Chemistry

Morgantown, West Virginia

2023

Keywords: Huntington's disease, amyloid formation, aggregation, lipid binding, cholesterol, post-translational modification, mass spectrometry, atomic force microscopy

Copyright 2023 Alyssa R. Stonebraker

Abstract

Investigation of Early Complex Formation of Huntingtin Protein With and Without Lipids

Alyssa R. Stonebraker

Huntington's disease (HD) is a fatal neurodegenerative disease caused by the expansion of the polyglutamine (polyQ) domain of the huntingtin protein (htt). The expansion of the polyQ domain beyond a threshold of approximately 35 repeats triggers complex toxic aggregation mechanisms and results in altered interactions between htt and lipid membranes. Many factors modulate these processes. One such modulator includes sequences flanking the polyQ domain, most notably the first 17 amino acids at the N-terminus of the protein (Nt17), and environmental factors including the presence of membranous structures. Nt17 has the propensity to form an amphipathic α -helix in the presence of binding partners, which can facilitate aggregation and lipid binding. These processes can be further modulated by overall membrane composition and physiochemical properties. Considering the influence of membrane composition and the known dysregulation of cholesterol homeostasis in HD, cholesterol may be a crucial membrane component that can modulate early htt interactions through influencing membrane properties such as permeability, fluidity, and overall organization. Early interactions may also be modulated through altered electrostatics, hydrophobicity, and hydrogen bonding introduced through mutations to residues within the Nt17 domain. A mechanistic understanding of such modulating factors and their impacts on early htt interactions can provide crucial insights into the toxic mechanism of HD. Early htt interactions were further explored in the studies presented here. Thioflavin T (ThT) aggregation assays, atomic force microscopy (AFM), polydiacetylene (PDA) lipid binding assays, and mass spectrometry (MS) were used to identify changes to aggregation, aggregate morphologies, htt/lipid binding, and htt/lipid complexation respectively. When htt was exposed to lipid systems composed of pure POPC, DOPC, and POPG distinctly different htt interactions with increasing amounts of exogenously added cholesterol were observed. Increasing cholesterol content increased aggregation for the DOPC systems, but reduced aggregation for the POPC and POPG systems. Htt/lipid binding decreased with increasing cholesterol for the POPC systems, while binding increased for the DOPC and POPG systems. Differences in htt/lipid complexation were also observed for each pure lipid system with increasing cholesterol content. When htt was incubated with Nt17 peptides with mutations that altered residue charges aggregation was significantly reduced, though the extent was dependent on the type of modification. Incorporation of Nt17 peptides into oligomeric structures resulted in minimal changes to oligomer/lipid interactions, though monomeric peptide/lipid complexation was altered with the introduction of modifications.

Acknowledgements

I would like to take some time to express my deepest thanks and appreciation to those who have helped guide and support my PhD journey. From the beginning of my undergraduate career throughout my graduate career, everyone I've met along the way has had a major role in helping me complete the studies presented here.

Starting with my undergraduate career, I must thank the entirety of the chemistry department at Kutztown University of Pennsylvania for laying the foundation that I needed to succeed at the graduate level and for always inspiring me to reach higher. Special thanks to my undergraduate advisor Dr. Matthew Junker, whose guidance supported my success; to Dr. Darren Achey, who not only convinced me to attend the university but also provided me with my earliest opportunities for engaging with and teaching students; to Dr. Rolf Mayrhofer who inspired my passion for physical chemistry and pushed my academic career forward by offering course work specific to the type of work I wanted to do in the future; and great thanks to Dr. Tom Betts, who pushed me to explore research opportunities and who I heavily credit with my decision to attend graduate school. I also want to acknowledge every other professor in the department for their contributions to my academic career, as well as professors in the biology and physics department who also helped to solidify the direction of my graduate career. The opportunities and support I had at Kutztown University undoubtedly helped me get to where I am today.

Throughout my graduate career I am incredibly grateful to have been advised by Dr. Justin Legleiter and Dr. Stephen Valentine. I had the opportunity to gain valuable research experience as an undergraduate in Dr. Legleiter's lab during a REU offered through the chemistry department here at WVU. Prior to that experience, I had little intention of continuing

my academic career beyond my undergraduate degree. However, I very much enjoyed the research and his mentorship coupled with that of his graduate students at the time inspired me to continue my academic career. I returned to WVU the next year as a graduate student in his lab, and I haven't looked back since. After joining the lab, Dr. Legleiter also facilitated collaboration and recommended co-advisement with Dr. Stephen Valentine. Having been co-advised between a biophysical group and analytical group allowed me to explore two areas of chemistry I've come to greatly appreciate. The support I had and the skills I gained across both labs are invaluable to my career moving forward and I will be forever grateful for these opportunities to learn and grow as a chemist. In addition to my advisors, I would also like to thank my committee, Dr. Peng Li, Dr. Blake Mertz, and Dr. David Smith, and my labmates for further enhancing my graduate career through their support, recommendations, and collaborations.

Furthermore, I would like to thank the WVU Foundation for presenting me with a Ruby Distinguished Doctoral Fellowship for the first three years of my graduate degree. This fellowship allowed me to focus heavily on my research during those three years, helping to ultimately accelerate my degree timeline, in addition to providing funding that allowed me to travel to conferences to present my work, make valuable connections, and broaden my knowledge in my field. I would also like to thank the C. Eugene Bennett department of chemistry for presenting me with the John R. Conrad Endowed Scholarship that provided additional support during my final year.

Beyond the academic support, I would also like to thank those who have supported me outside of the university. Of course, the never-ending support from my family throughout both my undergraduate and graduate careers has been immeasurable, and I will be forever grateful for them pushing me to reach for the best and encouraging me to never give up through the hardest

times. Finally, I would like to thank the friends that I've met along the way that have stood by my side and helped support my academic endeavors while also helping me maintain a crucial work-life balance; your efforts have not gone unnoticed or unappreciated.

In closing, I could never put into words the appreciation I have for the support of the various people and organizations mentioned here. I never would have made it this far in my academic career or have accomplished as much as I did over the years without everyone. Thank you all.

Table of Contents

Abstract	ii
Acknowledgements	iii
Table of Contents	vi
List of Figures	ix
List of Tables	xi
List of Symbols and Abbreviations	xiii
1. Introduction: The Structure and Function of the Huntingtin Protein and its Implications in Huntington’s Disease	1
1.1 Amyloids and Amyloid Diseases.....	1
1.2 Huntington’s Disease and the Huntingtin Protein.....	3
1.3 Huntingtin Aggregation and Toxicity.....	5
1.4 Structure and Function of Nt17.....	8
1.5 Huntingtin-Lipid Interactions.....	11
1.6 Influences of the Environment on Huntingtin Interactions.....	13
1.7 Dissertation Rationale.....	16
1.8 References.....	17
2. Cholesterol Impacts the Formation of Huntingtin/Lipid Complexes and Subsequent Aggregation	29
2.1 Abstract.....	29
2.2 Introduction.....	30
2.3 Materials and Methods.....	32
2.3.1 Purification of GST-Htt-Exon1 Fusion Protein.....	32

2.3.2 Lipid Vesicle Preparation.....	33
2.3.4 Thioflavin T (ThT) Aggregation Assay.....	33
2.3.5 Polydiacetylene (PDA) Lipid Binding Assay.....	34
2.3.6 Atomic Force Microscopy (AFM).....	35
2.3.7 Pulled-Tip Capillary Emitter and Capillary Vibrating Sharp-Edge Spray Ionization (cVSSI) Device Fabrication.....	35
2.3.8 Capillary Vibrating Sharp-Edge Electrospray Ionization Mass Spectrometry (cVSSI-MS).....	36
2.4 Results.....	36
2.4.1 Lipids Alter Htt-Exon1(46Q) Aggregation in a Composition-Dependent Manner.....	36
2.4.2 Htt-Exon1(46Q)/Lipid Interactions are Altered in a Composition-Dependent Manner.....	45
2.4.3 Cholesterol Content Alters Complex Formation Between Lipids and the Lipid Binding Domain of Htt-Exon1(46Q).....	47
2.5 Discussion.....	52
2.6 References.....	60
3. Charge Within Nt17 Peptides Modulates Huntingtin Aggregation and Lipid Binding Events.....	67
3.1 Abstract.....	67
3.2 Introduction.....	67
3.3 Materials and Methods.....	70
3.3.1 Preparation of Synthetic Peptides.....	70

3.3.2 GST-Htt-Exon1 Fusion Protein Purification.....	70
3.3.3 Lipid Vesicle Preparation.....	71
3.3.4 Thioflavin T (ThT) Aggregation Assay.....	71
3.3.5 Polydiacetylene (PDA) Lipid Binding Assay.....	72
3.3.6 Atomic Force Microscopy (AFM).....	73
3.3.7 Pulled-Tip Capillary Emitter and Capillary Vibrating Sharp-Edge Spray Ionization (cVSSI) Device Fabrication.....	73
3.3.8 Capillary Vibrating Sharp-Edge Electrospray Ionization Mass Spectrometry (cVSSI-MS)	74
3.4 Results and Discussion.....	74
3.4.1 Incorporation of Modified Nt17 Peptides Inhibits Fibril Formation and Alters Oligomer Morphologies.....	74
3.4.2 Modifications Within Nt17 Alters Complex Formation Between Peptide and Lipids.....	81
3.4.3 Oligomer/Lipid Interactions are Modified by the Incorporation of Modified Nt17 Peptides.....	94
3.5 References.....	97
 4. Future Directions and Concluding Remarks	
4.1 Introduction.....	103
4.2 Research in Progress: Proteomics of <i>C. elegans</i> HD Model.....	105
4.3 Lipidomics: An Approach to Lipid Dysregulation.....	111
4.4 Conclusions.....	114
4.5 References.....	116

List of Figures

1. Introduction: The Structure and Function of the Huntingtin Protein and its

Implications in Huntington's Disease

- 1.1. Schematic of a normal protein folding energy landscape and the misfolding/amyloid energy landscape.
- 1.2. The mutation within the htt gene that causes the expression of pathogenic htt protein.
- 1.3. A generic aggregation scheme of polyQ-containing proteins.
- 1.4. The amphipathic α -helical structure of Nt17 and sites available for post-translational modification.
- 1.5. Generic phospholipid structure and how varied shapes contribute to key membrane properties such as curvature and packing.

2. Cholesterol Impacts the Formation of Huntingtin/Lipid Complexes and Subsequent Aggregation

- 2.1. ThT aggregation assays for htt-exon1(46Q) incubated in the presence of different lipid vesicles with varying amounts of exogenously added cholesterol.
- 2.2. Representative AFM images of all experimental conditions.
- 2.3. AFM analysis of observed htt-exon1(46Q) aggregate species morphologies under varied lipid conditions.
- 2.4. PDA/lipid binding assays for htt-exon1(46Q) incubated with different lipid systems with varied amounts of exogenously added cholesterol.
- 2.5. Mass spectrum and analysis of Nt17/lipid complex formation in the presence of pure POPC vesicles and POPC vesicles with 20% exogenously added cholesterol using cVSSI-MS.

2.6. Mass spectrum and analysis of Nt17/lipid complex formation in the presence of pure DOPC vesicles and DOPC vesicles with 20% exogenously added cholesterol using cVSSI-MS.

2.7. Mass spectrum and analysis of Nt17/lipid complex formation in the presence of pure POPG vesicles and POPG vesicles with 20% exogenously added cholesterol using cVSSI-MS.

3. Charge Within Nt17 Peptides Modulates Huntingtin Aggregation and Initial Lipid Binding Events

3.1. ThT aggregation assay data for htt-exon1 mimic peptide Nt17Q₃₅P₁₀ incubated alone or with each Nt17 peptide.

3.2. Representative AFM images for all peptide conditions.

3.3. AFM analysis of observed htt-exon1(46Q) oligomeric aggregates in the absence and presence of each Nt17 peptide.

3.4. Analysis of Nt17/lipid complexation in the presence of POPC/POPS (75/25% w/w) vesicles using cVSSI-MS.

3.5. The percent POPS composition for each identified complex of a peptide.

3.6. The relative percent of the total monomeric (1M), dimeric (2M), trimeric (3M), and tetrameric (4M) species that are lipid bound for each peptide.

3.7. PDA/lipid binding assays for htt-exon1(46Q) incubated alone or with each Nt17 peptide in the presence of different lipid systems.

4. Future Directions and Concluding Remarks

4.1. A generic proteomics experimental workflow.

4.2. A generic lipidomics experimental workflow.

List of Tables

Table 1.1. The impacts of various lipid systems on htt interactions.

Table 2.1. Significance of oligomer height, fibril height, and fibril contour length relative to the htt control.

Table 2.2. Identified ions for Nt17 incubated with pure POPC, DOPC, and POPG vesicles and the same vesicles with 20% exogenously added cholesterol with their corresponding mass to charge ratios and charge states.

Table 2.3. Summary of the trends observed with each lipid system for all experiments performed.

Table 3.1. Identified ions of wild-type Nt17 peptide incubated with POPC/POPS lipid vesicles with their respective possible iterations, contribution of each iteration, RMSD from iteration determinations, percent relative peak areas, and SEM from triplicate spectra.

Table 3.2. Identified ions of K6Q mutant Nt17 peptide incubated with POPC/POPS lipid vesicles with their respective possible iterations, contribution of each iteration, RMSD from iteration determinations, percent relative peak areas, and SEM from triplicate spectra.

Table 3.3. Identified ions of K9Q mutant Nt17 peptide incubated with POPC/POPS lipid vesicles with their respective possible iterations, contribution of each iteration, RMSD from iteration determinations, percent relative peak areas, and SEM from triplicate spectra.

Table 3.4. Identified ions of K15Q mutant Nt17 peptide incubated with POPC/POPS lipid vesicles with their respective possible iterations, contribution of each iteration, RMSD from iteration determinations, average percent relative peak areas, and SEM from triplicate spectra.

Table 3.5. Identified ions of T3D mutant Nt17 peptide incubated with POPC/POPS lipid vesicles with their respective possible iterations, contribution of each iteration, RMSD from iteration determinations, average percent relative peak areas, and SEM from triplicate spectra.

Table 3.6. Identified ions of S13D mutant Nt17 peptide incubated with POPC/POPS lipid vesicles with their respective possible iterations, contribution of each iteration, RMSD from iteration determinations, average percent relative peak areas, and SEM from triplicate spectra.

Table 3.7. Identified ions of S16D mutant Nt17 peptide incubated with POPC/POPS lipid vesicles with their respective possible iterations, contribution of each iteration, RMSD from iteration determinations, average percent relative peak areas, and SEM from triplicate spectra.

List of Symbols and Abbreviations

α -syn	Alpha-synuclein
A β	Amyloid-beta
AD	Alzheimer's disease
AFM	Atomic force microscopy
BSA	Bovine serum albumin
<i>C. elegans</i>	Nematode worm <i>Caenorhabditis elegans</i>
CNS	Central nervous system
CR	Colorimetric response
CSF	Cerebrospinal fluid
cVSSI	Capillary vibrating sharp-edge spray ionization
DDA	Data dependent acquisition
dH ₂ O	Deionized water
DIA	Data independent acquisition
DMSO	Dimethyl sulfoxide
DOPC	1,2-dioleoyl-sn-glycero-3-phosphocholine
DPC	Dodecylphosphocholine
DTT	Dithiothreitol
<i>E. coli</i>	Bacteria <i>Escherichia coli</i>
EDTA	Ethylenediaminetetraacetic acid
EGCG	Epigallocatechin 3-gallate
emPAI	Exponentially modified protein abundance index

ER	Endoplasmic reticulum
FFA	Free fatty acid
FUDR	5-fluorodeoxyuridine
GC-MS	Gas chromatography-mass spectrometry
GM1	Ganglioside
GST	Glutathione S-transferase
HD	Huntington's disease
HFIP	Hexafluoroisopropanol
Htt	Huntingtin protein
Htt-exon1(46Q)	Htt-exon1 with 46 glutamine repeats
HUFAs	Highly unsaturated fatty acids
IA	Iodoacetamide
IMS-MS	Ion mobility spectrometry-mass spectrometry
IPTG	Isopropyl-thio-galactopyranoside
K6Q	Lysine 6 to glutamine mutation
K9Q	Lysine 9 to glutamine mutation
K15Q	Lysine 15 to glutamine mutation
LN2	Liquid nitrogen
LPA	Lysophosphatidic acid
LPC	Lysophosphatidylcholine
MRM	Multiple reaction monitoring
MS	Mass spectrometry
MS/MS	Tandem mass spectrometry

NGM	Nematode growth media
NMR	Nuclear magnetic resonance
nESI	Nano-electrospray ionization
Nt17	The first 17 amino acids at the N-terminus of htt
Nt17Q ₃₅ P ₁₀	Htt-exon1 mimic peptide consisting of the Nt17 domain, 35 glutamine residues and 10 proline residues
PD	Parkinson's disease
PDA	Polydiacetylene
PolyP	Polyproline
PolyQ	Polyglutamine
POPC	1-palmitoyl-2-oleoyl-sn-glycero-3-phosphocholine
POPE	1-palmitoyl-2-oleoyl-sn-glycero-3-phosphoethanolamine
POPG	1-palmitoyl-2-oleoyl-sn-glycero-3-(phospho-rac-(1-glycerol))
POPS	1-palmitoyl-2-oleoyl-sn-glycero-3-phospho-L-serine
PTMs	Post-translational modifications
RPLC-MS	Reversed-phase liquid chromatography-mass spectrometry
S13D	Serine 13 to glutamic acid mutation
S16D	Serine 16 to glutamic acid mutation
SEM	Standard error of the mean
SM	Sphingomyelin
SRM	Selected reaction monitoring
T3D	Threonine 3 to glutamic acid mutation
t ₅₀	Time required to reach half of the maximum signal

TBLE	Total brain lipid extract
TFA	Trifluoroacetic acid
ThT	Thioflavin-T

1. The Structure and Function of the Huntingtin Protein and its Implications in Huntington's Disease

1.1 Amyloids and Amyloid Diseases

Multiple neurodegenerative diseases, including Alzheimer's disease (AD), Parkinson's disease (PD), and Huntington's disease (HD), are defined by the accumulation and subsequent deposition of proteinaceous materials in a variety of cellular compartments and tissues. Pathogenesis results from the misfolding and subsequent toxic aggregation of specific proteins, i.e. amyloid-beta ($A\beta$) and tau in AD, alpha-synuclein (α -syn) in PD, and huntingtin (htt) in HD. Clinically, these neurodegenerative diseases are characterized by impaired motor and cognitive functions, while pathological manifestations include neuronal cell dysfunction and death.¹⁻³ More specifically, the hallmark of these diseases is the aggregation of proteins into β -sheet rich fibrillar structures, termed amyloid, that are deposited in the brain.^{4,5} Amyloids are resistant to proteolytic degradation⁶ and are fundamentally characterized by cross- β motifs in which β -strands are organized perpendicular to the fibril axis.⁷⁻⁹

Amyloid diseases are often referred to as protein misfolding diseases, as they result from the misfolding and subsequent aggregation of normally functional proteins. Generically, the process of protein folding can be described by a folding energy landscape^{10,11} (Figure 1.1). As dictated by the primary amino acid sequence, synthesized proteins progress through the energy landscape and fold into a conformation of lower energy, also known as the native conformation. This folding is driven by hydrophobic effects in which hydrophobic residues are shielded from water in the protein interior while hydrophilic residues are solvent-exposed at the protein

surface.^{12,13} Along the energy landscape that leads to the native conformation, there are other local minima in which partially folded intermediates can become trapped.^{14,15}

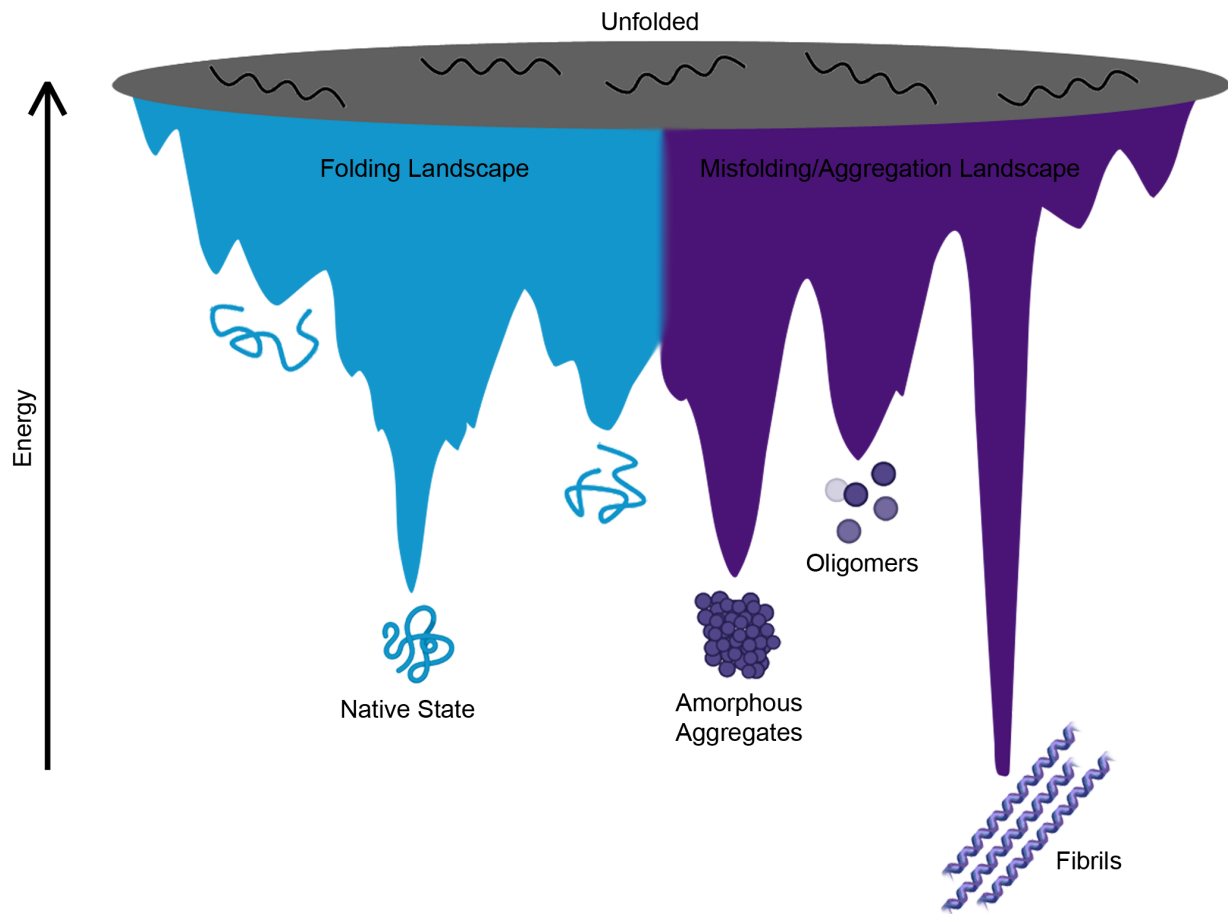


Figure 1.1. Schematic of both the normal protein folding energy landscape and the misfolding/amyloid energy landscape.¹⁶ Unfolded proteins follow a folding landscape to the lowest energy native folded state (blue). Monomers may sample misfolded intermediate states that encourage altered interaction to promote aggregation into various species (purple).

In the case of protein misfolding diseases, the partially folded states expose aggregation-prone domains of the protein, which ultimately results in increased intermolecular interactions that facilitate the transition to an aggregation energy landscape.¹⁷ With an increase in both intermolecular and intramolecular interactions in the aggregation pathway, there are many local minima along the energy landscape corresponding to many different protein conformations and

aggregate species.¹⁷ More specifically, amyloid forming proteins result in monomeric and multimeric species rich in β -sheets, which expose hydrophobic residues and promote the formation of amyloid fibrils.^{18,19} While the stability of these aggregates is heavily dependent on the specific protein, the energy minimum along the aggregation pathway for these proteins is much lower than that of the native conformation, and thus these misfolded and aggregated species are more thermodynamically stable.²⁰ These altered conformations associated with amyloid forming proteins change their biological properties and lead to a toxic gain of function,^{17,21} as the proteins accumulate and aggregate in tissues as a result of disrupted protein homeostasis.²²

1.2 Huntington's Disease and the Huntingtin Protein

HD is a fatal neurodegenerative disease that is clinically characterized by cognitive, motor, and psychiatric decline resulting from autosomal dominant inheritance of a mutation on chromosome 4 that encodes for htt.³ The disease results from a mutation that causes an expansion in a region of CAG trinucleotide repeats, which encodes for a polyglutamine (polyQ) domain near the N-terminus of htt (Figure 1.2). Expansion of the polyQ domain beyond a threshold of approximately 35 repeats correlates to disease.^{23,24} Larger polyQ domains beyond this threshold face a lower energetic penalty for associating and forming β -sheet rich structures,^{25,26} increasing the likelihood that htt will misfold with increasing polyQ length. Both toxic htt aggregate formation and age of HD onset are also directly related to polyQ length; with increasing polyQ length aggregation increases while age of onset decreases.^{23,24,27} Typical onset occurs between 21 and 50 years old with a median repeat length of 45. Late onset HD occurs in individuals over 50 years old with a lower median polyQ repeat length of 42, while juvenile onset occurs between 2 and 20 years old and has an increased median repeat length of 60.²⁷

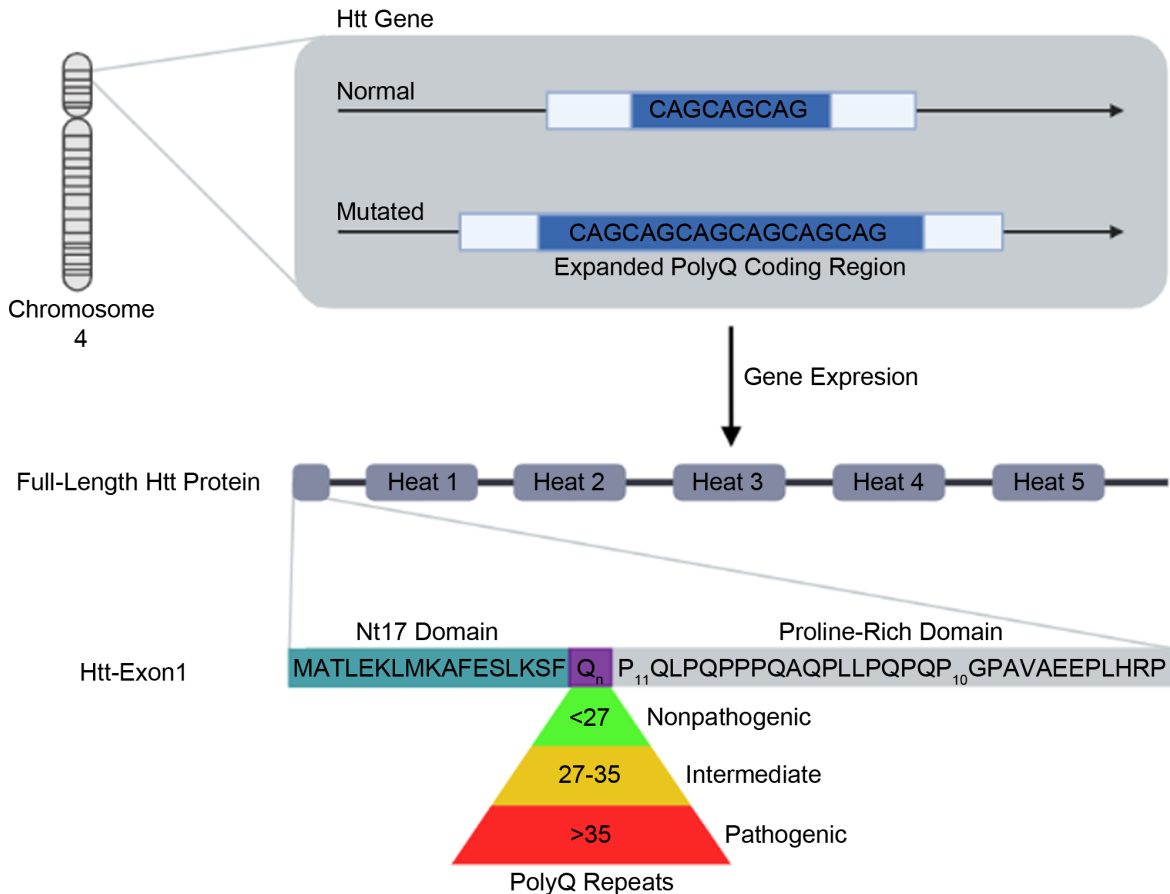


Figure 1.2. The mutation within the htt gene that causes the expression of pathogenic htt protein.¹⁶ The htt gene is found on chromosome 4, and an expansion within the polyQ coding region causes the expression of pathogenic htt protein. The expanded polyQ domain is located within the N-terminal region of the protein known as htt-exon1. Htt-exon1 also contains the Nt17 and proline-rich domains. A polyQ domain with <27 repeats is nonpathogenic, 27-35 repeats is intermediate, and >35 repeats is pathogenic.

Full-length htt is approximately 3142 amino acids with a molecular weight of approximately 350 kDa,²⁸ but ultimately the size is dependent on the length of the polyQ domain. Purification of full-length htt was not made possible until recently,²⁹ and as a result many studies were performed using biologically relevant N-terminal fragments of htt, including the htt-exon1 fragment. This specific fragment is stable and is consistently produced in the brain via proteolysis of full length htt,³⁰ and has been identified as the most toxic fragment of htt that is naturally occurring,³¹ as it has been identified in post-mortem brains of HD patients.³² with

implications in the accumulation and aggregation of htt in the striatum.³³ Htt-exon1 is comprised of three critical domains. The polyQ domain begins at residue 18, and on the N-terminal side of the polyQ domain are the first 17 amino acids (Nt17) which are crucial to facilitating aggregation^{34–36} and lipid binding.^{37–39} On the C-terminal side of the polyQ domain is a proline rich domain that consists of two polyproline (polyP) stretches that modulate both nucleation of htt⁴⁰ and lipid interactions.³⁷ Importantly, the expression of htt-exon1 with an expanded polyQ domain in knock-in mice recapitulated both HD-like phenotypes and age-dependent accumulation of htt much like what has been observed with expression of full length htt.³³ Oligomeric and fibrillar species formed by purified htt-exon1 are also morphologically similar to aggregate species isolated from knock-in mouse models,⁴¹ supporting the use of htt-exon1 for physiologically relevant in-vitro studies.

1.3 Huntingtin Aggregation and Toxicity

Beyond HD, there are eight additional diseases caused by the aggregation of proteins containing expanded polyQ domains: spinocerebellar ataxias (types 1, 2, 6, 7, and 17), Machado-Joseph disease, spinal and bulbar muscular atrophy, dentatorubral pallidoluysian atrophy, and X-linked 1.⁴² Beyond the polyQ threshold of approximately 35 repeats, there is a lower energetic penalty with respect to the formation of β -sheet rich structures, and thus aggregate formation is promoted.^{25,26} Pure polyQ peptides on their own can aggregate,^{43–45} and the incorporation of a polyQ domain into a protein is sufficient to induce the complex polyQ-mediated aggregation process.⁴⁶ This process consists of multiple mechanistic pathways made up of a variety of intermediate species that occur simultaneously, producing heterogenous mixtures of aggregate species that can include oligomers, fibrils, and inclusions,^{34,47,48} and are categorized as “on

pathway” or “off pathway” based on whether their mechanisms of aggregation ultimately lead to the formation of β -sheet rich fibrillar structures or not (Figure 1.3).

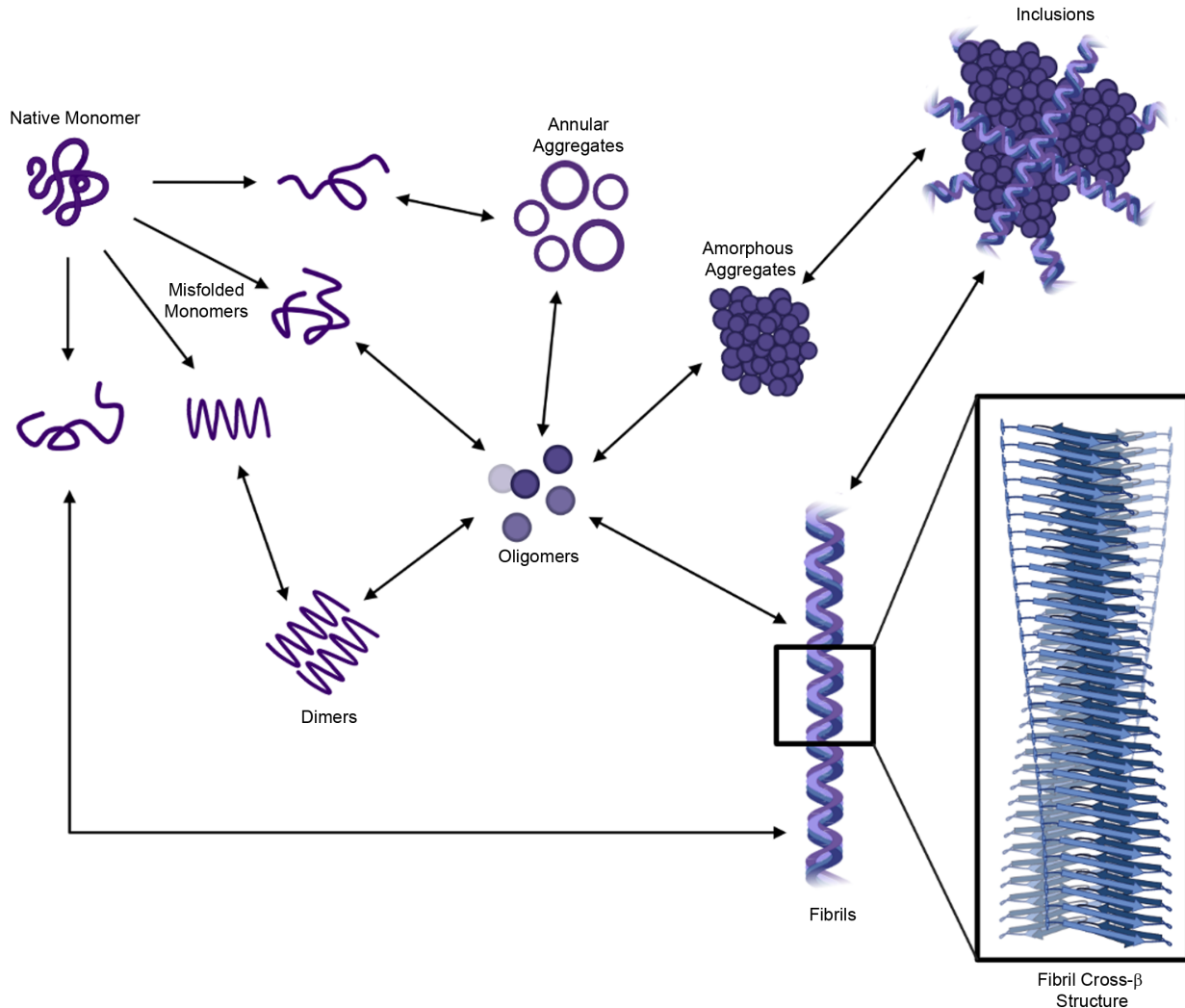


Figure 1.3. A generic aggregation scheme of polyQ-containing proteins. The complex aggregation pathway of polyQ-containing proteins begins with a protein monomer sampling a misfolded conformation. From there, the misfolded monomers can aggregate into a variety of intermediate species including dimers, oligomers, and annular aggregates or a misfolded monomer can undergo direct nucleation to form fibrillar structures. The intermediate species then from higher-order aggregates such as amorphous aggregates or fibrils, which can accumulate together to form large inclusions.

The exact aggregation mechanisms that occur for polyQ-containing proteins are specific to each individual protein, though overall they follow a generic on pathway aggregation scheme.¹⁹ Initially, a protein monomer undergoes a thermodynamically unfavorable transition into a non-native conformation.²⁵ These non-native conformations can be associated with aggregation, and it is through intramolecular and intermolecular interactions the polyQ domain that a β -sheet rich nucleus is formed in the rate-limiting step known as nucleation.^{8,9,49} Once the nucleus is formed, monomer addition can occur during what is known as the elongation phase to ultimately yield β -sheet rich fibril formation.^{8,49} Pathways promoted by different protein conformations that are off pathway can occur simultaneously. Some examples of off pathway species include annular aggregates, amorphous aggregates, and off-pathway oligomers.⁴⁸ Furthermore, a higher order aggregate species known as inclusions, the hallmark aggregate species of HD deposited in the brain, are formed when monomers and other aggregate species, such as fibrils and amorphous aggregates, accumulate together.⁵⁰

The complexities underlying the various aggregation pathways of htt, which are all occurring simultaneously, allow for variations within individual subsets of aggregate species.^{36,51} For example, early differences in monomeric conformations result in the formation of oligomers that can have either non-amyloid α -helix rich structures or cross- β interactions and they can vary greatly in size,⁵¹⁻⁵³ which demonstrates a high degree of structural variation. Fibril structures are generally more consistent, displaying a β -hairpin-based polyQ core structure,^{54,55} but variation in structure, and subsequently neurotoxicity, can be introduced based on flanking sequences present.^{56,57} It is important to note that additional factors such as polyQ length⁵⁰ and the cellular environment⁵⁸⁻⁶⁰ can also modulate aggregation pathways, the types of aggregate species produced, and aggregate structures/morphologies.

The elucidation of the dominant toxic mechanism responsible for dysfunction in HD is difficult. Multiple hypotheses surrounding the toxicity of amyloids have been proposed: the amyloid cascade hypothesis, amyloid fibrils having the ability to catalyze the formation of toxic on-pathway oligomeric species, fibrils having protective effects while off-pathway oligomeric species are toxic due to their ability to insert into and disrupt membrane systems, the entire process involving amyloid formation is toxic, and toxicity is the result of induced cellular stress.⁷ Most debate surrounding toxicity is due to the heterogeneity of aggregate species resulting from various aggregation pathways occurring simultaneously. Identifying which species is most toxic, as many species are involved in various mechanisms,^{51,61} is a difficult task. In cell culture, oligomeric species form early⁶² and the formation of dimeric and tetrameric structures have been identified as early markers of cellular pathology.⁵³ Other cell survival studies point to the toxicity of diffuse htt aggregates,⁶³ specifically oligomeric aggregates^{64,65} in addition to amorphous aggregates and fibrils.^{66,67} Fibrils have also demonstrated toxic properties by inducing apoptotic cell death through the ability to interact with and subsequently permeabilize lipid membranes.⁶⁶ Conversely, some aggregate species have also demonstrated protective effects. It is hypothesized that inclusions are protective as they sequester diffuse htt,^{68,69} which is supported by inclusions exhibiting potential neuroprotective effects by reducing neural cell death.⁷⁰ The complexity surrounding these aggregate species and their various mechanisms make it increasingly difficult to identify a primary species responsible for htt toxicity and highlight the complexity of HD pathogenesis.

1.4 Structure and Function of Nt17

The Nt17 domain of htt is crucial to pathogenesis due to its role in promoting aggregation.^{35,52} Nt17 is intrinsically disordered in bulk solution, but in the presence of binding

partners it undergoes a conformational shift to an amphipathic α -helix,^{71,72} consisting of a predominantly hydrophobic side and a predominantly hydrophilic side (Figure 1.4a). The formation of this amphipathic α -helix is critical to driving aggregation, as Nt17 α -helices associate through intermolecular interactions to form multimeric structures including more compact globular structures and elongated helical bundles.³⁴ This variation in multimeric species exposes different residues to the solvent depending on the structural organization, altering Nt17-driven oligomerization and downstream aggregation.^{34,73} One such multimeric structure observed is an α -helical tetramer structure,^{34,52,73} which can ultimately build up to α -helix rich oligomeric species, making it crucial to the early stages of aggregation.^{35,36} However other multimeric species, for example a dimer with partial α -helical character, can form without undergoing further oligomerization, such as a nonproductive dimer with partial α -helical character.⁷³ In addition to the role of Nt17 in oligomer formation, it is also important in the formation of fibrillar aggregates. The formation of α -helix rich oligomers lowers the energetic barrier for the transition to β -sheet rich aggregates by bringing the polyQ domains close in proximity.^{52,53,73,74}

Nt17 is implicated in initiating aggregation, but its ability to form an amphipathic α -helix also functions in lipid binding.^{75,76} Pure polyQ peptides do not appreciably interact and insert into lipid membranes, but if the polyQ domain is flanked by Nt17 on the N-terminal side there is significant membrane interaction and disruption.³⁷ The interaction of Nt17 with lipid bilayers is summarized by four general steps: approach, reorganization, anchoring, and insertion.³⁸ Long-range electrostatic interactions between the peptide and lipid headgroups drive the approach, and once near the bilayer surface conformational changes to the peptide bring hydrophobic residues close in proximity to the hydrophobic core of the membrane. The peptide anchors as one hydrophobic residue is positioned in the hydrophobic membrane core, after which the peptide

inserts into the membrane more as additional conformational changes allow additional hydrophobic residues to partition into the membrane core. Overall, the end result is a stabilized α -helical structure nearly parallel with the surface of the membrane with the hydrophobic residues of the peptide buried in the hydrophobic core of the membrane.^{38,39,72} The precise mechanisms of interaction between Nt17 and membranes are more nuanced, and interactions are heavily influenced by both lipid composition and physiochemical properties.^{77–79}

Another key factor to consider in terms of htt aggregation and lipid interactions with respect to Nt17 are sites that are subject to post-translational modifications (PTMs). Commonly observed PTMs include phosphorylation,^{80–83} acetylation,^{58,82} ubiquitination,⁸⁴ SUMOylation,^{85,86} and oxidation^{87,88} while some less commonly observed modifications include palmitoylation^{89,90} and transglutamination⁹¹ (Figure 1.4b). PTMs influence htt/lipid interactions,^{58,83,86} aggregation,^{58,80,83,85} and toxicity^{80,85,92} with the exact effects being dependent on the type and location of the modification.

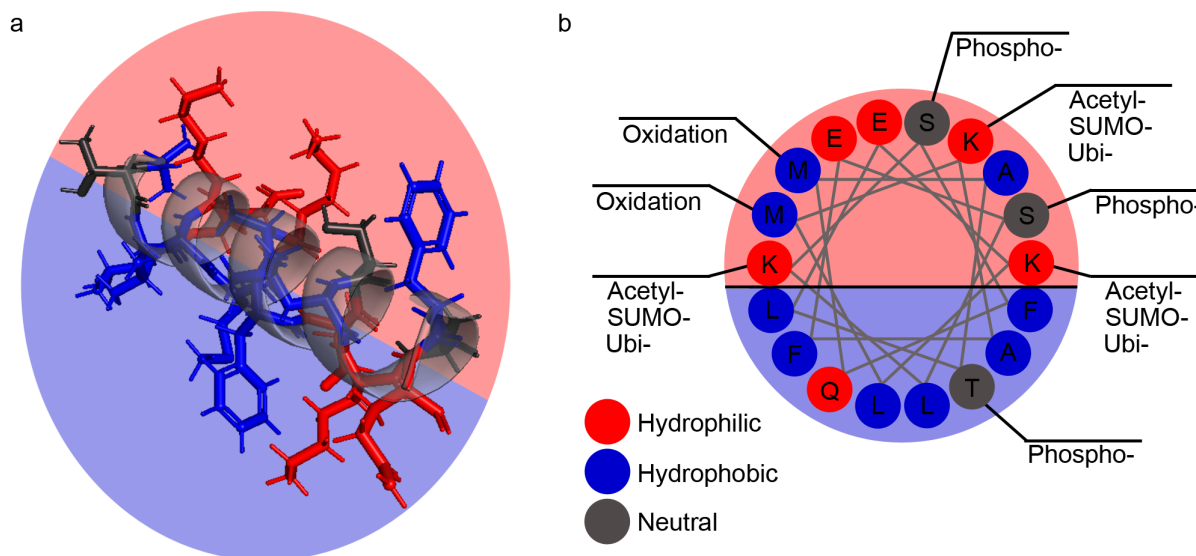


Figure 1.4. The amphipathic α -helical structure of Nt17 and sites available for post-translational modification. (a) A three-dimensional representation of the amphipathic α -helical structure of a monomeric Nt17 domain from the 6N8C tetramer PDB structure rendered in

PyMol. (b) Another representation of the amphipathic α -helical structure of Nt17 that highlights locations available for post-translational modification.

1.5 Huntingtin-Lipid Interactions

A variety of normal functions have been attributed to htt and many of those functions, e.g. synaptic transmission,^{93,94} vesicle transport,^{93,94} and axonal transport,⁹⁵ require direct interactions with a variety of lipid membrane systems. Htt also localizes to the endoplasmic reticulum (ER),⁹⁶⁻⁹⁸ mitochondrial,⁹⁹⁻¹⁰³ nuclear,^{97,98} and plasma membranes.¹⁰⁴ Studies with htt knockout mice indicate that htt is an essential protein, as increased apoptosis and death in the early embryonic stage was observed,^{105,106} while heterozygous knockout mice still exhibited neuronal degeneration.^{106,107} Functions of htt as is related to lipid membranes, when disrupted, have deleterious effects including organelle dysfunction,^{103,108,109} cell death,¹¹⁰ and ultimately brain degeneration,⁹⁵ which supports the notion that the disruption of htt interactions with membranes plays a role in HD pathology.

Interactions between htt and lipid membranes are critical to normal and proper function, but upon expansion of the polyQ domain to a pathogenic length these interactions are altered.^{111,112} There is a polyQ length dependence on the ability of htt-exon1 to bind to and disrupt membranes,^{112,113} with longer polyQ correlating to faster aggregation^{52,114} and these aggregate species subsequently interact with and disrupt membrane systems.¹¹⁵⁻¹¹⁷ Oligomeric species disrupt brain lipid membranes, causing toxicity in neurons.¹¹⁶ Fibrils interact with ER, altering morphology and dynamics.¹¹⁶ Htt inclusions also interact directly with the ER as well as the mitochondria, ultimately resulting in ER membrane deformation, impaired organization, and altered membrane dynamics¹⁰⁹ while damaged and fragmented mitochondria accumulate at the periphery of htt inclusions and have increased respiration rates.¹¹⁸ Inclusions also sequester

membranous structures through such interactions.¹¹⁸ This evidence indicates that interactions of htt with various membrane systems could contribute to HD pathology.

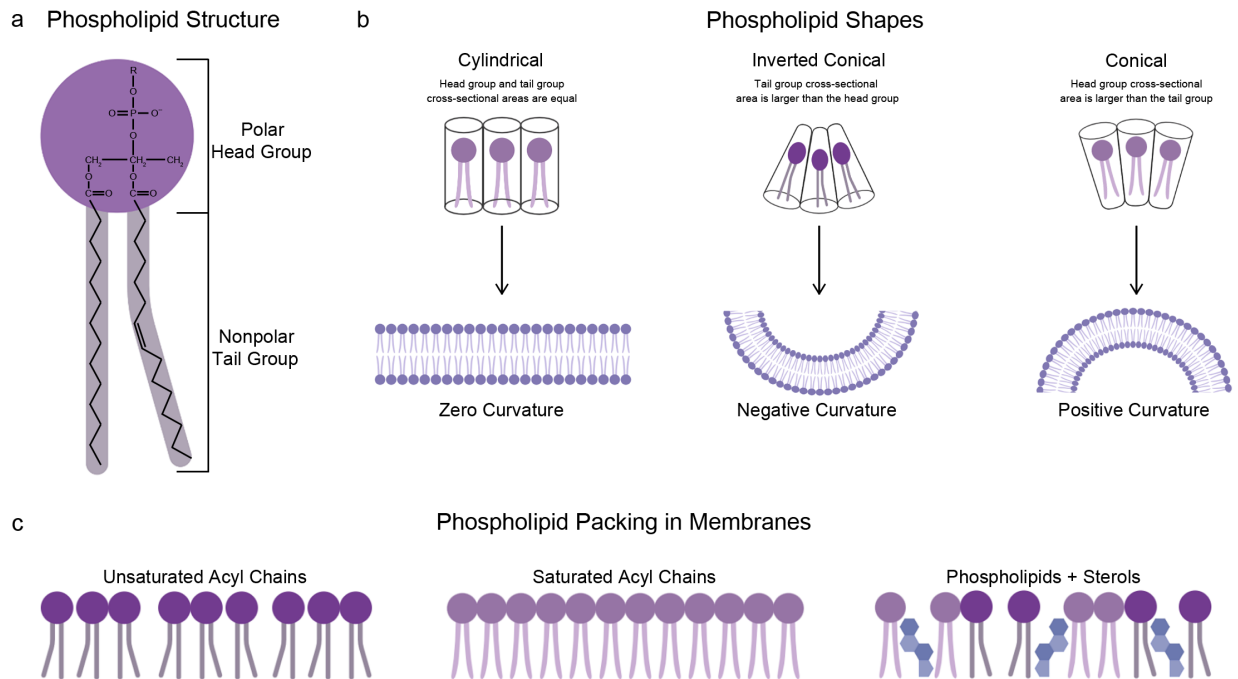


Figure 1.5. Generic phospholipid structure and how varied shapes contribute to key membrane properties such as curvature and packing. (a) The generic structure of a phospholipid consists of a polar headgroup and nonpolar tails that can be saturated or unsaturated. (b) Phospholipids have distinct shapes including cylindrical, inverted conical, and conical. These distinct shapes directly influence membrane curvature and result in zero curvature, negative curvature, or positive curvature membranes respectively based on the relative cross-sectional sizes of the head and tail groups. (c) The degree of saturation and other membrane components influence membrane packing. Unsaturated phospholipids pack less tightly relative to saturated phospholipids, while the inclusion of sterols further influences phospholipid packing within a membrane.

The overall composition and the physiochemical properties of different lipids can further modulate protein/lipid interactions. Lipids spontaneously assemble into bilayers in aqueous solution, such that the hydrophilic head groups are solvent exposed and hydrophobic tail groups are at the membrane interior and shielded from water. Individual properties of different lipids such as headgroup charge, headgroup size, tail length, and tail saturation all influence the overall

shape of the lipid and further dictates the distinct physical properties of a bilayer (Figure 1.5). The size of the lipid headgroup influences curvature,¹¹⁹ while tail properties influence both packing and fluidity.¹²⁰ Increased membrane fluidity and curvature increases the incidence and size of membrane defects,¹²¹ which is important to htt/lipid interactions specifically as Nt17 can detect these defects.¹²² Additionally, headgroup charge is a critical factor to consider as negatively charged lipids such as 1-palmitoyl-2-oleoyl-sn-glycero-3-(phospho-rac-(1-glycerol)) (POPG) and 1-palmitoyl-2-oleoyl-sn-glycero-3-phospho-L-serine (POPS) increase fibril formation relative to zwitterionic 1-palmitoyl-2-oleoyl-sn-glycero-3-phosphoethanolamine (POPE) and 1-palmitoyl-2-oleoyl-sn-glycero-3-phosphocholine (POPC),⁷⁸ likely the result of favorable electrostatic interactions with the net positive charge of Nt17.¹²³ Physicochemical properties of different membrane systems are heavily influenced by the overall composition,¹²⁴ contributing to altered htt/lipid interactions with changing composition. For membranes composed of total brain lipid extract (TBLE), incorporation of membrane components such as sphingomyelin (SM) or ganglioside (GM1) reduces htt/lipid interactions, while SM also increases htt-induced permeability of lipid vesicles but GM1 has no such effect.¹²⁵ Interactions between htt and lipid membranes is multi-faceted and dependent on a variety of lipid properties. Gaining a better understanding of how changes to different membrane properties influences htt interactions can provide additional insight into HD pathology and toxic mechanism.

1.6 Influences of the Environment on Huntingtin Interactions

There are many factors of the environment that can influence amyloid aggregation kinetics, fibril formation, and aggregate structures such as pH,^{126–129} temperature,^{130–134} salt concentration,^{135–137} and/or chemical treatments.^{58,87,88,138–140} Compared to aqueous solvent, simulating the cellular environment using macromolecular crowders also influences aggregation

and htt interactions at the interfaces of different surfaces.¹⁴¹ Another important modulating factor to consider is the presence of lipid membranes. Nt17 has critical roles in both lipid binding and facilitating early interactions to promote aggregation, and subsequently early interactions between htt and membranes can influence aggregation (Table 1.1). A computational study demonstrates that the presence of dodecylphosphocholine (DPC) micelles promotes the formation of the Nt17 α -helix and stabilizes it, whereas in bulk solution the α -helix is quick to unfold.¹⁴² This phenomenon is a likely contributor to changes in htt aggregation and interactions in the presence of lipid membranes. For example, membranes composed of a combination of POPC and POPS catalyze htt aggregation.¹⁴³ Conversely, vesicles composed solely of TBLE reduce htt fibril formation^{60,125} while in TBLE systems with increasing SM or cholesterol content oligomer¹²⁵ and fibril formation,⁵⁹ respectively, are reduced. Meanwhile, vesicles composed of 1,2-dioleoyl-sn-glycero-3-phosphocholine (DOPC), SM, and cholesterol have no impact on aggregation.¹¹⁶ Despite containing similar components, each system has different effects. Pure lipid systems differing only by head groups⁷⁸ or by tail groups⁷⁹ have also demonstrated different effects on aggregation, lipid binding, and htt/lipid complexation as a function of composition and subsequent physiochemical properties. This demonstrates the complexity of htt aggregation in the presence of lipids. Beyond their ability to stabilize the Nt17 domain specifically, lipids have also been demonstrated to have a stabilizing effect on certain aggregate species, such as oligomers.³⁷ Beyond direct interactions at membrane surfaces, some aggregate species have also been shown to sequester lipids; htt inclusions often include multi-vesicular membranes and mitochondria at their surfaces¹¹⁸ while also interacting directly with and disrupting the ER membrane.¹⁰⁹ Beyond the modulation of interactions directly involving membranous surfaces, simply the presence of membranes alters other htt interactions simultaneously. For example, the

presence of TBLE or POPC vesicles eliminated the ability of the small molecule curcumin to inhibit htt fibril formation compared to in bulk solution, while the small molecule epigallocatechin 3-gallate (EGCG) was a successful inhibitor both with and without lipid present.⁶⁰ This added level of complexity could be an additional consideration for HD pathology and progression.

Table 1.1. Impacts of various lipid systems on htt interactions.

Lipid System	Impacts on Htt Interactions	Reference(s)
POPG	Increase htt aggregation, promote fibril formation, increased htt/lipid interactions	78
POPS	Increase htt aggregation, promote fibril formation, increased htt/lipid interactions	78
POPC	Minimal impact on htt aggregation	78, 79
POPE	Minimal impact on aggregation, inhibits aggregation at high lipid:protein ratio	78
DMPC	Increase htt aggregation, promote fibril formation	79
DOPC	Inhibit htt aggregation, reduce fibril formation	79
DOPC/SM/Cholesterol	No impact on htt aggregation	116
POPC/POPS	Increase htt aggregation	143
TBLE	Inhibit htt aggregation, reduce fibril formation	60, 125
TBLE/Cholesterol	Inhibit aggregation, reduce fibril formation	59
TBLE/SM	Reduced htt/lipid interactions, vesicles more susceptible to permeabilization	125
TBLE/GM1	Reduced htt/lipid interactions	125

1.7 Dissertation Rationale

Normal htt functions necessitate its interactions with a variety of membrane systems with unique compositions. However, in the case of mutant htt with pathogenic polyQ lengths toxic aggregation is initiated and interactions between mutant htt and membrane systems also induces

toxic effects. One direct result of such toxic interactions is the resulting dysfunction in various organelles and the degeneration of neurons as HD progresses. It has been established that membranes alter htt aggregation pathways, especially early interactions, and there is evidence to support that such effects are dependent on membrane composition. Here, we further elaborate on the specific effects of membrane composition on both htt aggregation and lipid binding in addition to exploring how the alteration of early htt/lipid interactions impacts downstream interactions.

In Chapter 2, the specific impact of membrane cholesterol content is explored. Model lipid systems of POPC, DOPC, and POPG were chosen due to their differing head and tail groups, varying their physiochemical properties. Varied levels of exogenously added cholesterol were added to each system, then each system was exposed to htt-exon1(46Q). The effects of cholesterol content on aggregation, lipid binding, and htt/lipid complex formation were evaluated using thioflavin-T (ThT) assays, atomic force microscopy (AFM), polydiacetylene (PDA) lipid binding assays, and mass spectrometry (MS). This chapter reveals that increasing cholesterol content has significant impacts on fibril formation, lipid binding, and complex formation, but that the exact effects change in a lipid composition dependent manner.

In Chapter 3, the impact of peptide charge on early htt interactions is explored. Free Nt17 peptides, either wild-type or modified to mimic acetylation or phosphorylation of specific amino acids, were utilized to identify impacts of such modifications on aggregation as well as lipid binding and htt/lipid complex formation in the presence of POPC/POPS and TBLE membrane systems. The impact of monomeric peptides on aggregation and htt/complexation was evaluated using ThT assays and MS respectively. The impact of peptide incorporation into oligomers on aggregate morphology and lipid binding were evaluated using AFM and PDA lipid binding

assays respectively. This chapter reveals that peptide effects, both at the monomeric and oligomeric levels, were unique to each modification type and location of the modification.

1.8 References

- (1) Chung, J. A.; Cummings, J. L. NEUROBEHAVIORAL AND NEUROPSYCHIATRIC SYMPTOMS IN ALZHEIMER'S DISEASE. *Neurol. Clin.* **2000**, *18* (4), 829–846. [https://doi.org/10.1016/S0733-8619\(05\)70228-0](https://doi.org/10.1016/S0733-8619(05)70228-0).
- (2) Moore, D. J.; West, A. B.; Dawson, V. L.; Dawson, T. M. MOLECULAR PATHOPHYSIOLOGY OF PARKINSON'S DISEASE. *Annu. Rev. Neurosci.* **2005**, *28* (1), 57–87. <https://doi.org/10.1146/annurev.neuro.28.061604.135718>.
- (3) McColgan, P.; Tabrizi, S. J. Huntington's Disease: A Clinical Review. *Eur. J. Neurol.* **2018**, *25* (1), 24–34. <https://doi.org/10.1111/ene.13413>.
- (4) Carrell, R. W.; Lomas, D. A. Conformational Disease. *The Lancet* **1997**, *350* (9071), 134–138. [https://doi.org/10.1016/S0140-6736\(97\)02073-4](https://doi.org/10.1016/S0140-6736(97)02073-4).
- (5) Dobson, C. M. Protein Misfolding, Evolution and Disease. *Trends Biochem. Sci.* **1999**, *24* (9), 329–332. [https://doi.org/10.1016/S0968-0004\(99\)01445-0](https://doi.org/10.1016/S0968-0004(99)01445-0).
- (6) Soto, C. Unfolding the Role of Protein Misfolding in Neurodegenerative Diseases. *Nat. Rev. Neurosci.* **2003**, *4* (1), 49–60. <https://doi.org/10.1038/nrn1007>.
- (7) Riek, R.; Eisenberg, D. S. The Activities of Amyloids from a Structural Perspective. *Nature* **2016**, *539* (7628), 227–235. <https://doi.org/10.1038/nature20416>.
- (8) Chiti, F.; Dobson, C. M. Protein Misfolding, Amyloid Formation, and Human Disease: A Summary of Progress Over the Last Decade. *Annu. Rev. Biochem.* **2017**, *86* (1), 27–68. <https://doi.org/10.1146/annurev-biochem-061516-045115>.
- (9) Dobson, C. M. The Amyloid Phenomenon and Its Links with Human Disease. *Cold Spring Harb. Perspect. Biol.* **2017**, *9* (6), a023648. <https://doi.org/10.1101/cshperspect.a023648>.
- (10) Dill, K. A.; Chan, H. S. From Levinthal to Pathways to Funnels. *Nat. Struct. Mol. Biol.* **1997**, *4* (1), 10–19. <https://doi.org/10.1038/nsb0197-10>.
- (11) Onuchic, J. N.; Luthey-Schulten, Z.; Wolynes, P. G. THEORY OF PROTEIN FOLDING: The Energy Landscape Perspective. *Annu. Rev. Phys. Chem.* **1997**, *48* (1), 545–600. <https://doi.org/10.1146/annurev.physchem.48.1.545>.
- (12) Lins, L.; Brasseur, R. The Hydrophobic Effect in Protein Folding. *FASEB J.* **1995**, *9* (7), 535–540. <https://doi.org/10.1096/fasebj.9.7.7737462>.
- (13) Xi, E.; Patel, A. J. The Hydrophobic Effect, and Fluctuations: The Long and the Short of It. *Proc. Natl. Acad. Sci.* **2016**, *113* (17), 4549–4551. <https://doi.org/10.1073/pnas.1603014113>.
- (14) Bryngelson, J. D.; Onuchic, J. N.; Socci, N. D.; Wolynes, P. G. Funnels, Pathways, and the Energy Landscape of Protein Folding: A Synthesis. *Proteins Struct. Funct. Genet.* **1995**, *21* (3), 167–195. <https://doi.org/10.1002/prot.340210302>.
- (15) Vendruscolo, M.; Paci, E.; Karplus, M.; Dobson, C. M. Structures and Relative Free Energies of Partially Folded States of Proteins. *Proc. Natl. Acad. Sci.* **2003**, *100* (25), 14817–14821. <https://doi.org/10.1073/pnas.2036516100>.
- (16) Created with BioRender.Com.
- (17) Jahn, T. R.; Radford, S. E. Folding versus Aggregation: Polypeptide Conformations on Competing Pathways. *Arch. Biochem. Biophys.* **2008**, *469* (1), 100–117. <https://doi.org/10.1016/j.abb.2007.05.015>.

- (18) Reynaud, E. Protein Misfolding and Degenerative Diseases. *Nat. Educ.* **2010**, *9* (3), 1–7.
- (19) Adegbuyiro, A.; Sedighi, F.; Pilkington, A. W.; Groover, S.; Legleiter, J. Proteins Containing Expanded Polyglutamine Tracts and Neurodegenerative Disease. *Biochemistry* **2017**, *56* (9), 1199–1217. <https://doi.org/10.1021/acs.biochem.6b00936>.
- (20) Wetzel, R. Kinetics and Thermodynamics of Amyloid Fibril Assembly. *Acc. Chem. Res.* **2006**, *39* (9), 671–679. <https://doi.org/10.1021/ar050069h>.
- (21) Shorter, J.; Lindquist, S. Prions as Adaptive Conduits of Memory and Inheritance. *Nat. Rev. Genet.* **2005**, *6* (6), 435–450. <https://doi.org/10.1038/nrg1616>.
- (22) Finkel, T. Radical Medicine: Treating Ageing to Cure Disease. *Nat. Rev. Mol. Cell Biol.* **2005**, *6* (12), 971–976. <https://doi.org/10.1038/nrm1763>.
- (23) Snell, R. G.; MacMillan, J. C.; Cheadle, J. P.; Fenton, I.; Lazarou, L. P.; Davies, P.; MacDonald, M. E.; Gusella, J. F.; Harper, P. S.; Shaw, D. J. Relationship between Trinucleotide Repeat Expansion and Phenotypic Variation in Huntington’s Disease. *Nat. Genet.* **1993**, *4* (4), 393–397. <https://doi.org/10.1038/ng0893-393>.
- (24) Penney, J. B.; Vonsattel, J.-P.; Macdonald, M. E.; Gusella, J. F.; Myers, R. H. CAG Repeat Number Governs the Development Rate of Pathology in Huntington’s Disease. *Ann. Neurol.* **1997**, *41* (5), 689–692. <https://doi.org/10.1002/ana.410410521>.
- (25) Bhattacharyya, A. M.; Thakur, A. K.; Wetzel, R. Polyglutamine Aggregation Nucleation: Thermodynamics of a Highly Unfavorable Protein Folding Reaction. *Proc. Natl. Acad. Sci.* **2005**, *102* (43), 15400–15405. <https://doi.org/10.1073/pnas.0501651102>.
- (26) Chen, S.; Ferrone, F. A.; Wetzel, R. Huntington’s Disease Age-of-Onset Linked to Polyglutamine Aggregation Nucleation. *Proc. Natl. Acad. Sci.* **2002**, *99* (18), 11884–11889. <https://doi.org/10.1073/pnas.182276099>.
- (27) The U.S.–Venezuela Collaborative Research Project*; Wexler, N. S. Venezuelan Kindreds Reveal That Genetic and Environmental Factors Modulate Huntington’s Disease Age of Onset. *Proc. Natl. Acad. Sci.* **2004**, *101* (10), 3498–3503. <https://doi.org/10.1073/pnas.0308679101>.
- (28) Macdonald, M. A Novel Gene Containing a Trinucleotide Repeat That Is Expanded and Unstable on Huntington’s Disease Chromosomes. *Cell* **1993**, *72* (6), 971–983. [https://doi.org/10.1016/0092-8674\(93\)90585-E](https://doi.org/10.1016/0092-8674(93)90585-E).
- (29) Li, W.; Serpell, L. C.; Carter, W. J.; Rubinsztein, D. C.; Huntington, J. A. Expression and Characterization of Full-Length Human Huntingtin, an Elongated HEAT Repeat Protein. *J. Biol. Chem.* **2006**, *281* (23), 15916–15922. <https://doi.org/10.1074/jbc.M511007200>.
- (30) Landles, C.; Sathasivam, K.; Weiss, A.; Woodman, B.; Moffitt, H.; Finkbeiner, S.; Sun, B.; Gafni, J.; Ellerby, L. M.; Trotter, Y.; Richards, W. G.; Osmand, A.; Paganetti, P.; Bates, G. P. Proteolysis of Mutant Huntingtin Produces an Exon 1 Fragment That Accumulates as an Aggregated Protein in Neuronal Nuclei in Huntington Disease. *J. Biol. Chem.* **2010**, *285* (12), 8808–8823. <https://doi.org/10.1074/jbc.M109.075028>.
- (31) Barbaro, B. A.; Lukacsovich, T.; Agrawal, N.; Burke, J.; Bornemann, D. J.; Purcell, J. M.; Worthge, S. A.; Caricasole, A.; Weiss, A.; Song, W.; Morozova, O. A.; Colby, D. W.; Marsh, J. L. Comparative Study of Naturally Occurring Huntingtin Fragments in Drosophila Points to Exon 1 as the Most Pathogenic Species in Huntington’s Disease. *Hum. Mol. Genet.* **2015**, *24* (4), 913–925. <https://doi.org/10.1093/hmg/ddu504>.
- (32) DiFiglia, M.; Sapp, E.; Chase, K. O.; Davies, S. W.; Bates, G. P.; Vonsattel, J. P.; Aronin, N. Aggregation of Huntingtin in Neuronal Intranuclear Inclusions and Dystrophic

- Neurites in Brain. *Science* **1997**, *277* (5334), 1990–1993.
<https://doi.org/10.1126/science.277.5334.1990>.
- (33) Yang, H.; Yang, S.; Jing, L.; Huang, L.; Chen, L.; Zhao, X.; Yang, W.; Pan, Y.; Yin, P.; Qin, Z. S.; Tang, B.; Li, S.; Li, X.-J. Truncation of Mutant Huntingtin in Knock-in Mice Demonstrates Exon1 Huntingtin Is a Key Pathogenic Form. *Nat. Commun.* **2020**, *11* (1), 2582.
<https://doi.org/10.1038/s41467-020-16318-1>.
- (34) Arndt, J. R.; Kondalaji, S. G.; Maurer, M. M.; Parker, A.; Legleiter, J.; Valentine, S. J. Huntingtin N-Terminal Monomeric and Multimeric Structures Destabilized by Covalent Modification of Heteroatomic Residues. *Biochemistry* **2015**, *54* (28), 4285–4296.
<https://doi.org/10.1021/acs.biochem.5b00478>.
- (35) Williamson, T. E.; Vitalis, A.; Crick, S. L.; Pappu, R. V. Modulation of Polyglutamine Conformations and Dimer Formation by the N-Terminus of Huntingtin. *J. Mol. Biol.* **2010**, *396* (5), 1295–1309. <https://doi.org/10.1016/j.jmb.2009.12.017>.
- (36) Vitalis, A.; Pappu, R. V. Assessing the Contribution of Heterogeneous Distributions of Oligomers to Aggregation Mechanisms of Polyglutamine Peptides. *Biophys. Chem.* **2011**, *159* (1), 14–23. <https://doi.org/10.1016/j.bpc.2011.04.006>.
- (37) Burke, K. A.; Kauffman, K. J.; Umbaugh, C. S.; Frey, S. L.; Legleiter, J. The Interaction of Polyglutamine Peptides with Lipid Membranes Is Regulated by Flanking Sequences Associated with Huntingtin. *J. Biol. Chem.* **2013**, *288* (21), 14993–15005.
<https://doi.org/10.1074/jbc.M112.446237>.
- (38) Côté, S.; Wei, G.; Mousseau, N. Atomistic Mechanisms of Huntingtin N-Terminal Fragment Insertion on a Phospholipid Bilayer Revealed by Molecular Dynamics Simulations: Htt^{NT}Q_N Insertion on a Phospholipid Bilayer. *Proteins Struct. Funct. Bioinforma.* **2014**, *82* (7), 1409–1427. <https://doi.org/10.1002/prot.24509>.
- (39) Côté, S.; Binette, V.; Salnikov, E. S.; Bechinger, B.; Mousseau, N. Probing the Huntingtin 1-17 Membrane Anchor on a Phospholipid Bilayer by Using All-Atom Simulations. *Biophys. J.* **2015**, *108* (5), 1187–1198. <https://doi.org/10.1016/j.bpj.2015.02.001>.
- (40) Arndt, J. R.; Chaibva, M.; Beasley, M.; Kiani Karanji, A.; Ghassabi Kondalaji, S.; Khakinejad, M.; Sarver, O.; Legleiter, J.; Valentine, S. J. Nucleation Inhibition of Huntingtin Protein (Htt) by Polyproline PPII Helices: A Potential Interaction with the N-Terminal α -Helical Region of Htt. *Biochemistry* **2020**, *59* (4), 436–449.
<https://doi.org/10.1021/acs.biochem.9b00689>.
- (41) Sathasivam, K.; Lane, A.; Legleiter, J.; Warley, A.; Woodman, B.; Finkbeiner, S.; Paganetti, P.; Muchowski, P. J.; Wilson, S.; Bates, G. P. Identical Oligomeric and Fibrillar Structures Captured from the Brains of R6/2 and Knock-in Mouse Models of Huntington's Disease. *Hum. Mol. Genet.* **2010**, *19* (1), 65–78. <https://doi.org/10.1093/hmg/ddp467>.
- (42) Fan, H.-C.; Ho, L.-I.; Chi, C.-S.; Chen, S.-J.; Peng, G.-S.; Chan, T.-M.; Lin, S.-Z.; Harn, H.-J. Polyglutamine (PolyQ) Diseases: Genetics to Treatments. *Cell Transplant.* **2014**, *23* (4–5), 441–458. <https://doi.org/10.3727/096368914X678454>.
- (43) Perutz, M. F.; Johnson, T.; Suzuki, M.; Finch, J. T. Glutamine Repeats as Polar Zippers: Their Possible Role in Inherited Neurodegenerative Diseases. *Proc. Natl. Acad. Sci.* **1994**, *91* (12), 5355–5358. <https://doi.org/10.1073/pnas.91.12.5355>.
- (44) Chen, S.; Berthelie, V.; Yang, W.; Wetzel, R. Polyglutamine Aggregation Behavior in Vitro Supports a Recruitment Mechanism of Cytotoxicity. *J. Mol. Biol.* **2001**, *311* (1), 173–182.
<https://doi.org/10.1006/jmbi.2001.4850>.

- (45) Chen, S.; Berthelie, V.; Hamilton, J. B.; O’Nuallai, B.; Wetzel, R. Amyloid-like Features of Polyglutamine Aggregates and Their Assembly Kinetics †. *Biochemistry* **2002**, *41* (23), 7391–7399. <https://doi.org/10.1021/bi011772q>.
- (46) Stott, K.; Blackburn, J. M.; Butler, P. J.; Perutz, M. Incorporation of Glutamine Repeats Makes Protein Oligomerize: Implications for Neurodegenerative Diseases. *Proc. Natl. Acad. Sci.* **1995**, *92* (14), 6509–6513. <https://doi.org/10.1073/pnas.92.14.6509>.
- (47) Counterman, A. E.; Hilderbrand, A. E.; Barnes, C. A. S.; Clemmer, D. E. Formation of Peptide Aggregates during ESI: Size, Charge, Composition, and Contributions to Noise. *J. Am. Soc. Mass Spectrom.* **2001**, *12* (9), 1020–1035. [https://doi.org/10.1016/S1044-0305\(01\)00283-5](https://doi.org/10.1016/S1044-0305(01)00283-5).
- (48) Burke, K. A.; Godbey, J.; Legleiter, J. Assessing Mutant Huntingtin Fragment and Polyglutamine Aggregation by Atomic Force Microscopy. *Methods* **2011**, *53* (3), 275–284. <https://doi.org/10.1016/j.ymeth.2010.12.028>.
- (49) Eisenberg, D.; Jucker, M. The Amyloid State of Proteins in Human Diseases. *Cell* **2012**, *148* (6), 1188–1203. <https://doi.org/10.1016/j.cell.2012.02.022>.
- (50) Legleiter, J.; Mitchell, E.; Lotz, G. P.; Sapp, E.; Ng, C.; DiFiglia, M.; Thompson, L. M.; Muchowski, P. J. Mutant Huntingtin Fragments Form Oligomers in a Polyglutamine Length-Dependent Manner in Vitro and in Vivo. *J. Biol. Chem.* **2010**, *285* (19), 14777–14790. <https://doi.org/10.1074/jbc.M109.093708>.
- (51) Xi, W.; Wang, X.; Laue, T. M.; Denis, C. L. Multiple Discrete Soluble Aggregates Influence Polyglutamine Toxicity in a Huntington’s Disease Model System. *Sci. Rep.* **2016**, *6* (1), 34916. <https://doi.org/10.1038/srep34916>.
- (52) Jayaraman, M.; Kodali, R.; Sahoo, B.; Thakur, A. K.; Mayasundari, A.; Mishra, R.; Peterson, C. B.; Wetzel, R. Slow Amyloid Nucleation via α -Helix-Rich Oligomeric Intermediates in Short Polyglutamine-Containing Huntingtin Fragments. *J. Mol. Biol.* **2012**, *415* (5), 881–899. <https://doi.org/10.1016/j.jmb.2011.12.010>.
- (53) Sahoo, B.; Arduini, I.; Drombosky, K. W.; Kodali, R.; Sanders, L. H.; Greenamyre, J. T.; Wetzel, R. Folding Landscape of Mutant Huntingtin Exon1: Diffusible Multimers, Oligomers and Fibrils, and No Detectable Monomer. *PLOS ONE* **2016**, *11* (6), e0155747. <https://doi.org/10.1371/journal.pone.0155747>.
- (54) Kar, K.; Hoop, C. L.; Drombosky, K. W.; Baker, M. A.; Kodali, R.; Arduini, I.; van der Wel, P. C. A.; Horne, W. S.; Wetzel, R. β -Hairpin-Mediated Nucleation of Polyglutamine Amyloid Formation. *J. Mol. Biol.* **2013**, *425* (7), 1183–1197. <https://doi.org/10.1016/j.jmb.2013.01.016>.
- (55) Hoop, C. L.; Lin, H.-K.; Kar, K.; Magyarfalvi, G.; Lamley, J. M.; Boatz, J. C.; Mandal, A.; Lewandowski, J. R.; Wetzel, R.; van der Wel, P. C. A. Huntingtin Exon 1 Fibrils Feature an Interdigitated β -Hairpin-Based Polyglutamine Core. *Proc. Natl. Acad. Sci.* **2016**, *113* (6), 1546–1551. <https://doi.org/10.1073/pnas.1521933113>.
- (56) Shen, K.; Calamini, B.; Fauerbach, J. A.; Ma, B.; Shahmoradian, S. H.; Serrano Lachapel, I. L.; Chiu, W.; Lo, D. C.; Frydman, J. Control of the Structural Landscape and Neuronal Proteotoxicity of Mutant Huntingtin by Domains Flanking the PolyQ Tract. *eLife* **2016**, *5*, e18065. <https://doi.org/10.7554/eLife.18065>.
- (57) Lin, H.-K.; Boatz, J. C.; Krabbendam, I. E.; Kodali, R.; Hou, Z.; Wetzel, R.; Dolga, A. M.; Poirier, M. A.; van der Wel, P. C. A. Fibril Polymorphism Affects Immobilized Non-Amyloid Flanking Domains of Huntingtin Exon1 Rather than Its Polyglutamine Core. *Nat. Commun.* **2017**, *8* (1), 15462. <https://doi.org/10.1038/ncomms15462>.

- (58) Chaibva, M.; Jawahery, S.; Pilkington, A. W.; Arndt, J. R.; Sarver, O.; Valentine, S.; Matysiak, S.; Legleiter, J. Acetylation within the First 17 Residues of Huntingtin Exon 1 Alters Aggregation and Lipid Binding. *Biophys. J.* **2016**, *111* (2), 349–362. <https://doi.org/10.1016/j.bpj.2016.06.018>.
- (59) Gao, X.; Campbell, W. A.; Chaibva, M.; Jain, P.; Leslie, A. E.; Frey, S. L.; Legleiter, J. Cholesterol Modifies Huntingtin Binding to, Disruption of, and Aggregation on Lipid Membranes. *Biochemistry* **2016**, *55* (1), 92–102. <https://doi.org/10.1021/acs.biochem.5b00900>.
- (60) Beasley, M.; Stonebraker, A. R.; Hasan, I.; Kapp, K. L.; Liang, B. J.; Agarwal, G.; Groover, S.; Sedighi, F.; Legleiter, J. Lipid Membranes Influence the Ability of Small Molecules To Inhibit Huntingtin Fibrillization. *Biochemistry* **2019**, *58* (43), 4361–4373. <https://doi.org/10.1021/acs.biochem.9b00739>.
- (61) Stefani, M.; Dobson, C. M. Protein Aggregation and Aggregate Toxicity: New Insights into Protein Folding, Misfolding Diseases and Biological Evolution. *J. Mol. Med.* **2003**, *81* (11), 678–699. <https://doi.org/10.1007/s00109-003-0464-5>.
- (62) Takahashi, Y.; Okamoto, Y.; Popiel, H. A.; Fujikake, N.; Toda, T.; Kinjo, M.; Nagai, Y. Detection of Polyglutamine Protein Oligomers in Cells by Fluorescence Correlation Spectroscopy. *J. Biol. Chem.* **2007**, *282* (33), 24039–24048. <https://doi.org/10.1074/jbc.M704789200>.
- (63) Arrasate, M.; Finkbeiner, S. Protein Aggregates in Huntington’s Disease. *Exp. Neurol.* **2012**, *238* (1), 1–11. <https://doi.org/10.1016/j.expneurol.2011.12.013>.
- (64) Nucifora, L. G.; Burke, K. A.; Feng, X.; Arbez, N.; Zhu, S.; Miller, J.; Yang, G.; Ratovitski, T.; Delannoy, M.; Muchowski, P. J.; Finkbeiner, S.; Legleiter, J.; Ross, C. A.; Poirier, M. A. Identification of Novel Potentially Toxic Oligomers Formed in Vitro from Mammalian-Derived Expanded Huntingtin Exon-1 Protein. *J. Biol. Chem.* **2012**, *287* (19), 16017–16028. <https://doi.org/10.1074/jbc.M111.252577>.
- (65) Kim, Y. E.; Hosp, F.; Frottin, F.; Ge, H.; Mann, M.; Hayer-Hartl, M.; Hartl, F. U. Soluble Oligomers of PolyQ-Expanded Huntingtin Target a Multiplicity of Key Cellular Factors. *Mol. Cell* **2016**, *63* (6), 951–964. <https://doi.org/10.1016/j.molcel.2016.07.022>.
- (66) Pieri, L.; Madiona, K.; Bousset, L.; Melki, R. Fibrillar α -Synuclein and Huntingtin Exon 1 Assemblies Are Toxic to the Cells. *Biophys. J.* **2012**, *102* (12), 2894–2905. <https://doi.org/10.1016/j.bpj.2012.04.050>.
- (67) Drombosky, K. W.; Rode, S.; Kodali, R.; Jacob, T. C.; Palladino, M. J.; Wetzel, R. Mutational Analysis Implicates the Amyloid Fibril as the Toxic Entity in Huntington’s Disease. *Neurobiol. Dis.* **2018**, *120*, 126–138. <https://doi.org/10.1016/j.nbd.2018.08.019>.
- (68) Saudou, F.; Finkbeiner, S.; Devys, D.; Greenberg, M. E. Huntingtin Acts in the Nucleus to Induce Apoptosis but Death Does Not Correlate with the Formation of Intranuclear Inclusions. *Cell* **1998**, *95* (1), 55–66. [https://doi.org/10.1016/S0092-8674\(00\)81782-1](https://doi.org/10.1016/S0092-8674(00)81782-1).
- (69) Arrasate, M.; Mitra, S.; Schweitzer, E. S.; Segal, M. R.; Finkbeiner, S. Inclusion Body Formation Reduces Levels of Mutant Huntingtin and the Risk of Neuronal Death. *Nature* **2004**, *431* (7010), 805–810. <https://doi.org/10.1038/nature02998>.
- (70) Ramdzan, Y. M.; Trubetskov, M. M.; Ormsby, A. R.; Newcombe, E. A.; Sui, X.; Tobin, M. J.; Bongiovanni, M. N.; Gras, S. L.; Dewson, G.; Miller, J. M. L.; Finkbeiner, S.; Moily, N. S.; Niclis, J.; Parish, C. L.; Purcell, A. W.; Baker, M. J.; Wilce, J. A.; Waris, S.; Stojanovski, D.; Böcking, T.; Ang, C.-S.; Ascher, D. B.; Reid, G. E.; Hatters, D. M. Huntingtin Inclusions Trigger Cellular Quiescence, Deactivate Apoptosis, and Lead to Delayed Necrosis. *Cell Rep.* **2017**, *19* (5), 919–927. <https://doi.org/10.1016/j.celrep.2017.04.029>.

- (71) Michalek, M.; Salnikov, E. S.; Werten, S.; Bechinger, B. Membrane Interactions of the Amphipathic Amino Terminus of Huntingtin. *Biochemistry* **2013**, *52* (5), 847–858. <https://doi.org/10.1021/bi301325q>.
- (72) Michalek, M.; Salnikov, E. S.; Bechinger, B. Structure and Topology of the Huntingtin 1–17 Membrane Anchor by a Combined Solution and Solid-State NMR Approach. *Biophys. J.* **2013**, *105* (3), 699–710. <https://doi.org/10.1016/j.bpj.2013.06.030>.
- (73) Kotler, S. A.; Tugarinov, V.; Schmidt, T.; Cecon, A.; Libich, D. S.; Ghirlando, R.; Schwieters, C. D.; Clore, G. M. Probing Initial Transient Oligomerization Events Facilitating Huntingtin Fibril Nucleation at Atomic Resolution by Relaxation-Based NMR. *Proc. Natl. Acad. Sci.* **2019**, *116* (9), 3562–3571. <https://doi.org/10.1073/pnas.1821216116>.
- (74) Thakur, A. K.; Jayaraman, M.; Mishra, R.; Thakur, M.; Chellgren, V. M.; L Byeon, I.-J.; Anjum, D. H.; Kodali, R.; Creamer, T. P.; Conway, J. F.; M Gronenborn, A.; Wetzel, R. Polyglutamine Disruption of the Huntingtin Exon 1 N Terminus Triggers a Complex Aggregation Mechanism. *Nat. Struct. Mol. Biol.* **2009**, *16* (4), 380–389. <https://doi.org/10.1038/nsmb.1570>.
- (75) Brass, V.; Bieck, E.; Montserret, R.; Wölk, B.; Hellings, J. A.; Blum, H. E.; Penin, F.; Moradpour, D. An Amino-Terminal Amphipathic α -Helix Mediates Membrane Association of the Hepatitis C Virus Nonstructural Protein 5A. *J. Biol. Chem.* **2002**, *277* (10), 8130–8139. <https://doi.org/10.1074/jbc.M111289200>.
- (76) Georgieva, E. R.; Xiao, S.; Borbat, P. P.; Freed, J. H.; Eliezer, D. Tau Binds to Lipid Membrane Surfaces via Short Amphipathic Helices Located in Its Microtubule-Binding Repeats. *Biophys. J.* **2014**, *107* (6), 1441–1452. <https://doi.org/10.1016/j.bpj.2014.07.046>.
- (77) Karanji, A. K.; Beasley, M.; Sharif, D.; Ranjbaran, A.; Legleiter, J.; Valentine, S. J. Investigating the Interactions of the First 17 Amino Acid Residues of Huntingtin with Lipid Vesicles Using Mass Spectrometry and Molecular Dynamics. *J. Mass Spectrom.* **2020**, *55* (1). <https://doi.org/10.1002/jms.4470>.
- (78) Beasley, M.; Groover, S.; Valentine, S. J.; Legleiter, J. Lipid Headgroups Alter Huntingtin Aggregation on Membranes. *Biochim. Biophys. Acta BBA - Biomembr.* **2021**, *1863* (1), 183497. <https://doi.org/10.1016/j.bbamem.2020.183497>.
- (79) Beasley, M.; Frazee, N.; Groover, S.; Valentine, S. J.; Mertz, B.; Legleiter, J. Physicochemical Properties Altered by the Tail Group of Lipid Membranes Influence Huntingtin Aggregation and Lipid Binding. *J. Phys. Chem. B* **2022**, *126* (16), 3067–3081. <https://doi.org/10.1021/acs.jpcc.1c10254>.
- (80) Aiken, C. T.; Steffan, J. S.; Guerrero, C. M.; Khashwji, H.; Lukacsovich, T.; Simmons, D.; Purcell, J. M.; Menhaji, K.; Zhu, Y.-Z.; Green, K.; LaFerla, F.; Huang, L.; Thompson, L. M.; Marsh, J. L. Phosphorylation of Threonine 3: IMPLICATIONS FOR HUNTINGTIN AGGREGATION AND NEUROTOXICITY. *J. Biol. Chem.* **2009**, *284* (43), 29427–29436. <https://doi.org/10.1074/jbc.M109.013193>.
- (81) Mishra, R.; Hoop, C. L.; Kodali, R.; Sahoo, B.; van der Wel, P. C. A.; Wetzel, R. Serine Phosphorylation Suppresses Huntingtin Amyloid Accumulation by Altering Protein Aggregation Properties. *J. Mol. Biol.* **2012**, *424* (1–2), 1–14. <https://doi.org/10.1016/j.jmb.2012.09.011>.
- (82) Chiki, A.; DeGuire, S. M.; Ruggeri, F. S.; Sanfelice, D.; Ansaloni, A.; Wang, Z.-M.; Cendrowska, U.; Burai, R.; Vieweg, S.; Pastore, A.; Dietler, G.; Lashuel, H. A. Mutant Exon1 Huntingtin Aggregation Is Regulated by T3 Phosphorylation-Induced Structural Changes and Crosstalk between T3 Phosphorylation and Acetylation at K6. *Angew. Chem. Int. Ed.* **2017**, *56* (19), 5202–5207. <https://doi.org/10.1002/anie.201611750>.

- (83) DeGuire, S. M.; Ruggeri, F. S.; Fares, M.-B.; Chiki, A.; Cendrowska, U.; Dietler, G.; Lashuel, H. A. N-Terminal Huntingtin (Htt) Phosphorylation Is a Molecular Switch Regulating Htt Aggregation, Helical Conformation, Internalization, and Nuclear Targeting. *J. Biol. Chem.* **2018**, *293* (48), 18540–18558. <https://doi.org/10.1074/jbc.RA118.004621>.
- (84) Kalchman, M. A.; Graham, R. K.; Xia, G.; Koide, H. B.; Hodgson, J. G.; Graham, K. C.; Goldberg, Y. P.; Gietz, R. D.; Pickart, C. M.; Hayden, M. R. Huntingtin Is Ubiquitinated and Interacts with a Specific Ubiquitin-Conjugating Enzyme. *J. Biol. Chem.* **1996**, *271* (32), 19385–19394. <https://doi.org/10.1074/jbc.271.32.19385>.
- (85) Steffan, J. S. SUMO Modification of Huntingtin and Huntington's Disease Pathology. *Science* **2004**, *304* (5667), 100–104. <https://doi.org/10.1126/science.1092194>.
- (86) Sedighi, F.; Adegbuyiro, A.; Legleiter, J. SUMOylation Prevents Huntingtin Fibrillization and Localization onto Lipid Membranes. *ACS Chem. Neurosci.* **2020**, *11* (3), 328–343. <https://doi.org/10.1021/acchemneuro.9b00509>.
- (87) Fox, J. H.; Connor, T.; Stiles, M.; Kama, J.; Lu, Z.; Dorsey, K.; Liebermann, G.; Sapp, E.; Cherny, R. A.; Banks, M.; Volitakis, I.; DiFiglia, M.; Berezovska, O.; Bush, A. I.; Hersch, S. M. Cysteine Oxidation within N-Terminal Mutant Huntingtin Promotes Oligomerization and Delays Clearance of Soluble Protein. *J. Biol. Chem.* **2011**, *286* (20), 18320–18330. <https://doi.org/10.1074/jbc.M110.199448>.
- (88) Adegbuyiro, A.; Stonebraker, A. R.; Sedighi, F.; Fan, C. K.; Hodges, B.; Li, P.; Valentine, S. J.; Legleiter, J. Oxidation Promotes Distinct Huntingtin Aggregates in the Presence and Absence of Membranes. *Biochemistry* **2022**, *acs.biochem.2c00212*. <https://doi.org/10.1021/acs.biochem.2c00212>.
- (89) Yanai, A.; Huang, K.; Kang, R.; Singaraja, R. R.; Arstikaitis, P.; Gan, L.; Orban, P. C.; Mullard, A.; Cowan, C. M.; Raymond, L. A.; Drisdell, R. C.; Green, W. N.; Ravikumar, B.; Rubinsztein, D. C.; El-Husseini, A.; Hayden, M. R. Palmitoylation of Huntingtin by HIP14 is Essential for Its Trafficking and Function. *Nat. Neurosci.* **2006**, *9* (6), 824–831. <https://doi.org/10.1038/nn1702>.
- (90) Young, F. B.; Butland, S. L.; Sanders, S. S.; Sutton, L. M.; Hayden, M. R. Putting Proteins in Their Place: Palmitoylation in Huntington Disease and Other Neuropsychiatric Diseases. *Prog. Neurobiol.* **2012**, *97* (2), 220–238. <https://doi.org/10.1016/j.pneurobio.2011.11.002>.
- (91) Kahlem, P.; Green, H.; Djian, P. Transglutaminase Action Imitates Huntington's Disease: Selective Polymerization of Huntingtin Containing Expanded Polyglutamine. *Mol. Cell* **1998**, *1* (4), 595–601. [https://doi.org/10.1016/S1097-2765\(00\)80059-3](https://doi.org/10.1016/S1097-2765(00)80059-3).
- (92) Pennuto, M.; Palazzolo, I.; Poletti, A. Post-Translational Modifications of Expanded Polyglutamine Proteins: Impact on Neurotoxicity. *Hum. Mol. Genet.* **2009**, *18* (R1), R40–R47. <https://doi.org/10.1093/hmg/ddn412>.
- (93) Li, S.-H.; Li, X.-J. Huntingtin-Protein Interactions and the Pathogenesis of Huntington's Disease. *Trends Genet.* **2004**, *20* (3), 146–154. <https://doi.org/10.1016/j.tig.2004.01.008>.
- (94) Cattaneo, E.; Zuccato, C.; Tartari, M. Normal Huntingtin Function: An Alternative Approach to Huntington's Disease. *Nat. Rev. Neurosci.* **2005**, *6* (12), 919–930. <https://doi.org/10.1038/nrn1806>.
- (95) Trushina, E.; Dyer, R. B.; Badger, J. D.; Ure, D.; Eide, L.; Tran, D. D.; Vrieze, B. T.; Legendre-Guillemain, V.; McPherson, P. S.; Mandavilli, B. S.; Van Houten, B.; Zeitlin, S.; McNiven, M.; Abersold, R.; Hayden, M.; Parisi, J. E.; Seeburg, E.; Dragatsis, I.; Doyle, K.; Bender, A.; Chacko, C.; McMurray, C. T. Mutant Huntingtin Impairs Axonal Trafficking in

- Mammalian Neurons In Vivo and In Vitro. *Mol. Cell. Biol.* **2004**, *24* (18), 8195–8209. <https://doi.org/10.1128/MCB.24.18.8195-8209.2004>.
- (96) De Rooij, K. Subcellular Localization of the Huntington's Disease Gene Product in Cell Lines by Immunofluorescence and Biochemical Subcellular Fractionation. *Hum. Mol. Genet.* **1996**, *5* (8), 1093–1099. <https://doi.org/10.1093/hmg/5.8.1093>.
- (97) Xia, J. Huntingtin Contains a Highly Conserved Nuclear Export Signal. *Hum. Mol. Genet.* **2003**, *12* (>12), 1393–1403. <https://doi.org/10.1093/hmg/ddg156>.
- (98) Atwal, R. S.; Xia, J.; Pinchev, D.; Taylor, J.; Epand, R. M.; Truant, R. Huntingtin Has a Membrane Association Signal That Can Modulate Huntingtin Aggregation, Nuclear Entry and Toxicity. *Hum. Mol. Genet.* **2007**, *16* (21), 2600–2615. <https://doi.org/10.1093/hmg/ddm217>.
- (99) Gu, M.; Gash, M. T.; Mann, V. M.; Javoy-Agid, F.; Cooper, J. M.; Schapira, A. H. V. Mitochondrial Defect in Huntington's Disease Caudate Nucleus. *Ann. Neurol.* **1996**, *39* (3), 385–389. <https://doi.org/10.1002/ana.410390317>.
- (100) Panov, A. V.; Gutekunst, C.-A.; Leavitt, B. R.; Hayden, M. R.; Burke, J. R.; Strittmatter, W. J.; Greenamyre, J. T. Early Mitochondrial Calcium Defects in Huntington's Disease Are a Direct Effect of Polyglutamines. *Nat. Neurosci.* **2002**, *5* (8), 731–736. <https://doi.org/10.1038/nn884>.
- (101) Choo, Y. S. Mutant Huntingtin Directly Increases Susceptibility of Mitochondria to the Calcium-Induced Permeability Transition and Cytochrome c Release. *Hum. Mol. Genet.* **2004**, *13* (14), 1407–1420. <https://doi.org/10.1093/hmg/ddh162>.
- (102) Chang, D. T. W.; Rintoul, G. L.; Pandipati, S.; Reynolds, I. J. Mutant Huntingtin Aggregates Impair Mitochondrial Movement and Trafficking in Cortical Neurons. *Neurobiol. Dis.* **2006**, *22* (2), 388–400. <https://doi.org/10.1016/j.nbd.2005.12.007>.
- (103) Orr, A. L.; Li, S.; Wang, C.-E.; Li, H.; Wang, J.; Rong, J.; Xu, X.; Mastroberardino, P. G.; Greenamyre, J. T.; Li, X.-J. N-Terminal Mutant Huntingtin Associates with Mitochondria and Impairs Mitochondrial Trafficking. *J. Neurosci.* **2008**, *28* (11), 2783–2792. <https://doi.org/10.1523/JNEUROSCI.0106-08.2008>.
- (104) Kegel, K. B.; Sapp, E.; Yoder, J.; Cuiffo, B.; Sobin, L.; Kim, Y. J.; Qin, Z.-H.; Hayden, M. R.; Aronin, N.; Scott, D. L.; Isenberg, G.; Goldmann, W. H.; DiFiglia, M. Huntingtin Associates with Acidic Phospholipids at the Plasma Membrane. *J. Biol. Chem.* **2005**, *280* (43), 36464–36473. <https://doi.org/10.1074/jbc.M503672200>.
- (105) Zeitlin, S.; Liu, J.-P.; Chapman, D. L.; Papaioannou, V. E.; Efstratiadis, A. Increased Apoptosis and Early Embryonic Lethality in Mice Nullizygous for the Huntington's Disease Gene Homologue. *Nat. Genet.* **1995**, *11* (2), 155–163. <https://doi.org/10.1038/ng1095-155>.
- (106) Nasir, J.; Floresco, S. B.; O'Kusky, J. R.; Diewert, V. M.; Richman, J. M.; Zeisler, J.; Borowski, A.; Marth, J. D.; Phillips, A. G.; Hayden, M. R. Targeted Disruption of the Huntington's Disease Gene Results in Embryonic Lethality and Behavioral and Morphological Changes in Heterozygotes. *Cell* **1995**, *81* (5), 811–823. [https://doi.org/10.1016/0092-8674\(95\)90542-1](https://doi.org/10.1016/0092-8674(95)90542-1).
- (107) O'Kusky, J. R.; Nasir, J.; Cicchetti, F.; Parent, A.; Hayden, M. R. Neuronal Degeneration in the Basal Ganglia and Loss of Pallido-Subthalamic Synapses in Mice with Targeted Disruption of the Huntington's Disease Gene. *Brain Res.* **1999**, *818* (2), 468–479. [https://doi.org/10.1016/S0006-8993\(98\)01312-2](https://doi.org/10.1016/S0006-8993(98)01312-2).
- (108) Gasset-Rosa, F.; Chillon-Marin, C.; Goginashvili, A.; Atwal, R. S.; Artates, J. W.; Tabet, R.; Wheeler, V. C.; Bang, A. G.; Cleveland, D. W.; Lagier-Tourenne, C. Polyglutamine-Expanded Huntingtin Exacerbates Age-Related Disruption of Nuclear Integrity and

- Nucleocytoplasmic Transport. *Neuron* **2017**, *94* (1), 48-57.e4. <https://doi.org/10.1016/j.neuron.2017.03.027>.
- (109) Bäuerlein, F. J. B.; Saha, I.; Mishra, A.; Kalemanov, M.; Martínez-Sánchez, A.; Klein, R.; Dudanova, I.; Hipp, M. S.; Hartl, F. U.; Baumeister, W.; Fernández-Busnadiego, R. In Situ Architecture and Cellular Interactions of PolyQ Inclusions. *Cell* **2017**, *171* (1), 179-187.e10. <https://doi.org/10.1016/j.cell.2017.08.009>.
- (110) Velier, J.; Kim, M.; Schwarz, C.; Kim, T. W.; Sapp, E.; Chase, K.; Aronin, N.; DiFiglia, M. Wild-Type and Mutant Huntingtins Function in Vesicle Trafficking in the Secretory and Endocytic Pathways. *Exp. Neurol.* **1998**, *152* (1), 34–40. <https://doi.org/10.1006/exnr.1998.6832>.
- (111) Kegel, K. B.; Sapp, E.; Alexander, J.; Valencia, A.; Reeves, P.; Li, X.; Masso, N.; Sobin, L.; Aronin, N.; DiFiglia, M. Polyglutamine Expansion in Huntingtin Alters Its Interaction with Phospholipids. *J. Neurochem.* **2009**, *110* (5), 1585–1597. <https://doi.org/10.1111/j.1471-4159.2009.06255.x>.
- (112) Kegel, K. B.; Schewkunow, V.; Sapp, E.; Masso, N.; Wanker, E. E.; DiFiglia, M.; Goldmann, W. H. Polyglutamine Expansion in Huntingtin Increases Its Insertion into Lipid Bilayers. *Biochem. Biophys. Res. Commun.* **2009**, *387* (3), 472–475. <https://doi.org/10.1016/j.bbrc.2009.07.039>.
- (113) Burke, K. A.; Hensal, K. M.; Umbaugh, C. S.; Chaibva, M.; Legleiter, J. Huntingtin Disrupts Lipid Bilayers in a PolyQ-Length Dependent Manner. *Biochim. Biophys. Acta BBA - Biomembr.* **2013**, *1828* (8), 1953–1961. <https://doi.org/10.1016/j.bbamem.2013.04.025>.
- (114) Slepko, N.; Bhattacharyya, A. M.; Jackson, G. R.; Steffan, J. S.; Marsh, J. L.; Thompson, L. M.; Wetzel, R. Normal-Repeat-Length Polyglutamine Peptides Accelerate Aggregation Nucleation and Cytotoxicity of Expanded Polyglutamine Proteins. *Proc. Natl. Acad. Sci.* **2006**, *103* (39), 14367–14372. <https://doi.org/10.1073/pnas.0602348103>.
- (115) Kegel, K. B.; Kim, M.; Sapp, E.; McIntyre, C.; Castaño, J. G.; Aronin, N.; DiFiglia, M. Huntingtin Expression Stimulates Endosomal–Lysosomal Activity, Endosome Tubulation, and Autophagy. *J. Neurosci.* **2000**, *20* (19), 7268–7278. <https://doi.org/10.1523/JNEUROSCI.20-19-07268.2000>.
- (116) Suopanki, J.; Gotz, C.; Lutsch, G.; Schiller, J.; Harjes, P.; Herrmann, A.; Wanker, E. E. Interaction of Huntingtin Fragments with Brain Membranes - Clues to Early Dysfunction in Huntington's Disease. *J. Neurochem.* **2006**, *96* (3), 870–884. <https://doi.org/10.1111/j.1471-4159.2005.03620.x>.
- (117) Guedes-Dias, P.; Holzbaur, E. L. F. Huntingtin Fibrils Poke Membranes. *Cell* **2017**, *171* (1), 32–33. <https://doi.org/10.1016/j.cell.2017.09.009>.
- (118) Riguet, N.; Mahul-Mellier, A.-L.; Maharjan, N.; Burtscher, J.; Croisier, M.; Knott, G.; Hastings, J.; Patin, A.; Reiterer, V.; Farhan, H.; Nasarov, S.; Lashuel, H. A. Nuclear and Cytoplasmic Huntingtin Inclusions Exhibit Distinct Biochemical Composition, Interactome and Ultrastructural Properties. *Nat. Commun.* **2021**, *12* (1), 6579. <https://doi.org/10.1038/s41467-021-26684-z>.
- (119) Cooke, I. R.; Deserno, M. Coupling between Lipid Shape and Membrane Curvature. *Biophys. J.* **2006**, *91* (2), 487–495. <https://doi.org/10.1529/biophysj.105.078683>.
- (120) *Molecular Biology of the Cell*, 4th ed.; Alberts, B., Ed.; Garland Science: New York, 2002.
- (121) Bennett, W. F. D.; Tieleman, D. P. The Importance of Membrane Defects—Lessons from Simulations. *Acc. Chem. Res.* **2014**, *47* (8), 2244–2251. <https://doi.org/10.1021/ar4002729>.

- (122) Arndt, J. R.; Chaibva, M.; Legleiter, J. The Emerging Role of the First 17 Amino Acids of Huntingtin in Huntington's Disease. *Biomol. Concepts* **2015**, *6* (1). <https://doi.org/10.1515/bmc-2015-0001>.
- (123) Tao, M.; Pandey, N. K.; Barnes, R.; Han, S.; Langen, R. Structure of Membrane-Bound Huntingtin Exon 1 Reveals Membrane Interaction and Aggregation Mechanisms. *Structure* **2019**, *27* (10), 1570-1580.e4. <https://doi.org/10.1016/j.str.2019.08.003>.
- (124) Haque, Md. E.; McIntosh, T. J.; Lentz, B. R. Influence of Lipid Composition on Physical Properties and PEG-Mediated Fusion of Curved and Uncurved Model Membrane Vesicles: "Nature's Own" Fusogenic Lipid Bilayer. *Biochemistry* **2001**, *40* (14), 4340–4348. <https://doi.org/10.1021/bi002030k>.
- (125) Chaibva, M.; Gao, X.; Jain, P.; Campbell, W. A.; Frey, S. L.; Legleiter, J. Sphingomyelin and GM1 Influence Huntingtin Binding to, Disruption of, and Aggregation on Lipid Membranes. *ACS Omega* **2018**, *3* (1), 273–285. <https://doi.org/10.1021/acsomega.7b01472>.
- (126) Wood, S. J.; Maleeff, B.; Hart, T.; Wetzel, R. Physical, Morphological and Functional Differences between PH 5.8 and 7.4 Aggregates of the Alzheimer's Amyloid Peptide A β . *J. Mol. Biol.* **1996**, *256* (5), 870–877. <https://doi.org/10.1006/jmbi.1996.0133>.
- (127) Fraser, P. E.; Nguyen, J. T.; Surewicz, W. K.; Kirschner, D. A. PH-Dependent Structural Transitions of Alzheimer Amyloid Peptides. *Biophys. J.* **1991**, *60* (5), 1190–1201. [https://doi.org/10.1016/S0006-3495\(91\)82154-3](https://doi.org/10.1016/S0006-3495(91)82154-3).
- (128) Bernstein, S. L.; Liu, D.; Wyttenbach, T.; Bowers, M. T.; Lee, J. C.; Gray, H. B.; Winkler, J. R. α -Synuclein: Stable Compact and Extended Monomeric Structures and PH Dependence of Dimer Formation. *J. Am. Soc. Mass Spectrom.* **2004**, *15* (10), 1435–1443. <https://doi.org/10.1016/j.jasms.2004.08.003>.
- (129) Eymsh, B.; Drobny, A.; Heyn, T. R.; Xiang, W.; Lucius, R.; Schwarz, K.; Keppler, J. K.; Zunke, F.; Arnold, P. Toxic Metamorphosis—How Changes from Lysosomal to Cytosolic PH Modify the Alpha-Synuclein Aggregation Pattern. *Biomacromolecules* **2020**, *21* (12), 4673–4684. <https://doi.org/10.1021/acs.biomac.0c00629>.
- (130) Sabaté, R.; Gallardo, M.; Estelrich, J. Temperature Dependence of the Nucleation Constant Rate in β Amyloid Fibrillogenesis. *Int. J. Biol. Macromol.* **2005**, *35* (1–2), 9–13. <https://doi.org/10.1016/j.ijbiomac.2004.11.001>.
- (131) Nekooki-Machida, Y.; Kurosawa, M.; Nukina, N.; Ito, K.; Oda, T.; Tanaka, M. Distinct Conformations of in Vitro and in Vivo Amyloids of Huntingtin-Exon1 Show Different Cytotoxicity. *Proc. Natl. Acad. Sci.* **2009**, *106* (24), 9679–9684. <https://doi.org/10.1073/pnas.0812083106>.
- (132) Cui, X.; Liang, Q.; Liang, Y.; Lu, M.; Ding, Y.; Lu, B. TR-FRET Assays of Huntingtin Protein Fragments Reveal Temperature and PolyQ Length-Dependent Conformational Changes. *Sci. Rep.* **2015**, *4* (1), 5601. <https://doi.org/10.1038/srep05601>.
- (133) Ariesandi, W.; Chang, C.-F.; Chen, T.-E.; Chen, Y.-R. Temperature-Dependent Structural Changes of Parkinson's Alpha-Synuclein Reveal the Role of Pre-Existing Oligomers in Alpha-Synuclein Fibrillization. *PLoS ONE* **2013**, *8* (1), e53487. <https://doi.org/10.1371/journal.pone.0053487>.
- (134) Mirau, P.; Farmer, B. L.; Pandey, R. B. Structural Variation of Alpha-Synuclein with Temperature by a Coarse-Grained Approach with Knowledge-Based Interactions. *AIP Adv.* **2015**, *5* (9), 092504. <https://doi.org/10.1063/1.4927544>.
- (135) Klement, K.; Wieligmann, K.; Meinhardt, J.; Hortschansky, P.; Richter, W.; Fändrich, M. Effect of Different Salt Ions on the Propensity of Aggregation and on the Structure of

- Alzheimer's A β (1-40) Amyloid Fibrils. *J. Mol. Biol.* **2007**, *373* (5), 1321–1333. <https://doi.org/10.1016/j.jmb.2007.08.068>.
- (136) Castelletto, V.; Hamley, I. W.; Cenker, C.; Olsson, U. Influence of Salt on the Self-Assembly of Two Model Amyloid Heptapeptides. *J. Phys. Chem. B* **2010**, *114* (23), 8002–8008. <https://doi.org/10.1021/jp102744g>.
- (137) Narayanan, S.; Reif, B. Characterization of Chemical Exchange between Soluble and Aggregated States of β -Amyloid by Solution-State NMR upon Variation of Salt Conditions. *Biochemistry* **2005**, *44* (5), 1444–1452. <https://doi.org/10.1021/bi048264b>.
- (138) Paik, S. R.; Lee, D.; Cho, H.-J.; Lee, E.-N.; Chang, C.-S. Oxidized Glutathione Stimulated the Amyloid Formation of α -Synuclein. *FEBS Lett.* **2003**, *537* (1–3), 63–67. [https://doi.org/10.1016/S0014-5793\(03\)00081-4](https://doi.org/10.1016/S0014-5793(03)00081-4).
- (139) Razzokov, J.; Yusupov, M.; Bogaerts, A. Oxidation Destabilizes Toxic Amyloid Beta Peptide Aggregation. *Sci. Rep.* **2019**, *9* (1), 5476. <https://doi.org/10.1038/s41598-019-41931-6>.
- (140) Adhikari, R.; Yang, M.; Saikia, N.; Dutta, C.; Alharbi, W. F. A.; Shan, Z.; Pandey, R.; Tiwari, A. Acetylation of A β 42 at Lysine 16 Disrupts Amyloid Formation. *ACS Chem. Neurosci.* **2020**, *11* (8), 1178–1191. <https://doi.org/10.1021/acchemneuro.0c00069>.
- (141) Groover, S. E.; Adegbuyiro, A.; Fan, C. K.; Hodges, B. L.; Beasley, M.; Taylor, K.; Stonebraker, A. R.; Siriwardhana, C.; Legleiter, J. Macromolecular Crowding in Solution Alters Huntingtin Interaction and Aggregation at Interfaces. *Colloids Surf. B Biointerfaces* **2021**, *206*, 111969. <https://doi.org/10.1016/j.colsurfb.2021.111969>.
- (142) Zhang, L.; Kang, H.; Vázquez, F. X.; Toledo-Sherman, L.; Luan, B.; Zhou, R. Molecular Mechanism of Stabilizing the Helical Structure of Huntingtin N17 in a Micellar Environment. *J. Phys. Chem. B* **2017**, *121* (18), 4713–4721. <https://doi.org/10.1021/acs.jpcc.7b01476>.
- (143) Pandey, N. K.; Isas, J. M.; Rawat, A.; Lee, R. V.; Langen, J.; Pandey, P.; Langen, R. The 17-Residue-Long N Terminus in Huntingtin Controls Stepwise Aggregation in Solution and on Membranes via Different Mechanisms. *J. Biol. Chem.* **2018**, *293* (7), 2597–2605. <https://doi.org/10.1074/jbc.M117.813667>.
- (144) Revival of 2DE-LC/MS in Proteomics and Its Potential for Large-Scale Study of Human Proteoforms. *Med One* **2018**. <https://doi.org/10.20900/mo.20180008>.

2. Cholesterol Impacts the Formation of Huntingtin/Lipid Complexes and Subsequent Aggregation

2.1 Abstract

Huntington's disease (HD) is a neurodegenerative disease resulting from an expansion of the polyglutamine (polyQ) domain within the huntingtin protein (htt). PolyQ expansion triggers toxic aggregation and alters htt/lipid interactions. The first 17 amino acids at the N-terminus of the protein (Nt17) have a propensity to form an amphipathic α -helix crucial to aggregation and membrane binding. Htt functions normally in processes including vesicle transport and synaptic transmission, and as such must interact closely with a variety of membrane systems including those of the endoplasmic reticulum, mitochondria, nuclear envelope, and plasma membrane. Membrane composition heavily influences both htt aggregation and lipid interactions, and cholesterol is a crucial membrane component that modulates properties such as fluidity, permeability, and organization. In HD, cholesterol homeostasis is disrupted, and likely plays a role in toxicity. The objective of these studies was to identify the impact of cholesterol on htt aggregation and lipid interactions in various lipid systems. Lipid systems of POPC, DOPC, and POPG with varied levels of exogenously added cholesterol were exposed to htt and the influences on aggregation, lipid binding, and htt/lipid complexation were evaluated using thioflavin-T aggregation assays, atomic force microscopy, colorimetric lipid binding assays, and mass spectrometry. The addition of cholesterol to DOPC vesicles enhanced htt aggregation. In the presence of vesicles of either POPC or POPG, the addition of cholesterol reduced htt aggregation. Htt/lipid binding decreased for POPC and increased for both DOPC and POPG with increasing cholesterol content, with observed differences in htt/lipid complexation. Altered

cholesterol content influences htt aggregation, lipid binding, and complexation differently depending on overall lipid composition.

2.2 Introduction

Huntington's disease (HD) is a fatal neurodegenerative disease caused by an expanded polyglutamine (polyQ) domain in the huntingtin protein (htt).¹ PolyQ domain expansion beyond a threshold of ~35 repeats^{2,3} results in the aggregation of htt into amyloid-like fibrils⁴⁻⁶ through a complex pathway that involves additional aggregate species including oligomers and amorphous aggregates.⁷ Peptide sequences directly adjacent to the polyQ domain heavily influence the aggregation process.⁸⁻¹⁰ One such sequence flanking the polyQ domain of htt is the first 17 amino acids at the N-terminus (Nt17).⁸⁻¹³ Nt17 accelerates aggregation as it can form an amphipathic α -helix that promotes early interactions of htt through intermolecular self-association to form oligomers.^{9,13,14} The interprotein association of Nt17 brings polyQ domains into close proximity, promoting fibril nucleation.^{13,15} The association of Nt17 into complexes on the order of dimers and tetramers was demonstrated by ion mobility spectrometry-linear ion trap mass spectrometry (IMS-MS)¹⁴ and α -helix rich structures of both Nt17 dimers and tetramers have been resolved by NMR.¹³

While a variety of functions have been attributed to htt, many of these, e.g. vesicle transport and synaptic transmission,^{16,17} require direct interaction with lipid membranes. Htt associates closely with a variety of membranes of varying lipid composition, localizing to the ER,¹⁸⁻²⁰ mitochondrial,²¹⁻²⁵ nuclear,^{19,20} and plasma membranes.²⁶ In addition to promoting aggregation, the propensity for Nt17 to form an α -helix causes it to facilitate lipid binding.^{9,27} As htt readily associates with lipids, the presence of lipid membranes can modify htt aggregation in a lipid composition dependent manner.²⁸⁻³⁴ Membranes comprised of total brain lipid extract

(TBLE) inhibit htt fibrilization compared with the absence of lipids.²⁸ Similarly, cellular lipid extracts also reduce htt aggregation.²⁹ Enriching TBLE with either sphingomyelin (SM) or ganglioside (GM1) content further modifies htt/lipid interactions and subsequent aggregation, with both SM and GM1 reducing htt insertion into the membrane and promoting distinct aggregate morphologies.³⁰ However, some pure lipid systems, like palmitoyl-2-oleoyl-glycero-3-phosphocholine (POPC)²⁸ or a mixture also containing 1-palmitoyl-2-oleoyl-sn-glycero-3-phospho-L-serine (POPS)³¹ enhance fibrillization. In particular, the POPS/POPC lipid system promotes a distinct aggregation pathway facilitated by Nt17 compared to aggregation in the absence of lipids.³¹ Generally, Nt17 displays higher affinity for anionic phospholipids, such as PS and phosphatidylglycerol (PG) lipids, compared to zwitterionic PC lipids.³² Beyond head group charge, studies on the impact of unsaturation in lipid tails revealed no direct correlation between htt aggregation and htt/lipid complexation, but that the orientation of Nt17 on the membrane surface is related to membrane defect sizes and how well the hydrophobic residues of Nt17 match those defect sizes.³³ Htt has also been shown to cause membrane damage, which is mediated by factors including polyQ length,^{26,27,35} cholesterol content,³⁶ and the presence of SM and GM1.³⁰ Thus, the distinct physiochemical properties of lipid systems resulting from varied composition potentially underlie the distinct interactions between htt and different lipid systems.

An important membrane component in the central nervous system is cholesterol, with ~25% of total body cholesterol being found in the brain.³⁶⁻³⁹ Brain cholesterol is synthesized locally due to the blood-brain barrier preventing uptake from circulation,³⁷⁻⁴⁰ and cholesterol is critical to effective signal transduction through its roles in myelination^{38,39} and lipid raft function.^{37-39,41} More broadly, cholesterol modulates physical membrane properties, including fluidity and permeability,^{42,43} organization,⁴¹ and ultimately membrane function.^{41,42} In HD,

cholesterol homeostasis is disrupted, though there are conflicting reports on whether cholesterol content is reduced³⁷⁻⁴⁰ or increased.⁴⁴ When htt was exposed to TBLE membranes enriched in cholesterol, the binding and insertion of htt into membranes was reduced, and membrane susceptibility to htt-induced damage was decreased.³⁶ Interestingly, cholesterol enrichment also promoted a distinct htt aggregation pattern on the membrane surface that resulted in elevated, plateau-like domains that extended several nanometers above the membrane surface.

Aggregation is heavily influenced by the cellular environment, and htt-lipid interactions are dependent on lipid system and composition. As cholesterol homeostasis is altered in HD, the influence of cholesterol content on htt aggregation and htt/lipid interactions may play a key role in pathogenesis. Our aim was to identify how the addition of cholesterol modulates the ability of htt to bind and complex with different lipid species with varying head groups and tails and evaluate the effect of these interactions on subsequent aggregation.

2.3 Materials and Methods

2.3.1 Purification of GST-Htt-Exon1 Fusion Protein

Glutathione S-transferase (GST)-htt-exon1 fusion proteins of disease length (46Q) were purified as previously described.⁴⁵ In short, GST-htt fusion proteins were expressed by induction in *Escherichia coli* with isopropyl-thio-galactopyranoside (IPTG) for four hours at 30 °C. The cells were lysed using lysozyme (0.5 mg/mL) and sonication with a sonic dismembrator (FisherSci), then liquid chromatography (BioRad LPLC) using a 5 mL GST affinity column was used to purify the fusion proteins. Sodium dodecyl-sulfate polyacrylamide gel electrophoresis (SDS-PAGE) was used to analyze fractions and verify the presence of htt, then the concentration was determined using Coomassie Bradford reagent. Prior to all experiments, high speed centrifugation of fusion protein solutions at 20,000 g at 4 °C for 45 mins removed pre-existing

aggregates then fusion proteins were incubated with Factor Xa (Promega, Madison, WI) to cleave the GST tag and initiate aggregation for experiments.

2.3.2 Lipid Vesicle Preparation

Stocks of DOPC, POPC, POPG, and cholesterol were dissolved in chloroform and mixed to the desired mass ratios at a total mass of 1 mg lipid per tube. Once mixed, the chloroform was evaporated off using a gentle stream of nitrogen to form a dried lipid film. Films were stored at -20 °C in parafilm-wrapped Eppendorf tubes until needed. On the day of experimentation, lipid films were rehydrated in tris buffer (pH=7.4) with agitation for a minimum of one hour. Lipid vesicles were formed via ten freeze-thaw cycles using liquid nitrogen and a thermomixer (45 °C), followed by one hour of bath sonication.

2.3.4 Thioflavin T (ThT) Aggregation Assay

Thioflavin T (ThT) assays were used to monitor htt fibril formation as a function of time in the presence and absence of different lipid systems. For each condition, htt-exon1(46Q) (10 μM) was incubated with ThT (125 μM) in black Costar 96-well plates with clear flat bottoms. For the lipid conditions, 100 μM of the desired lipid vesicle solution was added to result in a 10:1 lipid:protein ratio. Experiments were run at 37 °C for 18 h, and ThT fluorescence was recorded every 5 min using a SpectraMax M2 microplate reader (excitation 400 nm, emission 484 nm). Relative maximum fluorescence was calculated by normalizing the maximum fluorescence intensity of each condition to the maximum fluorescence of the huntingtin control (100%). Relevant controls were measured and subsequently subtracted from the curves to show the fluorescent signal strictly associated with htt aggregation. Each condition was performed a minimum of three times, and error bars represent the standard error.

2.3.5 Polydiacetylene (PDA) Lipid Binding Assay

To measure htt-lipid interaction, PDA lipid binding assays were performed using previously reported protocols.^{46,47} Briefly, monomeric 10,12-tricosadiynoic acid was mixed with the desired lipid system at a 2:3 molar ratio in a 4:1 chloroform/ethanol solution. Lipid films used in this step were formed by mixing lipids to the desired cholesterol content and then drying, as previously described. Once the lipid and 10,12-tricosadiynoic acid were mixed, the organic solvents were evaporated off with a gentle stream of nitrogen. Resulting films were rehydrated in tris buffer (70 °C) and sonicated to promote mixing. Periods of sonication did not exceed 5 min each to avoid extensive heating of the solution. Following sonication, lipid solutions were left at 4 °C overnight to allow for PDA/lipid vesicle formation. The following day, lipid solutions were equilibrated to 25 °C and irradiated at 254 nm to polymerize the 10,12-tricosadiynoic acid, resulting in a royal blue solution that would undergo a colorimetric shift to red when stress was applied to the vesicles. PDA/lipid vesicles were then incubated with htt-exon1(46Q) (10 μM) for 18 h at 30 °C. Absorbance of the blue (650 nm) and red (500 nm) wavelengths were recorded every 5 minutes on a SpectraMax M2 microplate reader with 1 minute of orbital shaking before each read. Negative controls consisted of equal parts PDA/lipid solution and neat buffer for each unique lipid mixture. As a positive control, PDA/lipid vesicles were incubated with equal part saturated NaOH (pH=12), which induces a colorimetric response by increasing repulsion among lipid head groups and causing stress on the vesicles.^{48,49} The NaOH results in the maximum colorimetric shift for each lipid system that can then be used to establish the sensitivity of different lipid/PDA systems and normalize results.⁵⁰ For each condition, the percent colorimetric response (% CR) was calculated using the following equation:

$$\% CR = \left(\frac{PB_0 - PB}{PB_0} \right) \times 100$$

where PB is defined as $A_{\text{blue}}/(A_{\text{blue}}+A_{\text{red}})$ for the negative control (PB₀) and sample condition (PB). Each condition was performed a minimum of three times, and error bars represent the standard error of the sample set.

2.3.6 Atomic Force Microscopy (AFM)

Purified htt-exon1(46Q) (10 μM) was incubated with and without lipid vesicles (100 μM for a 10:1 lipid:protein ratio) at 37 °C with constant orbital agitation. At the desired time points, 2 μL of each sample was deposited on freshly cleaved mica. One minute after deposition, the mica was rinsed with 200 μL of 18 M Ω water and dried with a gentle stream of clean air. Samples were imaged using a Nanoscope V Multi-Mode scanning probe microscope (VEECO) equipped with a closed loop vertical engage J-scanner. Silicon-cantilevers with a nominal spring constant of 40 N/m and a resonance frequency of 300 kHz were used. All images were collected with a scan rate of 1.99 Hz and cantilever drive frequencies at 10-20% of resonance. Images were analyzed using the Matlab image processing toolbox (MathWorks) as previously described.⁵¹

2.3.7 Pulled-Tip Capillary Emitter and Capillary Vibrating Sharp-Edge Spray Ionization (cVSSI) Device Fabrication.

Detailed descriptions of cVSSI devices have been provided previously.^{52,53} In short, a piezoelectric transducer was attached to the end of a glass slide coverslip using epoxy glue. A glass capillary emitter (0.5 mm I.D.) was pulled (Sutter Instrument Company, Novato, CA) and mechanically cut with a ceramic cutter to the desired I.D. (70-100 μm) verified under a microscope. The emitter was secured to the end opposite the piezoelectric transducer using glass glue. A blunt, fused silica capillary (250 μm I.D., 355 μm O.D., 5 cm-long) was inserted into the glass emitter and glued to the flat end using epoxy glue. PTFE tubing was used to connect a

syringe to the fused silica capillary of the cVSSI device. A 5 cm platinum wire was inserted into the PTFE tubing near the end connecting to the cVSSI device as an electrode for field-enabled experiments. RF signal (~ 94 kHz sine wave, 9-10 V_{pp}) was applied to the piezoelectric transducer via a function generator and connected amplifier.

2.3.8 Capillary Vibrating Sharp-Edge Electrospray Ionization-Mass Spectrometry (cVSSI-MS)

MS was used to investigate complexes formed between Nt17 peptide and various lipid vesicles with different cholesterol content. Lipid vesicles were formed by rehydrating films in 10 mM ammonium acetate solution, bath sonicated for 1 h, and subjected to 10 freeze-thaw cycles using liquid nitrogen. Nt17 peptide (10 μ M) was incubated with lipid vesicles (10:1 lipid:peptide ratio) for 24 h at 37 °C. Samples were analyzed using a Q-Exactive Hybrid Quadrupole mass spectrometer using cVSSI devices. Spectra were collected in both positive-ion and negative-ion mode over a mass-to-charge (m/z) ratio range of 350 to 4,000. Samples were infused at a flow rate of 10 μ L/min with 1.8 kV applied to the Pt wire. MS instrument parameters were: 250 °C capillary inlet temperature, 1×10^6 for the AGC, and 70,000 for MS resolution. Mass spectra for each sample were recorded in triplicate for 30 seconds each, with the high voltage turned off and the device flushed between each replicate to account for any device variability. Data were analyzed using the Xcalibur 2.2 software suite (Thermo Scientific).

2.4 Results

2.4.1 Lipids Alter Htt-Exon1(46Q) Aggregation in a Composition-Dependent Manner

The ability of lipid membranes to alter aggregation is well established.^{28-34,36} To determine how the addition of cholesterol impacts the ability of lipid membranes to influence htt aggregation, htt-exon1(46Q) (10 μ M) was incubated with vesicles of POPC, DOPC, or POPG

that contained no cholesterol or were enriched with either 10% or 20% cholesterol (% w/w) in a 10:1 lipid to protein molar ratio. Aggregation was monitored as a function of time using ThT, which fluoresces when bound to fibril associated β -sheet structure (Figure 2.1A-C). Htt-exon1(46Q) aggregation in the absence of lipids was measured for comparison. The maximum ThT signal for each condition was analyzed, then normalized to htt-exon1(46Q) alone to compare the extent of fibril formation (Figure 2.1D-F). The time required to reach 50% of the maximum signal (t_{50}) was also determined to evaluate if different lipid systems were altering initial aggregation events (Figure 2.1G-I).

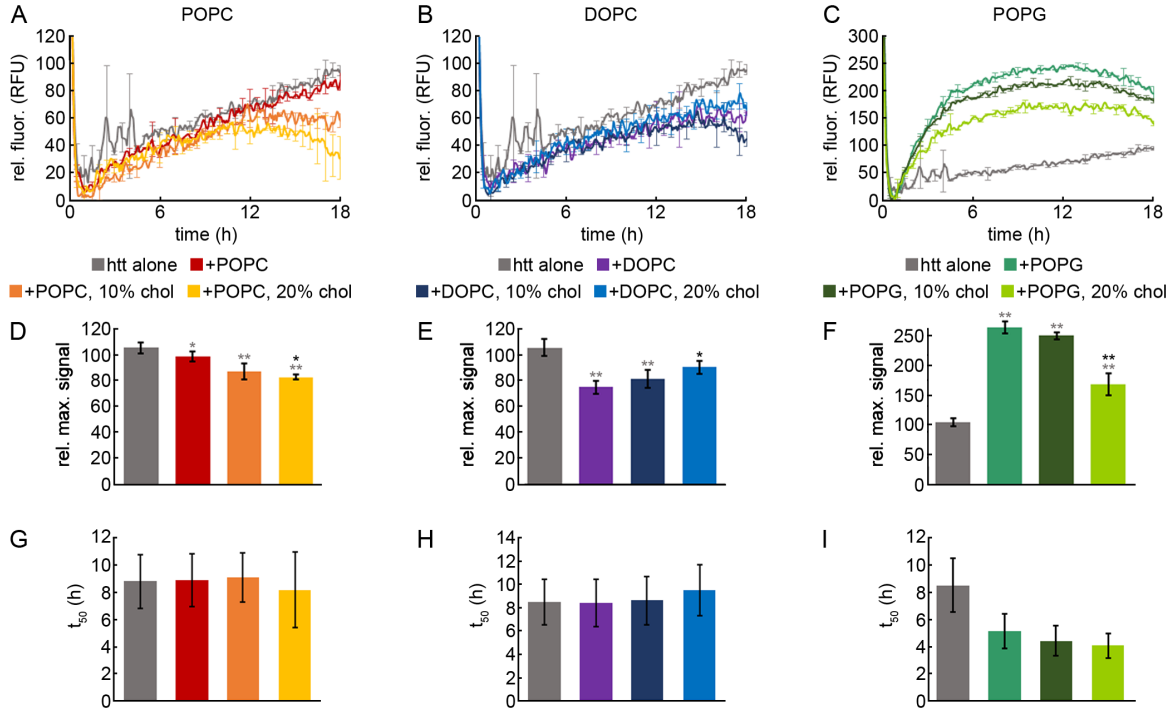


Figure 2.1. ThT aggregation assays for htt-exon1(46Q) incubated in the presence of different lipid vesicles with varying amounts of exogenously added cholesterol. Htt concentration was 10 μ M with a protein:lipid ratio of 1:10. Representative ThT assays for POPC (A), DOPC (B), and POPG (C) conditions are shown. The relative maximum signal for all POPC (D), DOPC (E), and POPG (F) conditions were calculated and averaged across all runs. The time to reach 50% of the maximum signal (t_{50}) for all POPC (G), DOPC (H), and POPG (I) conditions were determined and averaged across all runs. In panels A-C error bars are provided for every sixth data point (30 min) and represent the standard error of the mean (SEM) between triplicate wells of an individual run. Analysis in panels D-F were determined as averages over all trials, values are normalized as a percentage relative to the htt-exon1(46Q) control in the absence of

lipid, and error bars represent SEM. Analysis in panels G-H were determined as averages across all runs and error bars represent SEM. Using a Student's t-test, * represents a p-value <0.05 and ** represents a p-value of <0.01. Grey asterisks are for conditions relative to the htt control, black asterisks are for conditions relative to the pure lipid system.

The effect of lipid vesicles on htt-exon1(46Q) aggregation was dependent on both lipid composition and the amount of exogenously added cholesterol (Figure 2.1). Pure POPC vesicles had minimal, though statistically significant, impact on htt-exon1(46Q) aggregation with a 6% reduction in signal. The subsequent addition of exogenous cholesterol to POPC vesicles had an inhibitory effect, as addition of 10% and 20% exogenous cholesterol reduced the relative maximum signal by 11% and 16% respectively relative to the pure POPC vesicles (Figure 2.1D); however, there was no statistically significant difference in the t_{50} for all POPC conditions compared to control. The presence of pure DOPC vesicles inhibited htt-exon1(46Q) aggregation with a 30% reduction in relative maximum signal. Subsequent additions of exogenous cholesterol promoted aggregation relative to the pure lipid system, with 5% and 15% increases in signal for 10% and 20% exogenous cholesterol respectively. Even with some signal recovery for the conditions with exogenous cholesterol, aggregation overall was still reduced by 15%-23% relative to htt-exon1(46Q) alone (Figure 2.1E). The t_{50} was unaffected by the presence of DOPC vesicles (with and without cholesterol). Pure POPG vesicles promoted aggregation, with a 160% increase in signal. The addition of exogenous cholesterol reduced aggregation 14%-97% relative to the pure lipid system. Conditions containing exogenous cholesterol still promoted aggregation relative to htt-exon1(46Q) alone, with a 63%-146% increase in signal (Figure 2.1F). With POPG vesicles (with and without cholesterol) strongly increasing aggregation, the t_{50} appeared reduced relative to control, but this did not reach statistical significance.

To further investigate the effect of lipid composition and exogenous cholesterol content on htt-exon1(46Q) aggregation, morphology of htt aggregates was evaluated using AFM (Figures 2.2 and 2.3). Freshly prepared htt-exon1(46Q) (10 μ M) was incubated in the presence and absence of vesicles comprised of POPC, DOPC, or POPG (10:1 lipid:htt-exon1(46Q) molar ratio). Additional incubations were performed with vesicles of each lipid that contained either 10% or 20% exogenously added cholesterol. The 3 h time point was chosen because it typically results in a large oligomer population. The 8 h time point was chosen to obtain images of fibrils before extensive bundling, branching, and crossing occurred. Both oligomers and fibrils were observed across all incubation conditions (Figure 2.2). Fibril morphology appeared consistent with the htt-exon1(46Q) control for all POPC and DOPC lipid systems (Figure 2.2A-C), while a distinct spider-like fibril morphology was observed in the presence of all POPG lipid conditions (Figure 2.2D). Considering this observation, oligomer and fibril morphologies under each lipid condition were evaluated using automated Matlab scripts that determined morphological features for each individual aggregate. An oligomer was defined as any feature within an image composed of fewer than 50 pixels. For fibril analysis, fibrils were defined as any feature larger than 50 pixels (large amorphous aggregates were excluded by hand) with a contour length of at least 200 nm. In the case of the unique spider-like morphology observed under all POPG lipid conditions, the centers of the aggregates were much taller than the protruding fibrils, and thus were excluded for analysis of fibril height. The branching of POPG fibrils associated with the star-like morphology complicated the analysis of contour length. As a result, contour length represents the longest path through each star-like fibril.

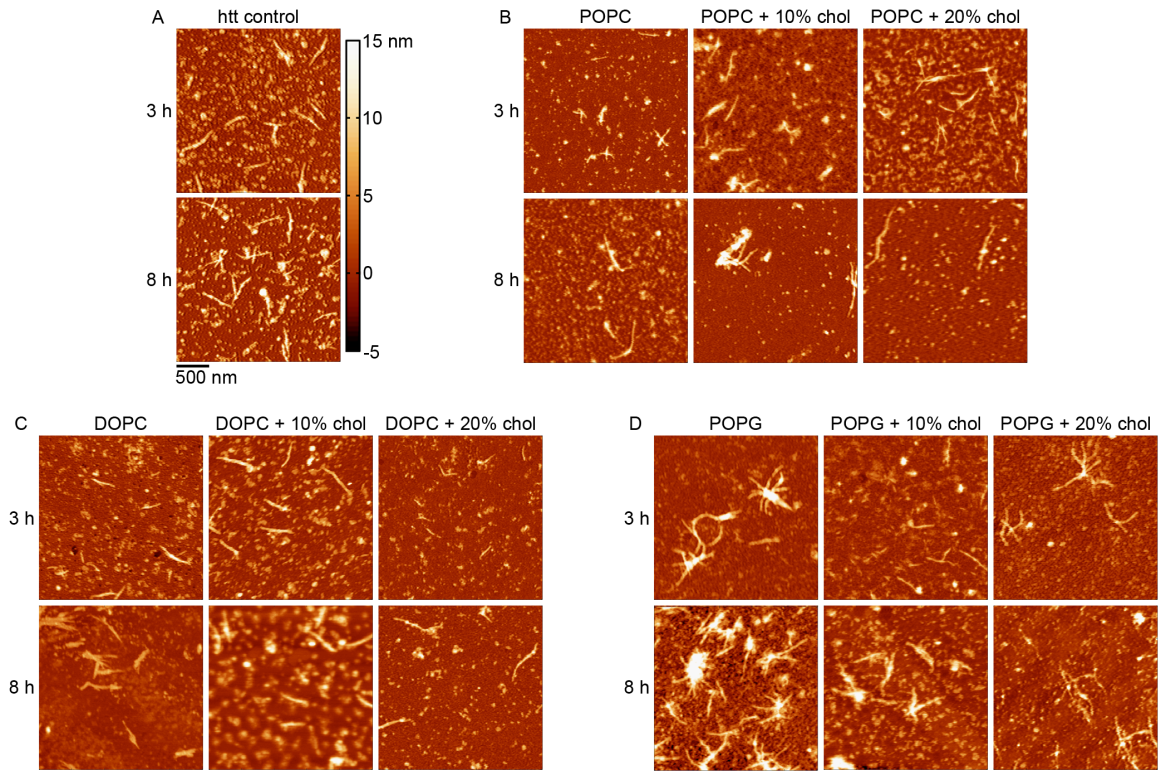


Figure 2.2. Representative AFM images of all experimental conditions. 10 μ M htt-exon1(46Q) incubated with no lipid (A), pure POPC and POPC with 10% or 20% exogenous cholesterol (B), pure DOPC and DOPC with 10% or 20% exogenous cholesterol (C), and pure POPG and POPG with 10% or 20% exogenous cholesterol (D). The protein:lipid ratio was 1:10. The colormap and scale bar is applicable to all images.

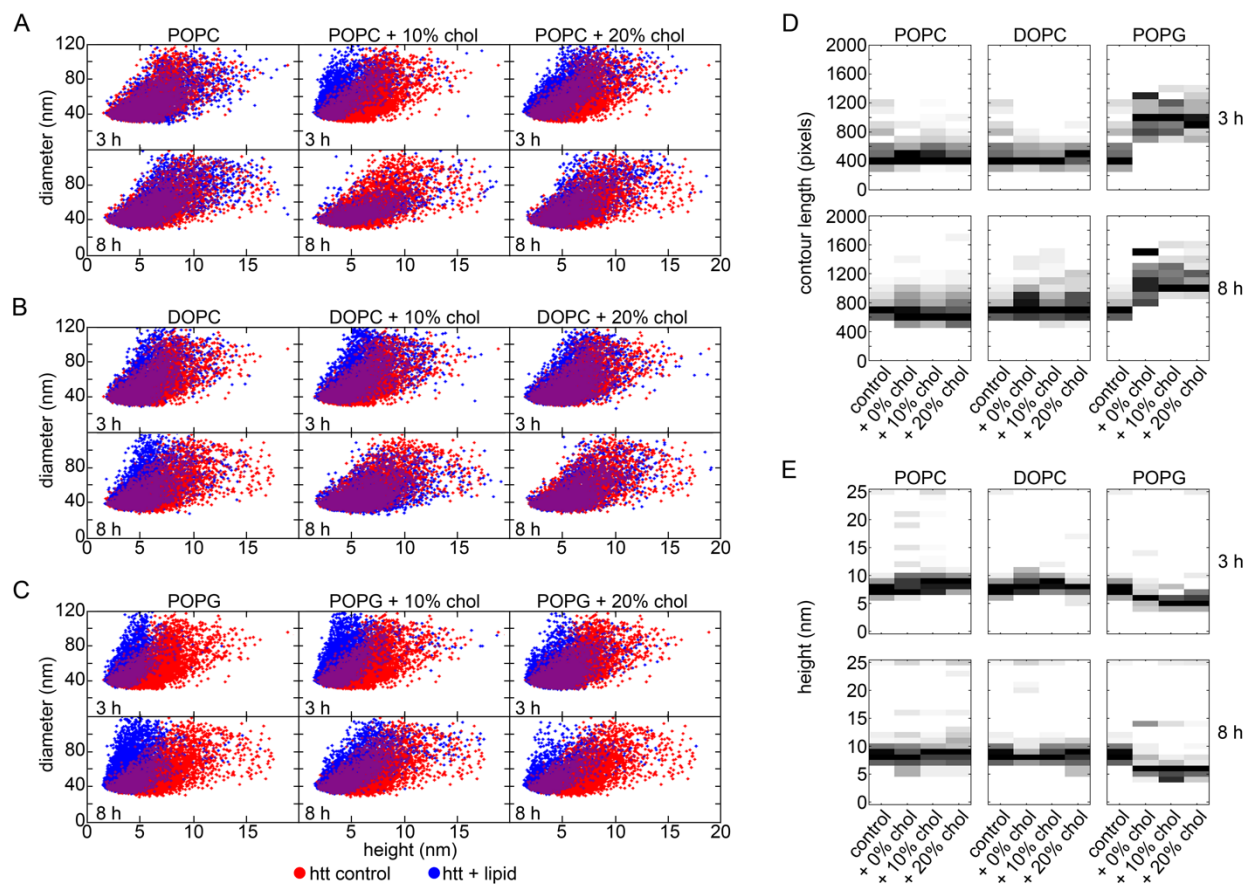


Figure 2.3. AFM analysis of observed htt-exon1(46Q) aggregate species morphologies under varied lipid conditions. Correlation plots of diameter and height each oligomer at 3h for htt-exon1(46Q) in the absence of lipid and incubated in the presence of pure POPC and POPC with 10% and 20% exogenous cholesterol (A), pure DOPC and DOPC with 10% and 20% exogenous cholesterol (B), pure POPG and POPG with 10% and 20% exogenous cholesterol (C). Histograms of fibril contour lengths comparing htt-exon1(46Q) in the absence of lipid to all POPC, DOPC, and POPG lipid conditions at 3 h and 8 h (D). Histograms of fibril heights comparing htt-exon1(46Q) in the absence of lipid to all POPC, DOPC, and POPG lipid conditions at 3 h and 8 h (E).

To deeper analyze if the lipid systems altered oligomer formation, oligomer morphology was evaluated by comparing the diameters and heights of oligomers identified in the htt-exon1(46Q) control at both the 3 h and 8 h time points to those identified when incubated with each lipid system (Figure 2.3A-C). Oligomers formed in the presence of pure POPC were not morphologically different from those formed in the absence of lipid at either 3 h or 8 h; however,

the addition of 10% or 20% cholesterol to POPC vesicles promoted a statistically significant shift to smaller oligomer heights at 3 h ($p < 0.01$ for each condition, Chi-squared test) while 8 h oligomers were not significantly different from the control (Figure 2.3A, Table 2.1). Under all DOPC lipid conditions, at both 3 h and 8 h, oligomers were not morphologically different from the htt-exon1(46Q) control (Figure 2.3B, Table 2.1). Under all POPG lipid conditions, at both 3 h and 8 h, oligomers shifted to significantly smaller heights ($p < 0.01$ for all conditions; Figure 2.3C, Table 2.1).

Fibril morphologies were compared by measuring the contour lengths of fibrils and the average height along the contour of the fibril. As the POPG star-like fibril morphology had a large height at the center where the branches connected, this was removed in calculating the average height along the contour. For branching structures, the longest path through the aggregate was considered the contour length. Fibril contour lengths for all POPC and DOPC systems were not significantly different from the htt-exon1(46Q) control at either 3 h or 8 h, while the POPG system shifted toward significantly longer fibrils at both timepoints (Figure 2.3D, Table 2.1). The control demonstrated mode fibril contour lengths of 400 nm at 3 h, which was consistent for all POPC and DOPC systems regardless of cholesterol content while POPG fibrils shifted to longer contour lengths of mode 1000 nm. Fibril contour length increased at 8 h for all conditions, with the control shifting to a mode length of 700 nm and the POPC and DOPC conditions, regardless of cholesterol content, demonstrating minimal deviations from the control. The POPG system contour lengths remained relatively consistent under all conditions with a mode of 1000-1100 nm. Much like with contour length, fibril heights along the contour for all POPC and DOPC systems were not significantly different from the htt-exon1(46Q) control at either 3 h or 8 h, while the POPG systems shifted toward significantly smaller heights ($p < 0.01$)

at both timepoints (Figure 2.3E, Table 2.1). Overall heights were consistent at both the 3 h and 8 h timepoints, with POPC and DOPC conditions, regardless of cholesterol content, demonstrating a mode height of approximately 7-8 nm, while POPG shifted smaller to mode heights of 5-6 nm. Generally, aggregate morphologies for the zwitterionic lipid systems were more consistent across all conditions relative to the htt-exon1(46Q) control. The most notable change was with the anionic POPG systems, where oligomers were typically smaller and fibrils displayed a unique morphology with increased contour length and reduced fibril height.

Table 2.1. Significance of oligomer height, fibril height, and fibril contour length relative to the htt control.

Oligomer Height		
<i>Condition</i>	<i>3 h Significance^a</i>	<i>8 h Significance^a</i>
Htt Control	N/A	N/A
POPC 0% Cholesterol	Not Significant	Not Significant
POPC 10% Cholesterol	Significant	Not Significant
POPC 20% Cholesterol	Significant	Not Significant
DOPC 0% Cholesterol	Not Significant	Not Significant
DOPC 10% Cholesterol	Not Significant	Not Significant
DOPC 20% Cholesterol	Not Significant	Not Significant
POPG 0% Cholesterol	Significant	Significant
POPG 10% Cholesterol	Significant	Significant
POPG 20% Cholesterol	Significant	Significant
Fibril Contour Length		
<i>Condition</i>	<i>3 h Significance^a</i>	<i>8 h Significance^a</i>
Htt Control	N/A	N/A
POPC 0% Cholesterol	Not Significant	Not Significant
POPC 10% Cholesterol	Not Significant	Not Significant
POPC 20% Cholesterol	Not Significant	Not Significant
DOPC 0% Cholesterol	Not Significant	Not Significant
DOPC 10% Cholesterol	Not Significant	Not Significant
DOPC 20% Cholesterol	Not Significant	Not Significant
POPG 0% Cholesterol	Significant	Significant
POPG 10% Cholesterol	Significant	Significant
POPG 20% Cholesterol	Significant	Significant
Fibril Height		
<i>Condition</i>	<i>3 h Significance^a</i>	<i>8 h Significance^a</i>
Htt Control	N/A	N/A
POPC 0% Cholesterol	Not Significant	Not Significant
POPC 10% Cholesterol	Not Significant	Not Significant
POPC 20% Cholesterol	Not Significant	Not Significant
DOPC 0% Cholesterol	Not Significant	Not Significant
DOPC 10% Cholesterol	Not Significant	Not Significant
DOPC 20% Cholesterol	Not Significant	Not Significant
POPG 0% Cholesterol	Significant	Significant
POPG 10% Cholesterol	Significant	Significant
POPG 20% Cholesterol	Significant	Significant

^a A condition is considered significant if the result from a Chi-Squared test was $p < 0.01$.

2.4.2 Htt-Exon1(46Q)/Lipid Interactions are Altered in a Composition-Dependent Manner.

Cholesterol content was shown to impact aggregation to different extents depending on lipid composition, indicating altered interactions between htt-exon1(46Q) and lipids. To directly evaluate htt-exon1(46Q) interactions with lipids and the influence of exogenous cholesterol, a colorimetric membrane binding assay with lipid/polydiacetylene (PDA) vesicles was used. The lipid components were POPC, DOPC, POPG, or the same pure lipid systems with 10% or 20% exogenously added cholesterol. When exposed to proteins, the colorimetric response (CR) of each system directly correlates to the extent of protein/lipid interaction, as there is a transition in the structure of the polymerized PDA backbone due to the binding and/or insertion of proteins into the vesicle (Figure 2.4A-C). The percent CR was obtained for each condition as described by equation 1. The maximum percent CR was then calculated by dividing the percent CR of the designated condition by the maximum percent CR from exposure of the lipid vesicles to NaOH, which was then normalized to 100%. Relative percent CR of each well was calculated by dividing the maximum percent CR of each well by the average maximum percent CR across triplicate wells of that condition normalized to 100%, which were then averaged across all separate runs (Figure 2.4D-F). The time required to reach 50% of the maximum signal (t_{50}) was also determined to evaluate the relative rate of htt-exon1 insertion into the vesicles (Figure 2.4G-I).

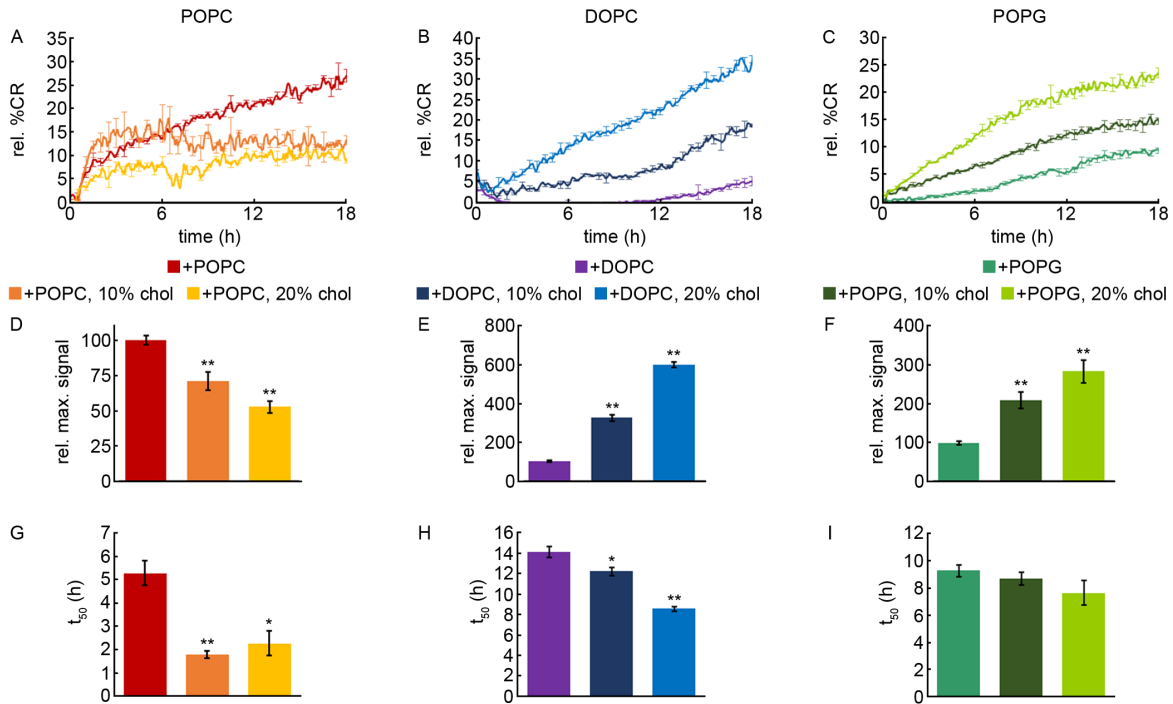


Figure 2.4. PDA/lipid binding assays for htt-exon1(46Q) incubated with different lipid systems with varied amounts of exogenously added cholesterol. Htt concentration was 10 μ M with a protein:lipid ratio of 1:10. Representative PDA assays for POPC (A), DOPC (B), and POPG (C) conditions are shown. The relative maximum signal for all POPC (D), DOPC (E), and POPG (F) conditions were calculated and averaged across all runs. The time to reach 50% of the maximum signal (t_{50}) for all POPC (G), DOPC (H), and POPG (I) conditions were determined and averaged across all runs. In panels A-C error bars are provided for every sixth data point (30 min) and SEM between triplicate wells of an individual run. Analysis in panels D-F were determined as averages over all trials, values are normalized as a percentage relative to the htt-exon1(46Q) control in the presence of pure lipid, and error bars represent SEM. Analysis in panels G-H were determined as averages across all runs and error bars represent SEM. Using a Student's t-test, * represents a p-value of <0.05 and ** represents a p-value of <0.01 relative to the pure lipid systems.

Incubation of htt-exon1(46Q) with POPC vesicles containing 10% and 20% cholesterol resulted in a decrease in the relative maximum signal by 30% and 48% respectively compared to interactions with pure POPC vesicles, indicating decreasing htt-exon1(46Q)/lipid interactions with increasing cholesterol content (Figure 2.4D). Despite the total binding signal reducing with the addition of cholesterol to POPC vesicles, the t_{50} was significantly reduced relative to the pure POPC system. This suggests that cholesterol alters the membrane in a manner that promotes

accessible binding sites, but that these sites are quickly saturated (Figure 2.4G). When htt-exon1(46Q) was incubated with DOPC vesicles containing 10% and 20% cholesterol there was an increase in the relative maximum signal of 225% and 500% respectively relative to interactions with pure DOPC vesicles, indicating increased htt-exon1(46Q)/lipid interactions with increasing cholesterol content (Figure 2.4E). The t_{50} for DOPC significantly decreased with the addition of cholesterol, suggesting that the addition of cholesterol creates more putative binding sites on the vesicle surface but that these sites are not necessarily more accessible (Figure 2.4H). In the case of POPG vesicles with 10% and 20% cholesterol, an increase in relative maximum signal by 110% and 184% respectively relative to interactions with pure POPG vesicles, indicating increased htt-exon1(46Q)/lipid interactions with increasing cholesterol content (Figure 2.4F). While the t_{50} decreased with the addition of cholesterol into POPG vesicles (Figure 2.4I), this change was not statistically significant.

2.4.3 Cholesterol Content Alters Complex Formation Between Lipids and the Lipid Binding Domain of Htt-Exon1(46Q).

The Nt17 domain of htt-exon1(46Q) facilitates interactions with lipid and can modify aggregation on membranes.¹⁰ Nt17 peptide has been shown to have a similar interaction mechanism with membrane as htt-exon1(46Q),³¹ and the mechanism does not change significantly with the addition of glutamines.⁵⁴ Therefore, synthetic Nt17 peptide was used to investigate the influence of lipid composition on the formation of protein/lipid complexes using capillary vibrating sharp-edge spray ionization (cVSSI)-MS due to the demonstrated ability of cVSSI to increase ion signals for field enabled experiments in both positive and negative mode.⁵³ Nt17 (10 μ M) was incubated with vesicles of POPC, DOPC, POPG, and the same pure lipid systems with 20% cholesterol, at a 10:1 lipid to peptide molar ratio for 24 h prior to analysis with

cVSSI-MS. The 24 h incubation time was chosen based on work using another small peptide, melittin, in which acyl chain transfer from lipid to peptide was observed in the presence of cholesterol,⁵⁵ allowing for the observation of potential cholesterol-aided acyl chain transfer to Nt17. Triplicate spectra of each sample were collected in positive ion mode. The integrated peak area of each identified complex was calculated by integrating the ion signal for each isotopic distribution of the given complex. The integrated peak areas of all complexes were normalized to that of the doubly-charged peptide monomer ($[M+2H]^{2+}$ at m/z 988.50). Complexes are represented in $[M+L]$ format, in which M represents Nt17 peptide and L represents the specified lipid.

Table 2.2. Identified ions for Nt17 incubated with pure POPC, DOPC, and POPG vesicles and the same vesicles with 20% exogenously added cholesterol with their corresponding mass to charge ratios and charge states.

Ion ^a	m/z	Charge State	Ion ^a	m/z	Charge State	Ion ^a	m/z	Charge State
<i>POPC 0% Cholesterol</i>			<i>DOPC 0% Cholesterol</i>			<i>POPG 0% Cholesterol</i>		
1Nt17 + 1POPC	1367.31	2	1Nt17 + 1DOPC	1380.32	2	1Nt17 + 1POPG	1361.78	2
2Nt17 + 1POPC	1569.55	3	1Nt17 + 1DOPC	2759.63	1	1Nt17 + 2POPG	1736.05	2
3Nt17 + 1POPC	1670.67	4	1Nt17 + 2DOPC	1773.11	2			
			1Nt17 + 3DOPC	2165.91	2			
			2Nt17 + 1DOPC	1578.22	3			
			2Nt17 + 1DOPC	2366.83	2			
			2Nt17 + 2DOPC	1840.09	3			
			2Nt17 + 3DOPC	2101.95	3			
			3Nt17 + 1DOPC	1677.18	4			
			3Nt17 + 3DOPC	2069.97	4			
			4Nt17 + 1DOPC	2170.43	4			
<i>POPC + 20% Cholesterol</i>			<i>DOPC + 20% Cholesterol</i>			<i>POPG + 20% Cholesterol</i>		
1Nt17 + 2POPC	1747.03	2	1Nt17 + 1DOPC	1380.32	2	1Nt17 + 1POPG	908.19	3
2Nt17 + 1POPC	1569.55	3	1Nt17 + 1DOPC	2759.63	1	1Nt17 + 1POPG	1361.78	2
2Nt17 + 2POPC	1822.74	3	1Nt17 + 2DOPC	1773.11	2	1Nt17 + 3POPG	2110.31	2
3Nt17 + 1POPC	1670.67	4	1Nt17 + 3DOPC	2165.91	2	2Nt17 + 2POPG	1361.78	4
			2Nt17 + 1DOPC	1578.22	3	2Nt17 + 2POPG	1815.38	3
			2Nt17 + 1DOPC	2366.83	2	2Nt17 + 3POPG	1548.91	4
			2Nt17 + 2DOPC	1840.09	3	2Nt17 + 3POPG	2064.88	3
			2Nt17 + 3DOPC	2101.95	3			
			3Nt17 + 1DOPC	1677.18	4			
			3Nt17 + 1DOPC	2235.90	3			
			4Nt17 + 1DOPC	2170.43	4			

^a The following monoisotopic masses were used to assign peaks: 1973.03 for Nt17 peptide, 759.58 for POPC lipid, 785.59 for DOPC lipid, and 748.53 for POPG lipid.

When Nt17 was incubated with pure POPC, complexes identified contained upwards of three peptide and one lipid molecules (Table 2.2; Figure 2.5A). The highest relative peak area was for [1M+1L] ($2.8\% \pm 0.90\%$) and smaller populations of [2M+1L] and [3M+1L] ($1.3\% \pm 0.45\%$ and $0.8\% \pm 0.30\%$ respectively). When 20% exogenous cholesterol was added to the lipid vesicles, complexes containing upwards of [3M+1L] and [2M+2L] were observed ($1.1\% \pm 0.25\%$ and $0.11\% \pm 0.03\%$ respectively). Complexes containing one peptide were less prevalent, with a total relative integrated peak area of 0.2%. Complexes containing two and three peptides,

however, were more prevalent in the 20% cholesterol system with total relative integrated peaks areas of 2.7% and 1.1% respectively (Figure 2.5B).

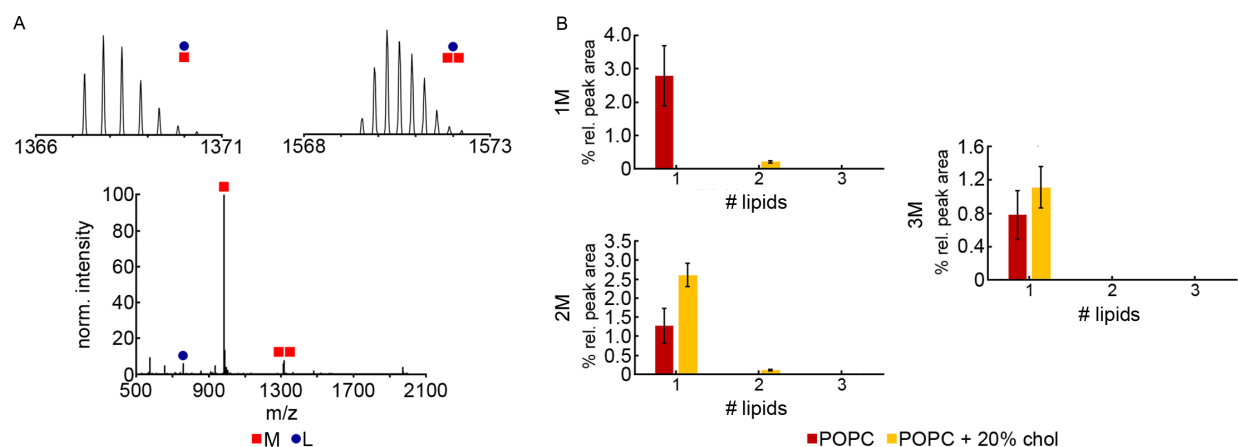


Figure 2.5. Mass spectrum and analysis of Nt17/lipid complex formation in the presence of pure POPC vesicles and POPC vesicles with 20% exogenously added cholesterol using cVSSI-MS. Peptides are denoted as M and lipids are denoted as L. The Nt17 concentration was 10 μ M and the peptide:lipid ratio was 1:10. (A) A representative mass spectrum of Nt17 incubated with pure POPC vesicles where insets show isotopic distributions of some identified peptide/lipid complexes. (B) The total percent relative peak areas for 1M, 2M, 3M, and 4M complexes identified after incubation with different POPC vesicle compositions. Error bars represent SEM.

Incubating Nt17 with pure DOPC yielded complexes containing upwards of [4M+3L] (Table 2.2; Figure 2.6A). Complexes containing one peptide account for the largest relative peak area at 27.5% total, followed by those containing two (10.3%), three (3.6%), and four peptides (1.0%). Complexes of up to [1M+3L] and [2M+3L] were observed (1.4% \pm 0.25% and 0.45% \pm 0.07% respectively) in addition to [3M+1L] and [4M+1L] complexes (3.3% \pm 0.36% and 0.98% \pm 0.25% respectively). With the addition of 20% exogenous cholesterol, again the largest total relative peak area was associated with complexes containing one peptide (17.7% total relative peak area) followed by two (8.0%), three (4.0%), and four peptides (1.2%). Similar in trend with the pure lipid system, complexes of up to [1M+3L] and [2M+3L] were observed (0.27% \pm 0.03% and 0.15% \pm 0.02%), with decreasing percent relative peak area linked to increasing lipid

monomers present in the complex. The complexes containing one or two peptides in the 20% cholesterol system, regardless of the number of lipids attached, were of a lower percent relative peak area compared to the pure lipid system. However, complexes containing three and four peptides, again regardless of the number of lipids in the complex, were of a higher percent relative peak area than those of the pure lipid system (Figure 2.6B).

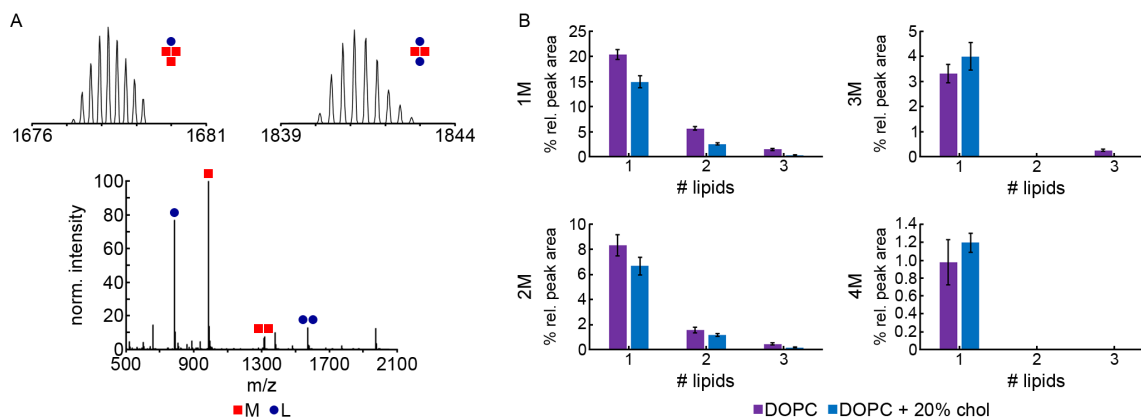


Figure 2.6. Mass spectrum and analysis of Nt17/lipid complex formation in the presence of pure DOPC vesicles and DOPC vesicles with 20% exogenously added cholesterol using cVSSI-MS. Peptides are denoted as M and lipids are denoted as L. The Nt17 concentration was 10 μ M and the peptide:lipid ratio was 1:10. (A) A representative mass spectrum of Nt17 incubated with pure DOPC vesicles where insets show isotopic distributions of some identified peptide/lipid complexes. (B) The total percent relative peak areas for 1M, 2M, 3M, and 4M complexes identified after incubation with different DOPC vesicle compositions. Error bars represent SEM.

When Nt17 was incubated with pure POPG, peptide/lipid complexes identified contained upwards of [1M+2L] (Table 2.2; Figure 2.7A). The complexes were predominantly [1M+1L] at $50.5\% \pm 5.6\%$, with [1M+2L] complexes being less prevalent at $9.7\% \pm 2.5\%$. When 20% cholesterol was added to the lipid vesicles, complexes containing two peptides were present in addition to complexes containing one peptide. In the 20% cholesterol condition [1M+1L] complexes were of a lower percent relative peak area at $22.3\% \pm 1.6\%$. [2M+2L] and [2M+3L]

complexes were observed with relative peak areas of $23.0\% \pm 2.1\%$ and $0.6\% \pm 0.30\%$ respectively (Figure 2.7B).

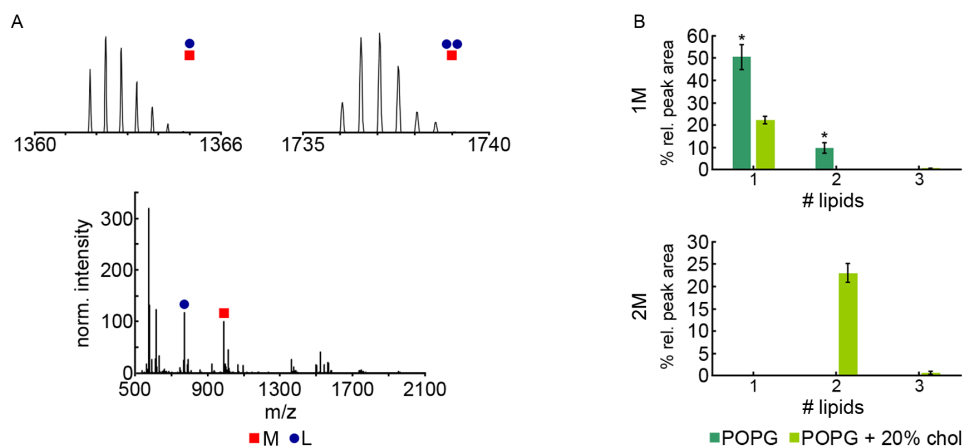


Figure 2.7. Mass spectrum and analysis of Nt17/lipid complex formation in the presence of pure POPG vesicles and POPG vesicles with 20% exogenously added cholesterol using cVSSI-MS. Peptides are denoted as M and lipids are denoted as L. The Nt17 concentration was $10 \mu\text{M}$ and the peptide:lipid ratio was 1:10. (A) A representative mass spectrum of Nt17 incubated with pure POPG vesicles where insets show isotopic distributions of some identified peptide/lipid complexes. (B) The total percent relative peak areas for 1M, 2M, 3M, and 4M complexes identified after incubation with different POPG vesicle compositions. Error bars represent SEM. The * represents conditions where $N=2$ and the error is represented as the difference between the high and the low values, as the third spectrum in the series shifted toward smaller species indicative of a discharge.

2.5 Discussion

Amyloid formation and subsequent interactions are influenced by the cellular environment.⁵⁶⁻⁵⁸ An important factor is the presence of cellular and subcellular membranes, where membrane composition further modulates amyloid formation and subsequent interactions. In this study, the impacts of cholesterol in simple lipid systems on htt-exon1(46Q) aggregation and binding was evaluated. In the case of POPC, increasing cholesterol content decreased fibril formation and htt/membrane interactions while promoting dimeric and trimeric Nt17/lipid complexes typically containing a single lipid. Increasing cholesterol content of DOPC vesicles

enhanced fibril formation and the ability of htt to bind to the membrane while promoting trimeric and tetrameric htt/lipid complexes that contained fewer lipid monomers. For pure POPG systems, increasing cholesterol content reduced fibril formation, increased htt/lipid interactions, and promoted the formation of dimeric htt/lipid complexes that included more lipid monomers. The data suggests inherently complex htt/lipid interactions and underlies the critical role of lipid composition on aggregation and lipid binding.

Previous studies in conjunction with this study highlight the complexity of htt aggregation mechanisms and lipid interactions.^{28-34,59} Physicochemical properties of lipids as a function of composition play a dominant role in such mechanisms, and small changes in features such as charge, tail group, or incorporation of other crucial membrane components can have varied impacts. Cholesterol dysregulation has been observed in HD, though debate remains with respect to cholesterol being downregulated³⁷⁻⁴⁰ or upregulated.⁴⁴ Cholesterol is a crucial component of membranes, with important roles in modulating properties such as fluidity and permeability,^{42,43} organization,⁴¹ and overall membrane function.^{41,42} Generally, cholesterol preferentially associates with large headgroup lipids, such as PC lipids, and lipids with more saturated tail groups.⁶⁰ When cholesterol is incorporated into membranes, there are changes to area per lipid, membrane thickness, bending and compressibility moduli, and lipid tail order parameters.^{61,62} In the case of POPC, the addition of cholesterol reduces overall fluidity and increases order,⁶³ which results in a decrease in membrane defects. This reduction in the presence of defects correlates to reduced lipid binding with increasing cholesterol content observed in the PDA assay. Despite overall reduced lipid binding, with the addition of exogenous cholesterol there was a significant decrease in t_{50} values. This indicates faster interaction between htt and cholesterol-containing POPC vesicles despite reduced interactions

overall. This could suggest that the incorporation of cholesterol influences early interactions of htt with the membrane by facilitating faster association, but due to reduced defects and fluidity overall binding is reduced. Increasing cholesterol content in DOPC lipid systems results in an increase in area per lipid,⁶⁴ causing more defects at the surface. Increasing the presence of defects correlates to increased lipid binding with increasing cholesterol content observed in the PDA assay. With increasing cholesterol content there was a significant reduction in t_{50} values relative to the pure lipid system. This suggests that with the addition of cholesterol causing an increase in defects htt more readily associates. POPG lipid systems form a tightly packed bilayer due to interlipid bridges and hydrogen bonding overcoming the electrostatic repulsion that exists between headgroups.⁶⁵ The addition of cholesterol to POPG systems could spread out the headgroups and allow for more interaction with htt as observed in the PDA assay. The t_{50} values for the POPG systems did not change significantly with the addition of cholesterol, indicating no significant changes in association based on cholesterol content, though overall lipid binding decreases with increasing cholesterol content. This could suggest that initial interactions are driven by electrostatics, but the addition of cholesterol likely spreads out the negative charge over the vesicle surface, reducing htt binding overall. Cholesterol content also varies throughout cellular and subcellular membranes. The plasma membrane contains the largest amount of cholesterol relative to phospholipid content, followed by late endosomes, the golgi, endoplasmic reticulum/nuclear envelope, and the mitochondria.⁶⁶ The role of cholesterol in modulating physiochemical properties of membranes, its presence and varied content in various cellular and subcellular membrane systems, and its dysregulated homeostasis in the case of HD make it a component of particular interest as its varying impact on membranes can broadly influence the ability of htt to interact with and aggregate on membranes. For example, the addition of

cholesterol to brain lipid extract completely alters the morphological impact on bilayers upon exposure to htt-exon1.³⁶

The addition of cholesterol altered htt aggregation and the ability to form complexes with all three model systems investigated here. Based on ThT assays, pure POPC had minimal impact on htt-exon1(46Q) fibril formation, pure DOPC reduced fibril formation, and pure POPG increased fibril formation; trends which align with previous studies.^{33,34} With increasing cholesterol content in the POPC and POPG systems, there was a decrease in fibril formation, while MS revealed Nt17/lipid complexes generally had a higher lipid content. In the case of DOPC, when cholesterol content was increased there was a reduction in fibrilization and MS revealed Nt17/lipid complexes that generally included fewer lipids. These trends suggest that the incorporation of more lipids into Nt17 complexes has a protective role against fibril formation. In the case of htt-lipid interactions revealed by PDA assays, increasing cholesterol content resulted in decreased lipid interactions with POPC systems and increased lipid interactions with DOPC and POPG systems. Trends in lipid binding may be attributed to changes noted in aggregation in the case of POPC and DOPC. With increasing cholesterol content POPC systems showed a reduction in both aggregation and lipid binding, while both trends increased in the case of DOPC. This suggests that with reduced aggregation in the case of POPC systems, interactions with the lipid may be smaller species as indicated by MS data (e.g., the absence of larger tetrameric species). Conversely, larger species including tetramers were present in the case of DOPC systems. The same trend was not observed in the case of POPG, where aggregation decreased with increasing cholesterol content while lipid binding increased. However, it is important to consider the influence cholesterol would have on the number and size of surface defects and, in the case of anionic POPG, charge distribution over the surface of vesicles. It is

likely that the inclusion of cholesterol in the systems used for this study also influences Nt17 orientation and insertion.

Based on computational studies, the interaction of Nt17 with phospholipid bilayers involves four basic steps: approach, reorganization, anchoring, and insertion;⁶⁷ however, the behaviors of amyloid proteins and their selective interactions with membranes is heavily dependent on physiochemical properties of the membrane system itself.⁵⁶ In the case of htt specifically, changes to lipid headgroups or tail groups change aggregation, lipid binding, Nt17 orientation at the membrane surface, and htt/lipid complex formation. With anionic lipid headgroups, electrostatics are likely the major influence on htt-lipid interactions, considering the net positive charge of the Nt17 domain.⁶⁸ This is consistent with previous studies demonstrating the localization of htt to acidic membranes²⁶ and anionic membranes enhancing fibril formation.³⁴ POPC/POPS membranes, for example enhances htt fibrillization via a unique Nt17-mediated mechanism based on membrane anchoring and two-dimensional diffusion.⁶⁹ Indeed, it appears that anionic character in lipid bilayers can result in a high local concentration at the interface without deep insertion,³⁴ allowing for easy diffusion of htt molecules along the bilayer. This is consistent with the observation of predominately monomeric Nt17 with pure POPG. The altered morphology of both htt oligomers and fibrils observed in the presence of POPG based vesicles compared to control also suggests a unique aggregation mechanism. Importantly, this is further mediated by the addition of cholesterol. With POPG, both the PDA assay and the increase in the number of complexes formed suggest that the addition of cholesterol facilitates a deeper penetration of htt into the bilayer. This more intimate interaction with lipids slows htt fibril formation relative to aggregation observed with pure POPG vesicles. Interestingly, the morphological changes of htt aggregates is less pronounced with increasing cholesterol. The

heavy influence of anionic lipids on aggregation is observed with other amyloid proteins. For example, acidic phospholipid membranes enhance α -syn fibrillization.⁷⁰

While anionic headgroups promote fibril formation, zwitterionic headgroups have varied impacts on htt fibrilization and indicate stronger htt-lipid interactions, resulting in a higher abundance of complexes containing multiple peptides. With zwitterionic lipids, aggregation was promoted by saturated tail groups, minimally affected by monounsaturated tail groups, and inhibited by polyunsaturated tail groups.³³ Computational studies with the same lipid systems demonstrated that the orientation and interactions between Nt17 and lipids also changed as a function of tail saturation, with Nt17 binding more tightly in a parallel orientation in the case of polyunsaturated lipids and less tightly in an orthogonal orientation in the case of saturated lipids.³³ In addition to orientation, defect sensing is also a common mechanism associated with amphipathic α -helix binding to membranes,⁷¹⁻⁷³ and this does appear to influence the affinity of Nt17 for membranes comprised of zwitterionic lipids.³³ The modifying impact of cholesterol on htt binding both POPC and DOPC vesicles is likely influenced by cholesterol impacting membrane fluidity and packing.

Minor changes to physiochemical properties as a function of lipid composition alters htt aggregation and lipid interactions in unique ways. This is a potential modifying factor to consider with respect to HD as changes to phospholipid metabolism (i.e. PC lipid metabolism) are observed in both HD patients^{74,75} and transgenic mouse models^{76,77} as a function of disease progression. While differentiating individual lipids within a class, i.e. saturated versus unsaturated PC lipids, is generally difficult there is interest in pursuing highly unsaturated fatty acids (HUFAs) as a treatment option for HD. The theory behind the approach focuses on potential neuroprotective effects of HUFAs due to their role in membrane function and ability to

alter the propensity of cells to undergo apoptosis.⁷⁸ Two studies utilizing different HUFAs as treatments for HD patients claimed significant efficacy; however, they are not considered sufficient to guide decisions with respect to treatment due to the small number of participants in each study.⁷⁸ Considering the complex nature of physiologically relevant systems whose lipid compositions are unique and likely variable with disease progression, it is important to understand the influence of systems beyond that of pure lipid systems alone to better understand mechanistic interactions of htt with various membranous systems such as organelles and the plasma membrane. The major phospholipid component of most cellular and subcellular membranes are PC lipids, but there are also varying ratios of PE, PI, and PS lipids in addition to others that are difficult to isolate and identify.^{42,43,66} Beyond phospholipid components, there are also varied amounts of other components such as sphingomyelin, gangliosides, and sterols such as cholesterol. In short, the ability of htt to interact with membranes is dependent on numerous factors related to membrane properties, i.e. fluidity, packing, thickness, and charge. The relative importance of each factor appears to be highly sensitive to lipid composition.

The ability of htt and its aggregate forms to directly bind and disrupt membranes underscores the development of organelle membrane damage observed in HD. Cytoplasmic htt inclusions formed in mammalian cell and primary neuron models of HD are enriched with and sequester organelle membrane fragments deriving from the ER and mitochondria,³⁵ suggesting that the aggregation process directly damages these surfaces. Indeed, htt fibrils directly impinge upon the ER membrane, compromising its integrity and dynamics.⁷⁹ In both HD patients and mouse models, htt aggregation exasperates age-dependent disruption of the nuclear envelope, leading to DNA damage.⁸⁰ Similar damage to organelle membranes (swollen mitochondria and absent nuclear membrane) develop in the striatum of a novel pig model of HD.⁸¹ Importantly,

each of these organelle membranes have unique lipid compositions. As lipid composition influences how htt interacts with and aggregates on these surfaces, mechanistic details of how htt damages different organelle membranes may vary. Even within mitochondria, htt aggregates impact inner and outer mitochondrial mimic membranes in distinct ways.⁸² Understanding how amyloid proteins aggregate in the presence of membranes and interact with them is critical to understanding the intricacies of toxic mechanisms attributable to htt aggregation. The intricacies of these interactions are demonstrated here with simple lipid systems enriched with cholesterol (Table 2.3). With increasing complexity of membrane composition, these htt/membrane interactions likely will become even more complicated. Future studies with more complex lipid systems could provide further detail on the intricacies of htt interactions with cholesterol-containing membranes and the relationship between such interactions and toxicity.

Table 2.3. Summary of the trends observed with each lipid system for all experiments performed.

Experiment	Results by Lipid System		
	<i>POPC</i>	<i>DOPC</i>	<i>POPG</i>
ThT Aggregation Assay	Pure POPC had minimal impact on fibril formation; subsequent additions of cholesterol decreased fibril formation	Pure DOPC reduced fibril formation; subsequent additions of cholesterol increased fibril formation	Pure POPG promoted fibril formation; subsequent additions of cholesterol reduced fibril formation
AFM: Oligomer Morphologies	Pure POPC did not change oligomer morphology; addition of exogenous cholesterol caused significant shift to smaller heights	No significant change to oligomer morphology with or without exogenous cholesterol	Significant shift to smaller oligomer heights both with and without exogenous cholesterol
AFM: Fibril Morphologies	Minimal change to fibril height in the presence of POPC with or without cholesterol	Minimal change to fibril height in the presence of DOPC with or without cholesterol	Shift to slightly smaller fibril heights in the presence of POPG both with and without cholesterol
PDA Lipid Binding Assay	Lipid binding decreased with increasing cholesterol content	Lipid binding increased with increasing cholesterol content	Lipid binding increased with increasing cholesterol content
MS: Peptide/Lipid Complexation	Increased cholesterol content favored dimer and trimer complexes; generally fewer lipids incorporated into complexes	Increased cholesterol content favored trimer and tetramer complexes; generally fewer lipids incorporated into complexes	Increasing cholesterol favored dimer complexes; generally more lipids incorporated into complexes

2.6 References

1. Macdonald M. A novel gene containing a trinucleotide repeat that is expanded and unstable on Huntington's disease chromosomes. *Cell*. 1993;72(6):971–983. doi:10.1016/0092-8674(93)90585-E
2. Snell RG, MacMillan JC, Cheadle JP, Fenton I, Lazarou LP, Davies P, MacDonald ME, Gusella JF, Harper PS, Shaw DJ. Relationship between trinucleotide repeat expansion and phenotypic variation in Huntington's disease. *Nature Genetics*. 1993;4(4):393–397. doi:10.1038/ng0893-393
3. Penney JB, Vonsattel J-P, Macdonald ME, Gusella JF, Myers RH. CAG repeat number governs the development rate of pathology in Huntington's disease. *Annals of Neurology*. 1997;41(5):689–692. doi:10.1002/ana.410410521
4. Scherzinger E, Lurz R, Turmaine M, Mangiarini L, Hollenbach B, Hasenbank R, Bates GP, Davies SW, Lehrach H, Wanker EE. Huntingtin-Encoded Polyglutamine Expansions Form Amyloid-like Protein Aggregates In Vitro and In Vivo. *Cell*. 1997;90(3):549–558. doi:10.1016/S0092-8674(00)80514-0
5. Scherzinger E, Sittler A, Schweiger K, Heiser V, Lurz R, Hasenbank R, Bates GP, Lehrach H, Wanker EE. Self-assembly of polyglutamine-containing huntingtin fragments into amyloid-like fibrils: Implications for Huntington's disease pathology. *Proceedings of the National Academy of Sciences*. 1999;96(8):4604–4609. doi:10.1073/pnas.96.8.4604
6. Chen S, Berthelier V, Hamilton JB, O'Nuallai B, Wetzel R. Amyloid-like Features of Polyglutamine Aggregates and Their Assembly Kinetics †. *Biochemistry*. 2002;41(23):7391–7399. doi:10.1021/bi011772q
7. Adegbuyiro A, Sedighi F, Pilkington AW, Groover S, Legleiter J. Proteins Containing Expanded Polyglutamine Tracts and Neurodegenerative Disease. *Biochemistry*. 2017;56(9):1199–1217. doi:10.1021/acs.biochem.6b00936
8. Nagarajan A, Jawahery S, Matysiak S. The Effects of Flanking Sequences in the Interaction of Polyglutamine Peptides with a Membrane Bilayer. *The Journal of Physical Chemistry B*. 2014;118(24):6368–6379. doi:10.1021/jp407900c
9. Arndt JR, Chaibva M, Legleiter J. The emerging role of the first 17 amino acids of huntingtin in Huntington's disease. *Biomolecular Concepts*. 2015 [accessed 2020 Feb 24];6(1). <https://www.degruyter.com/view/j/bmc.2015.6.issue-1/bmc-2015-0001/bmc-2015-0001.xml>. doi:10.1515/bmc-2015-0001
10. Burke KA, Kauffman KJ, Umbaugh CS, Frey SL, Legleiter J. The Interaction of Polyglutamine Peptides with Lipid Membranes Is Regulated by Flanking Sequences Associated with Huntingtin. *Journal of Biological Chemistry*. 2013;288(21):14993–15005. doi:10.1074/jbc.M112.446237
11. Mishra R, Hoop CL, Kodali R, Sahoo B, van der Wel PCA, Wetzel R. Serine Phosphorylation Suppresses Huntingtin Amyloid Accumulation by Altering Protein Aggregation Properties. *Journal of Molecular Biology*. 2012;424(1–2):1–14. doi:10.1016/j.jmb.2012.09.011
12. Chaibva M, Jawahery S, Pilkington AW, Arndt JR, Sarver O, Valentine S, Matysiak S, Legleiter J. Acetylation within the First 17 Residues of Huntingtin Exon 1 Alters Aggregation and Lipid Binding. *Biophysical Journal*. 2016;111(2):349–362. doi:10.1016/j.bpj.2016.06.018

13. Kotler SA, Tugarinov V, Schmidt T, Ceccon A, Libich DS, Ghirlando R, Schwieters CD, Clore GM. Probing initial transient oligomerization events facilitating Huntingtin fibril nucleation at atomic resolution by relaxation-based NMR. *Proceedings of the National Academy of Sciences*. 2019;116(9):3562–3571. doi:10.1073/pnas.1821216116
14. Arndt JR, Kondalaji SG, Maurer MM, Parker A, Legleiter J, Valentine SJ. Huntingtin N-Terminal Monomeric and Multimeric Structures Destabilized by Covalent Modification of Heteroatomic Residues. *Biochemistry*. 2015;54(28):4285–4296. doi:10.1021/acs.biochem.5b00478
15. Williamson TE, Vitalis A, Crick SL, Pappu RV. Modulation of Polyglutamine Conformations and Dimer Formation by the N-Terminus of Huntingtin. *Journal of Molecular Biology*. 2010;396(5):1295–1309. doi:10.1016/j.jmb.2009.12.017
16. Li S-H, Li X-J. Huntingtin–protein interactions and the pathogenesis of Huntington’s disease. *Trends in Genetics*. 2004;20(3):146–154. doi:10.1016/j.tig.2004.01.008
17. Cattaneo E, Zuccato C, Tartari M. Normal huntingtin function: an alternative approach to Huntington’s disease. *Nature Reviews Neuroscience*. 2005;6(12):919–930. doi:10.1038/nrn1806
18. De Rooij K. Subcellular localization of the Huntington’s disease gene product in cell lines by immunofluorescence and biochemical subcellular fractionation. *Human Molecular Genetics*. 1996;5(8):1093–1099. doi:10.1093/hmg/5.8.1093
19. Xia J. Huntingtin contains a highly conserved nuclear export signal. *Human Molecular Genetics*. 2003;12(>12):1393–1403. doi:10.1093/hmg/ddg156
20. Atwal RS, Xia J, Pinchev D, Taylor J, Epanand RM, Truant R. Huntingtin has a membrane association signal that can modulate huntingtin aggregation, nuclear entry and toxicity. *Human Molecular Genetics*. 2007;16(21):2600–2615. doi:10.1093/hmg/ddm217
21. Gu M, Gash MT, Mann VM, Javoy-Agid F, Cooper JM, Schapira AHV. Mitochondrial defect in Huntington’s disease caudate nucleus. *Annals of Neurology*. 1996;39(3):385–389. doi:10.1002/ana.410390317
22. Panov AV, Gutekunst C-A, Leavitt BR, Hayden MR, Burke JR, Strittmatter WJ, Greenamyre JT. Early mitochondrial calcium defects in Huntington’s disease are a direct effect of polyglutamines. *Nature Neuroscience*. 2002;5(8):731–736. doi:10.1038/nn884
23. Choo YS. Mutant huntingtin directly increases susceptibility of mitochondria to the calcium-induced permeability transition and cytochrome c release. *Human Molecular Genetics*. 2004;13(14):1407–1420. doi:10.1093/hmg/ddh162
24. Chang DTW, Rintoul GL, Pandipati S, Reynolds IJ. Mutant huntingtin aggregates impair mitochondrial movement and trafficking in cortical neurons. *Neurobiology of Disease*. 2006;22(2):388–400. doi:10.1016/j.nbd.2005.12.007
25. Orr AL, Li S, Wang C-E, Li H, Wang J, Rong J, Xu X, Mastroberardino PG, Greenamyre JT, Li X-J. N-Terminal Mutant Huntingtin Associates with Mitochondria and Impairs Mitochondrial Trafficking. *Journal of Neuroscience*. 2008;28(11):2783–2792. doi:10.1523/JNEUROSCI.0106-08.2008
26. Kegel KB, Sapp E, Yoder J, Cuiffo B, Sobin L, Kim YJ, Qin Z-H, Hayden MR, Aronin N, Scott DL, et al. Huntingtin Associates with Acidic Phospholipids at the Plasma Membrane. *Journal of Biological Chemistry*. 2005;280(43):36464–36473. doi:10.1074/jbc.M503672200

27. Burke KA, Hensal KM, Umbaugh CS, Chaibva M, Legleiter J. Huntingtin disrupts lipid bilayers in a polyQ-length dependent manner. *Biochimica et Biophysica Acta (BBA) - Biomembranes*. 2013;1828(8):1953–1961. doi:10.1016/j.bbamem.2013.04.025
28. Beasley M, Stonebraker AR, Hasan I, Kapp KL, Liang BJ, Agarwal G, Groover S, Sedighi F, Legleiter J. Lipid Membranes Influence the Ability of Small Molecules To Inhibit Huntingtin Fibrillization. *Biochemistry*. 2019;58(43):4361–4373. doi:10.1021/acs.biochem.9b00739
29. Levy GR, Shen K, Gavrilov Y, Smith PES, Levy Y, Chan R, Frydman J, Frydman L. Huntingtin's N-Terminus Rearrangements in the Presence of Membranes: A Joint Spectroscopic and Computational Perspective. *ACS Chemical Neuroscience*. 2019;10(1):472–481. doi:10.1021/acscchemneuro.8b00353
30. Chaibva M, Gao X, Jain P, Campbell WA, Frey SL, Legleiter J. Sphingomyelin and GM1 Influence Huntingtin Binding to, Disruption of, and Aggregation on Lipid Membranes. *ACS Omega*. 2018;3(1):273–285. doi:10.1021/acsomega.7b01472
31. Pandey NK, Isas JM, Rawat A, Lee RV, Langen J, Pandey P, Langen R. The 17-residue-long N terminus in huntingtin controls stepwise aggregation in solution and on membranes via different mechanisms. *Journal of Biological Chemistry*. 2018;293(7):2597–2605. doi:10.1074/jbc.M117.813667
32. Côté S, Binette V, Salnikov ES, Bechinger B, Mousseau N. Probing the Huntingtin 1-17 Membrane Anchor on a Phospholipid Bilayer by Using All-Atom Simulations. *Biophysical Journal*. 2015;108(5):1187–1198. doi:10.1016/j.bpj.2015.02.001
33. Beasley M, Frazee N, Groover S, Valentine SJ, Mertz B, Legleiter J. Physicochemical Properties Altered by the Tail Group of Lipid Membranes Influence Huntingtin Aggregation and Lipid Binding. *The Journal of Physical Chemistry B*. 2022;126(16):3067–3081. doi:10.1021/acs.jpcc.1c10254
34. Beasley M, Groover S, Valentine SJ, Legleiter J. Lipid headgroups alter huntingtin aggregation on membranes. *Biochimica et Biophysica Acta (BBA) - Biomembranes*. 2021;1863(1):183497. doi:10.1016/j.bbamem.2020.183497
35. Riguet N, Mahul-Mellier A-L, Maharjan N, Burtscher J, Croisier M, Knott G, Hastings J, Patin A, Reiterer V, Farhan H, et al. Nuclear and cytoplasmic huntingtin inclusions exhibit distinct biochemical composition, interactome and ultrastructural properties. *Nature Communications*. 2021;12(1):6579. doi:10.1038/s41467-021-26684-z
36. Gao X, Campbell WA, Chaibva M, Jain P, Leslie AE, Frey SL, Legleiter J. Cholesterol Modifies Huntingtin Binding to, Disruption of, and Aggregation on Lipid Membranes. *Biochemistry*. 2016;55(1):92–102. doi:10.1021/acs.biochem.5b00900
37. Korade Z, Kenworthy AK. Lipid rafts, cholesterol, and the brain. *Neuropharmacology*. 2008;55(8):1265–1273. doi:10.1016/j.neuropharm.2008.02.019
38. Valenza M, Cattaneo E. Emerging roles for cholesterol in Huntington's disease. *Trends in Neurosciences*. 2011;34(9):474–486. doi:10.1016/j.tins.2011.06.005
39. Vance JE. Dysregulation of cholesterol balance in the brain: contribution to neurodegenerative diseases. *Disease Models & Mechanisms*. 2012;5(6):746–755. doi:10.1242/dmm.010124
40. Valenza M. Dysfunction of the Cholesterol Biosynthetic Pathway in Huntington's Disease. *Journal of Neuroscience*. 2005;25(43):9932–9939. doi:10.1523/JNEUROSCI.3355-05.2005

41. Arora A, Raghuraman H, Chattopadhyay A. Influence of cholesterol and ergosterol on membrane dynamics: a fluorescence approach. *Biochemical and Biophysical Research Communications*. 2004;318(4):920–926. doi:10.1016/j.bbrc.2004.04.118
42. Subczynski WK, Pasenkiewicz-Gierula M, Widomska J, Mainali L, Raguz M. High Cholesterol/Low Cholesterol: Effects in Biological Membranes: A Review. *Cell Biochemistry and Biophysics*. 2017;75(3–4):369–385. doi:10.1007/s12013-017-0792-7
43. Wennberg CL, van der Spoel D, Hub JS. Large Influence of Cholesterol on Solute Partitioning into Lipid Membranes. *Journal of the American Chemical Society*. 2012;134(11):5351–5361. doi:10.1021/ja211929h
44. Trushina E, Singh RD, Dyer RB, Cao S, Shah VH, Parton RG, Pagano RE, McMurray CT. Mutant huntingtin inhibits clathrin-independent endocytosis and causes accumulation of cholesterol in vitro and in vivo. *Human Molecular Genetics*. 2006;15(24):3578–3591. doi:10.1093/hmg/ddl434
45. Muchowski PJ, Schaffar G, Sittler A, Wanker EE, Hayer-Hartl MK, Hartl FU. Hsp70 and Hsp40 chaperones can inhibit self-assembly of polyglutamine proteins into amyloid-like fibrils. *Proceedings of the National Academy of Sciences*. 2000;97(14):7841–7846. doi:10.1073/pnas.140202897
46. Zheng F, Wu Z, Chen Y. A quantitative method for the measurement of membrane affinity by polydiacetylene-based colorimetric assay. *Analytical Biochemistry*. 2012;420(2):171–176. doi:10.1016/j.ab.2011.09.026
47. Sokolovski M, Sheynis T, Kolusheva S, Jelinek R. Membrane interactions and lipid binding of casein oligomers and early aggregates. *Biochimica et Biophysica Acta (BBA) - Biomembranes*. 2008;1778(10):2341–2349. doi:10.1016/j.bbamem.2008.07.001
48. Jelinek R, Kolusheva S. Biomolecular Sensing with Colorimetric Vesicles. In: Schrader T, editor. *Creative Chemical Sensor Systems*. Vol. 277. Berlin, Heidelberg: Springer Berlin Heidelberg; 2007. p. 155–180. (Topics in Current Chemistry). http://link.springer.com/10.1007/128_2007_112. doi:10.1007/128_2007_112
49. Jelinek R, Kolusheva S. Polymerized lipid vesicles as colorimetric biosensors for biotechnological applications. *Biotechnology Advances*. 2001;19(2):109–118. doi:10.1016/S0734-9750(00)00064-1
50. Beasley M, Stonebraker AR, Legleiter J. Normalizing polydiacetylene colorimetric assays of vesicle binding across lipid systems. *Analytical Biochemistry*. 2020;609:113864. doi:10.1016/j.ab.2020.113864
51. Burke KA, Legleiter J. Atomic Force Microscopy Assays for Evaluating Polyglutamine Aggregation in Solution and on Surfaces. In: Hatters DM, Hannan AJ, editors. *Tandem Repeats in Genes, Proteins, and Disease*. Vol. 1017. Totowa, NJ: Humana Press; 2013. p. 21–40. (Methods in Molecular Biology). http://link.springer.com/10.1007/978-1-62703-438-8_2. doi:10.1007/978-1-62703-438-8_2
52. Ranganathan N, Li C, Suder T, Karanji AK, Li X, He Z, Valentine SJ, Li P. Capillary Vibrating Sharp-Edge Spray Ionization (cVSSI) for Voltage-Free Liquid Chromatography-Mass Spectrometry. *Journal of The American Society for Mass Spectrometry*. 2019;30(5):824–831. doi:10.1007/s13361-019-02147-0
53. Li C, Attanayake K, Valentine SJ, Li P. Facile Improvement of Negative Ion Mode Electrospray Ionization Using Capillary Vibrating Sharp-Edge Spray Ionization. *Analytical Chemistry*. 2020;92(3):2492–2502. doi:10.1021/acs.analchem.9b03983

54. Côté S, Wei G, Mousseau N. Atomistic mechanisms of huntingtin N-terminal fragment insertion on a phospholipid bilayer revealed by molecular dynamics simulations: [http ^{NT} _N Insertion on a Phospholipid Bilayer](https://doi.org/10.1002/prot.24509). *Proteins: Structure, Function, and Bioinformatics*. 2014;82(7):1409–1427. doi:10.1002/prot.24509
55. Britt HM, Mosely JA, Sanderson JM. The influence of cholesterol on melittin lipidation in neutral membranes. *Physical Chemistry Chemical Physics*. 2019;21(2):631–640. doi:10.1039/C8CP06661B
56. Burke KA, Yates EA, Legleiter J. Biophysical Insights into How Surfaces, Including Lipid Membranes, Modulate Protein Aggregation Related to Neurodegeneration. *Frontiers in Neurology*. 2013 [accessed 2022 Nov 11];4. <http://journal.frontiersin.org/article/10.3389/fneur.2013.00017/abstract>. doi:10.3389/fneur.2013.00017
57. Aisenbrey C, Borowik T, Byström R, Bokvist M, Lindström F, Misiak H, Sani M-A, Gröbner G. How is protein aggregation in amyloidogenic diseases modulated by biological membranes? *European Biophysics Journal*. 2008;37(3):247–255. doi:10.1007/s00249-007-0237-0
58. Gorbenko GP, Kinnunen PKJ. The role of lipid–protein interactions in amyloid-type protein fibril formation. *Chemistry and Physics of Lipids*. 2006;141(1–2):72–82. doi:10.1016/j.chemphyslip.2006.02.006
59. Ho CS, Khadka NK, She F, Cai J, Pan J. Polyglutamine aggregates impair lipid membrane integrity and enhance lipid membrane rigidity. *Biochimica et Biophysica Acta (BBA) - Biomembranes*. 2016;1858(4):661–670. doi:10.1016/j.bbamem.2016.01.016
60. Huang J. Chapter 12 Model Membrane Thermodynamics and Lateral Distribution of Cholesterol. In: *Methods in Enzymology*. Vol. 455. Elsevier; 2009. p. 329–364. <https://linkinghub.elsevier.com/retrieve/pii/S0076687908042122>. doi:10.1016/S0076-6879(08)04212-2
61. Saeedimazine M, Montanino A, Kleiven S, Villa A. Role of lipid composition on the structural and mechanical features of axonal membranes: a molecular simulation study. *Scientific Reports*. 2019;9(1):8000. doi:10.1038/s41598-019-44318-9
62. Hofsäß C, Lindahl E, Edholm O. Molecular Dynamics Simulations of Phospholipid Bilayers with Cholesterol. *Biophysical Journal*. 2003;84(4):2192–2206. doi:10.1016/S0006-3495(03)75025-5
63. Schumann-Gillett A, O’Mara ML. The effects of oxidised phospholipids and cholesterol on the biophysical properties of POPC bilayers. *Biochimica et Biophysica Acta (BBA) - Biomembranes*. 2019;1861(1):210–219. doi:10.1016/j.bbamem.2018.07.012
64. Alwarawrah M, Dai J, Huang J. A Molecular View of the Cholesterol Condensing Effect in DOPC Lipid Bilayers. *The Journal of Physical Chemistry B*. 2010;114(22):7516–7523. doi:10.1021/jp101415g
65. Zhao W, Róg T, Gurtovenko AA, Vattulainen I, Karttunen M. Atomic-Scale Structure and Electrostatics of Anionic Palmitoyloleoylphosphatidylglycerol Lipid Bilayers with Na⁺ Counterions. *Biophysical Journal*. 2007;92(4):1114–1124. doi:10.1529/biophysj.106.086272
66. van Meer G, Voelker DR, Feigenson GW. Membrane lipids: where they are and how they behave. *Nature Reviews Molecular Cell Biology*. 2008;9(2):112–124. doi:10.1038/nrm2330

67. Côté S, Wei G, Mousseau N. Atomistic mechanisms of huntingtin N-terminal fragment insertion on a phospholipid bilayer revealed by molecular dynamics simulations. *Proteins*. 2014;82(7):1409–1427. doi:10.1002/prot.24509
68. Tao M, Pandey NK, Barnes R, Han S, Langen R. Structure of Membrane-Bound Huntingtin Exon 1 Reveals Membrane Interaction and Aggregation Mechanisms. *Structure*. 2019;27(10):1570-1580.e4. doi:10.1016/j.str.2019.08.003
69. Pandey NK, Isas JM, Rawat A, Lee RV, Langen J, Pandey P, Langen R. The 17-residue-long N terminus in huntingtin controls stepwise aggregation in solution and on membranes via different mechanisms. *Journal of Biological Chemistry*. 2018;293(7):2597–2605. doi:10.1074/jbc.M117.813667
70. Iyer A, Claessens MMAE. Disruptive membrane interactions of alpha-synuclein aggregates. *Biochimica et Biophysica Acta (BBA) - Proteins and Proteomics*. 2019;1867(5):468–482. (Lipid-protein interactions in amyloid formation). doi:10.1016/j.bbapap.2018.10.006
71. Drin G, Casella J-F, Gautier R, Boehmer T, Schwartz TU, Antonny B. A general amphipathic α -helical motif for sensing membrane curvature. *Nature Structural & Molecular Biology*. 2007;14(2):138–146. doi:10.1038/nsmb1194
72. Drin G, Antonny B. Amphipathic helices and membrane curvature. *FEBS Letters*. 2010;584(9):1840–1847. doi:10.1016/j.febslet.2009.10.022
73. Hatzakis NS, Bhatia VK, Larsen J, Madsen KL, Bolinger P-Y, Kunding AH, Castillo J, Gether U, Hedegård P, Stamou D. How curved membranes recruit amphipathic helices and protein anchoring motifs. *Nature Chemical Biology*. 2009;5(11):835–841. doi:10.1038/nchembio.213
74. Mastrokolas A, Pool R, Mina E, Hettne KM, van Duijn E, van der Mast RC, van Ommen G, 't Hoen PAC, Prehn C, Adamski J, et al. Integration of targeted metabolomics and transcriptomics identifies deregulation of phosphatidylcholine metabolism in Huntington's disease peripheral blood samples. *Metabolomics*. 2016;12(8):137. doi:10.1007/s11306-016-1084-8
75. McGarry A, Gaughan J, Hackmyer C, Lovett J, Khadeer M, Shaikh H, Pradhan B, Ferraro TN, Wainer IW, Moaddel R. Cross-sectional analysis of plasma and CSF metabolomic markers in Huntington's disease for participants of varying functional disability: a pilot study. *Scientific Reports*. 2020;10(1):20490. doi:10.1038/s41598-020-77526-9
76. Hashimoto M, Watanabe K, Miyoshi K, Koyanagi Y, Tadano J, Miyawaki I. Multiplatform metabolomic analysis of the R6/2 mouse model of Huntington's disease. *FEBS Open Bio*. 2021;11(10):2807–2818. doi:10.1002/2211-5463.13285
77. Tsang TM, Woodman B, McLoughlin GA, Griffin JL, Tabrizi SJ, Bates GP, Holmes E. Metabolic Characterization of the R6/2 Transgenic Mouse Model of Huntington's Disease by High-Resolution MAS ¹H NMR Spectroscopy. *Journal of Proteome Research*. 2006;5(3):483–492. doi:10.1021/pr050244o
78. Anne Rosser, Stephen Dunnett. New drugs for Huntington's disease. *Neuroreport*. 2002;13(2):A21–A22.
79. Bäuerlein FJB, Saha I, Mishra A, Kalemanov M, Martínez-Sánchez A, Klein R, Dudanova I, Hipp MS, Hartl FU, Baumeister W, et al. In Situ Architecture and Cellular Interactions of PolyQ Inclusions. *Cell*. 2017;171(1):179-187.e10. doi:10.1016/j.cell.2017.08.009
80. Gasset-Rosa F, Chillon-Marinás C, Goginashvili A, Atwal RS, Artates JW, Tabet R, Wheeler VC, Bang AG, Cleveland DW, Lagier-Tourenne C. Polyglutamine-Expanded Huntingtin

- Exacerbates Age-Related Disruption of Nuclear Integrity and Nucleocytoplasmic Transport. *Neuron*. 2017;94(1):48-57.e4. doi:10.1016/j.neuron.2017.03.027
81. Yan S, Tu Z, Liu Z, Fan N, Yang H, Yang S, Yang W, Zhao Y, Ouyang Z, Lai C, et al. A Huntingtin Knockin Pig Model Recapitulates Features of Selective Neurodegeneration in Huntington's Disease. *Cell*. 2018;173(4):989-1002.e13. doi:10.1016/j.cell.2018.03.005
82. Adegbuyiro A, Sedighi F, Jain P, Pinti MV, Siriwardhana C, Hollander JM, Legleiter J. Mitochondrial membranes modify mutant huntingtin aggregation. *Biochimica et Biophysica Acta (BBA) - Biomembranes*. 2021;1863(10):183663. doi:10.1016/j.bbamem.2021.183663

3. Charge Within Nt17 Peptides Modulates Huntingtin Aggregation and Initial Lipid Binding Events

3.1 Abstract

Toxic aggregation of pathogenic huntingtin protein (htt) is implicated in Huntington's disease and influenced by various factors, including the first seventeen amino acids at the N-terminus (Nt17) and the presence of lipid membranes. Nt17 has a propensity to form an amphipathic α -helix in the presence of binding partners, which promotes the formation of α -helix rich oligomers in addition to facilitating htt/lipid interactions. Within the Nt17 domain, there are multiple sites that are subject to post-translational modification, including acetylation and phosphorylation. Acetylation can occur at lysine 6, 9, and/or 15 while phosphorylation can occur at threonine 3, serine 13, and/or serine 16. Modifications at these sites impact aggregation and lipid binding through the alteration of various intra- and intermolecular interactions. The effects of free Nt17 peptides containing such modifications on htt aggregation and lipid binding were measured using thioflavin-T aggregation assays, atomic force microscopy, lipid binding assays, and mass spectrometry. Free Nt17 peptides containing point mutations mimicking acetylation or phosphorylation significantly reduced fibril formation when incubated with htt-exon1(46Q), with observed shifts in oligomer morphologies. When exposed to lipid vesicles, changes to peptide/lipid complexation were observed and oligomers containing free Nt17 peptides demonstrated small reductions in lipid interactions.

3.2 Introduction

Huntington's disease (HD) is a fatal neurodegenerative disease resulting from an expansion in the poly-glutamine (polyQ) domain within the huntingtin (htt) protein.¹ The

expansion of the polyQ domain beyond a threshold of approximately 35 repeats^{2,3} causes htt to aggregate into amyloid-like fibrils.⁴⁻⁶ The aggregation pathway is very complex and involves various aggregate species including oligomers and amorphous aggregates.⁷ Sequences directly adjacent to the polyQ domain of the protein, including the first 17 amino acids at the N-terminus (Nt17), heavily influence htt interactions with respect to both aggregation⁸⁻¹³ and lipid binding.⁸⁻¹¹ Htt is an intrinsically disordered protein,^{14,15} but the Nt17 domain has a propensity to form an amphipathic α -helix that facilitates early interactions of htt through intermolecular association, promoting the formation of α -helix rich oligomers.^{9,13,16-18} Within these oligomers, polyQ domains are brought into close proximity, promoting fibril nucleation.^{13,19-21}

The Nt17 domain also facilitates lipid interactions and subsequent damage through its ability to form an amphipathic α -helix.^{16,22} Many of the normal functions attributed to htt, including vesicle transport and synaptic transmission,^{23,24} require interactions with a variety of lipid membrane systems. Specifically, htt associates closely with the endoplasmic reticulum (ER),²⁵⁻²⁷ mitochondrial,²⁸⁻³² nuclear,^{26,27} and plasma membranes.³³ Mutant htt aggregation damages organelle membranes. Inclusions interact with the ER, resulting in membrane deformation, impaired organization, and altered dynamics of the membrane.³⁴ Damaged and fragmented mitochondria accumulate at the periphery of htt inclusions and have increased respiration rates.³⁵ Interactions of htt at the nuclear envelope exacerbate age-related degeneration of the membrane and impairs nucleocytoplasmic transport.³⁶

Both aggregation and interactions between Nt17 and lipids are modulated by a variety of factors, including lipid composition. Compared to aggregation in bulk solution, total brain lipid extract (TBLE)³⁷ and cellular lipid extracts³⁸ reduce htt fibrillization. Some pure lipid systems, such as palmitoyl-2-oleoyl-glycero-3-phosphocholine (POPC)³⁷ and a mixture also containing 1-

palmitoyl-2-oleoyl-sn-glycero-3-phospho-L-serine (POPS)³⁹ enhance fibril formation, with the POPC/POPS system promoting a unique aggregation pathway facilitated by Nt17 versus aggregation observed in the absence of lipid.³⁹ Conversely, 1,2,-dioleoyl-sn-glycero-3-phosphocholine (DOPC) inhibits fibril formation.⁴⁰ Lipid physiochemical properties play a large role in htt/lipid interactions, with htt demonstrating preferential interactions with anionic phospholipids compared to zwitterionic lipids.⁴¹ Additionally, while changes to lipid tail groups did not display a direct correlation between aggregation and htt/lipid complexation, it was revealed that membrane defect sizes in conjunction with Nt17 orientation and hydrophobic residue sizes are critical to lipid interactions.⁴⁰ Changes to lipid composition by additional lipid components, including ganglioside (GM1) and sphingomyelin (SM) content, further modulate htt/lipid with the addition of either GM1 or SM to TBLE reducing the insertion of htt into the membrane and promoting unique aggregate morphologies.⁴²

A second modulating factor of htt interactions are several sites within Nt17 that are subject to post-translational modifications (PTMs). Such modifications include phosphorylation,^{12,43–45} acetylation,^{11,43} ubiquitination,⁴⁶ and SUMOylation.^{47,48} PTMs at these sites alter both the aggregation propensity^{11,12,43,45,48,49} and lipid interactions^{11,48} of htt. Specifically, phosphorylation within Nt17 reduces aggregate accumulation,⁴⁹ while lysine acetylation decreased the formation of large, globular oligomers and reduced membrane damage by altering Nt17/lipid association.¹¹ Peptides with other mutations have also been used as mutant htt inhibitors; the incubation of htt with analogs of human Nt17 and sequence variants from evolutionarily distant organisms inhibited aggregation⁵⁰ while other Nt17 derived peptides, especially those containing D-amino acids and sequences where cell penetrating sequences were attached, inhibited nucleation and subsequent aggregation.²¹

Aggregation is dependent on a variety of factors, including the presence of lipids and their composition in addition to post-translational modifications within the Nt17 domain. Considering the close association of htt with a variety of membrane systems and subsequent damage observed in HD, understanding htt-lipid interactions and how such interactions can be modulated is crucial to gaining a better understanding of the toxic mechanism and pathogenesis. Our aim was to identify how the incorporation of modified Nt17 peptides, with altered net charges, into oligomeric structures modulates aggregation, lipid binding, and htt/lipid complexation.

3.3 Materials and Methods

3.3.1 Preparation of Synthetic Peptides

Synthetic Nt17 peptides were solubilized in dimethyl sulfoxide (DMSO) to a stock concentration of 2,000 μM . Solubilized peptide was stored at $-20\text{ }^{\circ}\text{C}$ until needed. On the day of the experiment, solubilized peptide was thawed and diluted to the desired final concentration such that the concentration of DMSO was less than 1% in the final solution. A synthetic htt-exon1 mimic peptide consisting of Nt17, a 35 residue polyQ stretch, and a 10 residue polyproline stretch (referred to as Nt17Q₃₅P₁₀) was solubilized based on previously established protocols.^{6,51} Lyophilized peptide was treated with a 1:1 mixture of trifluoroacetic acid (TFA) and hexafluoroisopropanol (HFIP). The solvent was removed under vacuum, and the resulting dried films were reconstituted in DMSO to a stock concentration of 4,000 μM and stored at $-20\text{ }^{\circ}\text{C}$ until needed. On the day of the experiment, stock peptide was diluted to the desired final concentration such that the DMSO concentration was less than 1% in the final solution.

3.3.2 GST-Htt-Exon1 Fusion Protein Purification

Disease length (46Q) glutathione S-transferase (GST)-htt-exon1 fusion protein was

purified as previously described.⁵² In short, GST-htt fusion proteins were expressed by induction in *Escherichia coli* with isopropyl-thio-galactopyranoside (IPTG) at 30 °C for 4 h. Cells were lysed using lysozyme (0.5 mg/mL) and sonication with a sonic dismembrator (FisherSci). Liquid chromatography (BioRad LPLC) with a GST affinity column was then used to purify the fusion proteins and the concentration was determined with Coomassie Bradford reagent. High speed centrifugation at 20,000 g for 45 min at 4 °C removed any preexisting aggregates from fusion protein solutions. Incubation of fusion proteins with Factor Xa (Promega, Madison, WI) cleaved the GST tag and initiated aggregation for experiments.

3.3.3 Lipid Vesicle Preparation

Lyophilized lipids of POPC, POPS, and TBLE were dissolved in chloroform and aliquoted into Eppendorf tubes. Aliquots were allowed to dry overnight, and the dry films were stored at -20 °C until needed. POPC and POPS aliquots were redissolved in chloroform and mixed to obtain 75/25% w/w PC/PS samples, which were dried overnight and stored at -20 °C until needed. For experiments, the dried films were rehydrated in tris buffer (150 mM NaCl, Tris-HCl, pH 7.4) for 1 h at 30 °C. Rehydrated lipids were subjected to 10 freeze-thaw cycles using liquid nitrogen. Lipid solutions were then bath sonicated for 1 h and stored at 4 °C.

3.3.4 Thioflavin T (ThT) Aggregation Assay

ThT assays were used to monitor fibril formation of htt-exon1 mimic peptide Nt17Q₃₅P₁₀ incubated with and without various Nt17 peptides. For all conditions Nt17Q₃₅P₁₀ (5 μM) was incubated with ThT (125 μM) in black Costar 96-well plates with flat, clear bottoms. For conditions with Nt17 peptides, 20 μM of each peptide was added, resulting in an Nt17Q₃₅P₁₀:peptide ratio of 1:4. Assays were performed using a SpectraMax M2 microplate reader where ThT fluorescence was measured at 37 °C using excitation and emission

wavelengths of 440 nm and 480 nm respectively. Emission data was collected every 10 min over 18 h. A blank sample containing no peptide was used to collect background fluorescence and correct for background. Samples were run in triplicate and averaged.

3.3.5 Polydiacetylene (PDA) Lipid Binding Assays

Htt-exon1 interactions with lipids were measured using a PDA lipid binding assay using previously reported protocol.⁵³ Briefly, diacetylene monomers of 10,12-tricosadiynoic acid and the lipid system of choice were mixed at a 2:3 molar ratio in 4:1 chloroform/ethanol solution. The solution was evaporated off to yield dry lipid films that were reconstituted in 70 °C tris buffer. Lipid solutions were sonicated (amplitude 50) for 10 min using a dismembrator (FisherSci) and stored overnight at 4 °C to allow for self-assembly of vesicles. For experiments, lipid mixtures were irradiated at 254 nm for 10 min with constant stirring to polymerize the 10,12-tricosadiynoic acid, resulting in a dark blue solution which undergoes a colorimetric shift to red with increased fluorescence when exposed to mechanical stress. Experimental conditions were performed in triplicate in black Costar 96-well plates with flat, clear bottoms. Assays were performed using a SpectraMax M2 microplate reader where fluorescence was measured at 25 °C every 10 min over 18 h using excitation and emission wavelengths of 489 nm and 570 nm respectively. The positive control included saturated NaOH (pH 12) while the negative control consisted of PDA/lipid vesicles and tris buffer. Mutant Nt17 peptides were incubated with htt-exon1 in a 1:1 ratio for 3 h to obtain peptide-containing oligomers. Polymerized vesicles were exposed to htt-exon1(46Q) oligomers at a final concentration of 10 μM. Samples were run in triplicate and averaged.

3.3.6 Atomic Force Microscopy (AFM)

Purified htt-exon1(46Q) (10 μ M) was incubated with Nt17 peptides in a 1:1 protein:peptide ratio in the absence of lipids at 37 °C and 1,400 rpm using an orbital mixer. At selected timepoints, a 2 μ L aliquot of each condition was deposited onto freshly cleaved mica and allowed to sit for 1 min. Mica was then washed with 200 μ L of ultra-pure water and dried with a gentle stream of air. All images were collected with a Nanoscope V Multi-Mode scanning probe microscope (Veeco, Santa Barbara, CA) equipped with a closed loop vertical engage J-scanner. Silicon-oxide cantilevers with 300 kHz resonance frequency and 40 N/m nominal spring constant were used. Scan rates were set between 1 and 2 Hz with cantilever drive frequencies at 10% of resonance. The Matlab image processing toolbox (MathWorks) was used to analyze images as previously described.⁵⁴

3.3.7 Pulled-Tip Capillary Emitter and Capillary Vibrating Sharp-Edge Spray Ionization (cVSSI) Device Fabrication

Descriptions of cVSSI devices have been provided previously.^{55,56} Briefly, epoxy glue was used to secure a piezoelectric transducer to the end of a glass slide coverslip. A glass capillary emitter (0.5 mm I.D.) was pulled (Sutter Instrument Company, Novato, CA) and cut mechanically to the desired I.D. (70-100 μ m) verified under a microscope. The emitter tip was secured to the glass slide coverslip opposite the piezoelectric transducer with glass glue. Using epoxy glue, a fused silica capillary section (250 μ m I.D., 355 μ m O.D.) was inserted into the glass emitter and secured at the flat end. PTFE tubing was attached to the fused silica capillary at one end and secured to a syringe at the other to allow for sample infusion. A 5 cm platinum wire inserted into the end of the PTFE tubing nearest to the cVSSI device and secured with epoxy glue served as an electrode for field-enabled experiments.

3.3.8 Capillary Vibrating Sharp-Edge Electrospray Ionization Mass Spectrometry (cVSSI-MS)

Mutant Nt17 peptides (10 μ M) were incubated with PC/PS (75/25% w/w) lipid vesicles in a 1:10 ratio (peptide:lipid) at 37 °C for 5 h. Lipid vesicles were formed by rehydrating lipid films in 10 mM ammonium acetate, which were then subjected to 10 freeze-thaw cycles using liquid nitrogen followed by bath sonication for 1 h. Samples were analyzed using cVSSI devices and a Q-Exactive hybrid quadrupole Orbitrap (Thermo Fisher, San Jose, CA) mass spectrometer. Spectra were collected in positive ion mode over a mass-to-charge (m/z) range of 300 to 4,000. Samples were infused at a rate of 10 μ L/min with 1.8 kV applied to the Pt wire. The resolving power and AGC target were set to 70,000 and 1×10^6 , respectively. The inlet capillary temperature was maintained at 250 °C. Mass spectra were recorded in triplicate for 30 s each. Between spectra collections the voltage supply to the cVSSI device was turned off and sample was allowed to flow without voltage. Turning off the voltage between collections took into account any variability across triplicate spectra, represented as the standard error of the mean (SEM), that may result from changing devices or variations in plume generation and droplet sizes. Data were analyzed using the Xcalibur 2.2 software suite (Thermo Scientific).

3.4 Results and Discussion

3.4.1 Incorporation of Modified Nt17 Peptides Inhibits Fibril Formation and Alters

Oligomer Morphologies. To determine how the addition of free Nt17 peptides with various modifications impacts fibril formation, Nt17Q₃₅P₁₀ peptide (5 μ M) was incubated with Nt17 peptides in a 1:4 Nt17Q₃₅P₁₀:Nt17 peptide molar ratio. Fibril formation was monitored as a function of time using ThT, which exhibits enhanced fluorescence when bound to fibril-associated β -sheet structure (Figure 3.1). Nt17Q₃₅P₁₀ aggregation in the absence of Nt17 peptides

was measured for comparison. The ThT signal for each condition was averaged across triplicate runs.

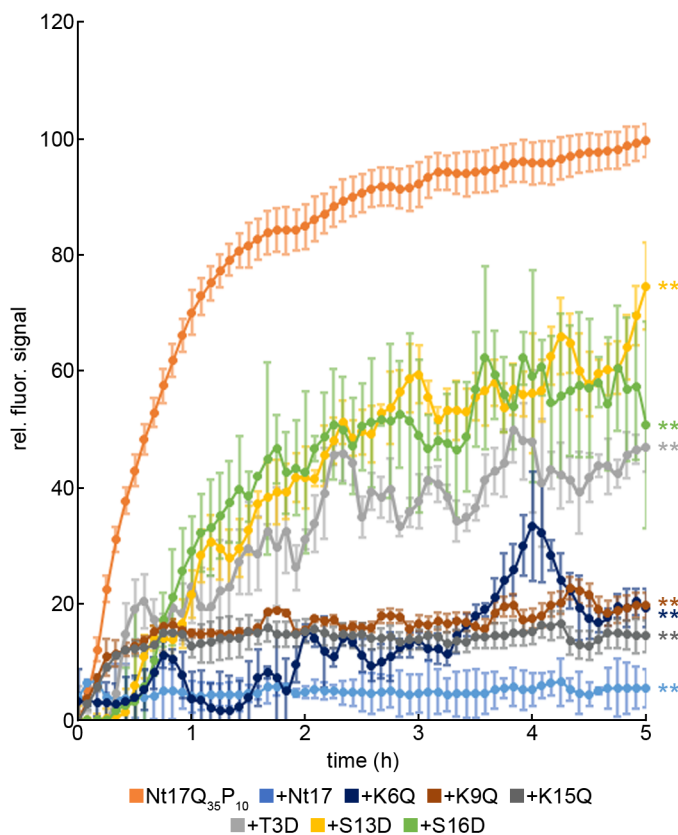


Figure 3.1. ThT aggregation assay data for htt-exon1 mimic peptide Nt17Q₃₅P₁₀ incubated alone or with each Nt17 peptide. Nt17Q₃₅P₁₀ concentration was approximately 5 μ M, and incubations with peptide were approximately a 1:4 Nt17Q₃₅P₁₀:peptide ratio. Conditions were calculated and averaged across all runs, then normalized to the Nt17Q₃₅P₁₀ control. Error bars represent SEM. Using a Student's t-test, ** represents a p-value of <0.01 relative to the Nt17Q₃₅P₁₀ control.

As Nt17 peptides are known inhibitors of htt aggregation,^{21,50} the impact of incubating Nt17Q₃₅P₁₀ with Nt17 peptides was dependent on the specific Nt17 peptide used, though all peptides significantly reduced fibril formation ($p < 0.01$) relative to the Nt17Q₃₅P₁₀ control. Wild-type Nt17 peptide, with no mutations, was the most efficient at inhibiting fibril formation. Wild-type Nt17 peptides completely inhibited fibril formation with a 92.2% reduction in signal relative to the Nt17Q₃₅P₁₀ control. Nt17 peptides containing mutations mimicking acetylation (K6Q,

K9Q, or K15Q), which effectively remove a positive charge from within Nt17, were also efficient at inhibiting fibril formation, but less efficient than wild-type Nt17 peptide. Nt17 peptides with K6Q, K9Q, and K15Q reduced fluorescent signal relative to the Nt17Q₃₅P₁₀ control by 79.9%, 74.3%, and 74.3% respectively. Nt17 peptides containing mutations mimicking phosphorylation (T3D, S13D, or S16D), which add a negative charge to Nt17, were the least efficient at inhibiting fibril formation. Relative to the Nt17Q₃₅P₁₀ control, Nt17 peptides containing T3D, S13D, or S16D resulted in a 46.4%, 25.0%, and 29.3% reduction in signal respectively.

To further investigate the effect of Nt17 peptide incorporation on htt aggregation, the morphologies of pure htt-exon1(46Q) oligomers and Nt17 peptide-containing oligomers were evaluated using AFM (Figures 3.2 and 3.3). Considering that incorporation of the Nt17 peptides is likely targeting oligomers, the analysis focused on these structures. Freshly prepared htt-exon1(46Q) (10 μ M) was incubated in the presence and absence of Nt17 peptides in a 1:1 protein:peptide molar ratio, and oligomers were observed over all incubation conditions after 3 h. Morphologies were evaluated using automated Matlab scripts that determined morphological features of each individually identified oligomer. Within a collected image, an oligomer was defined as any feature that contained less than 50 pixels.

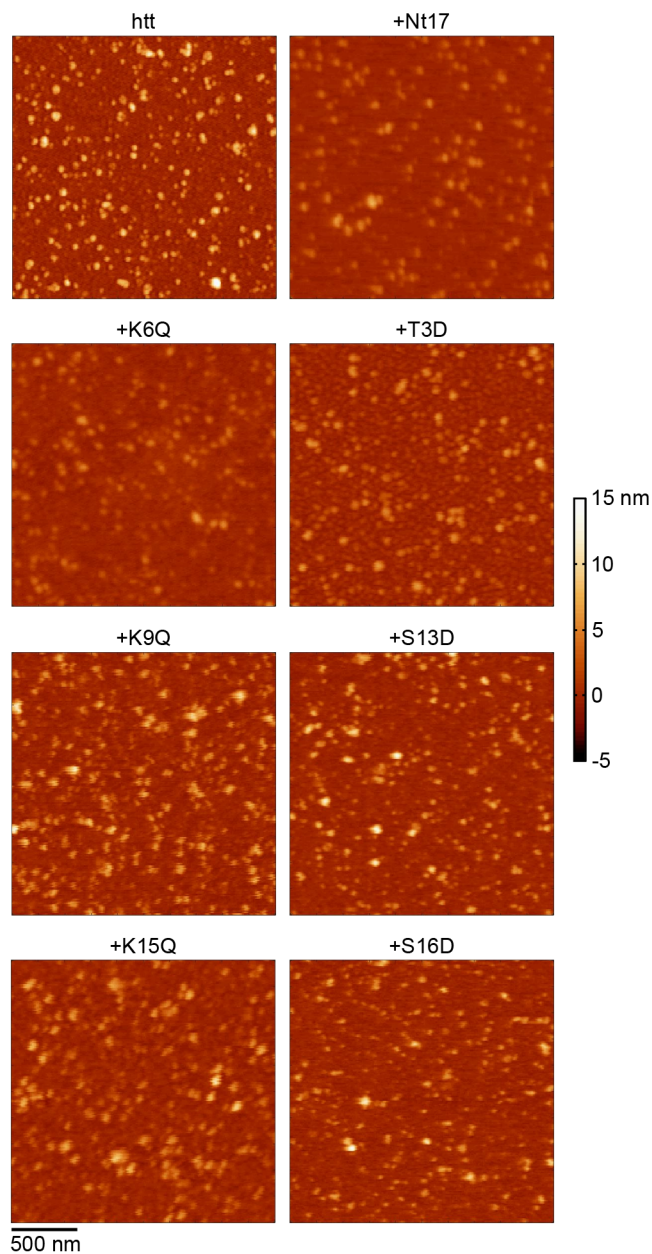


Figure 3.2. Representative AFM images for all peptide conditions. 10 μ M htt-exon1(46Q) incubated alone or with each Nt17 peptide for 3 h. The protein:peptide ratio was 1:1. The colormap and scale bar are applicable to all images.

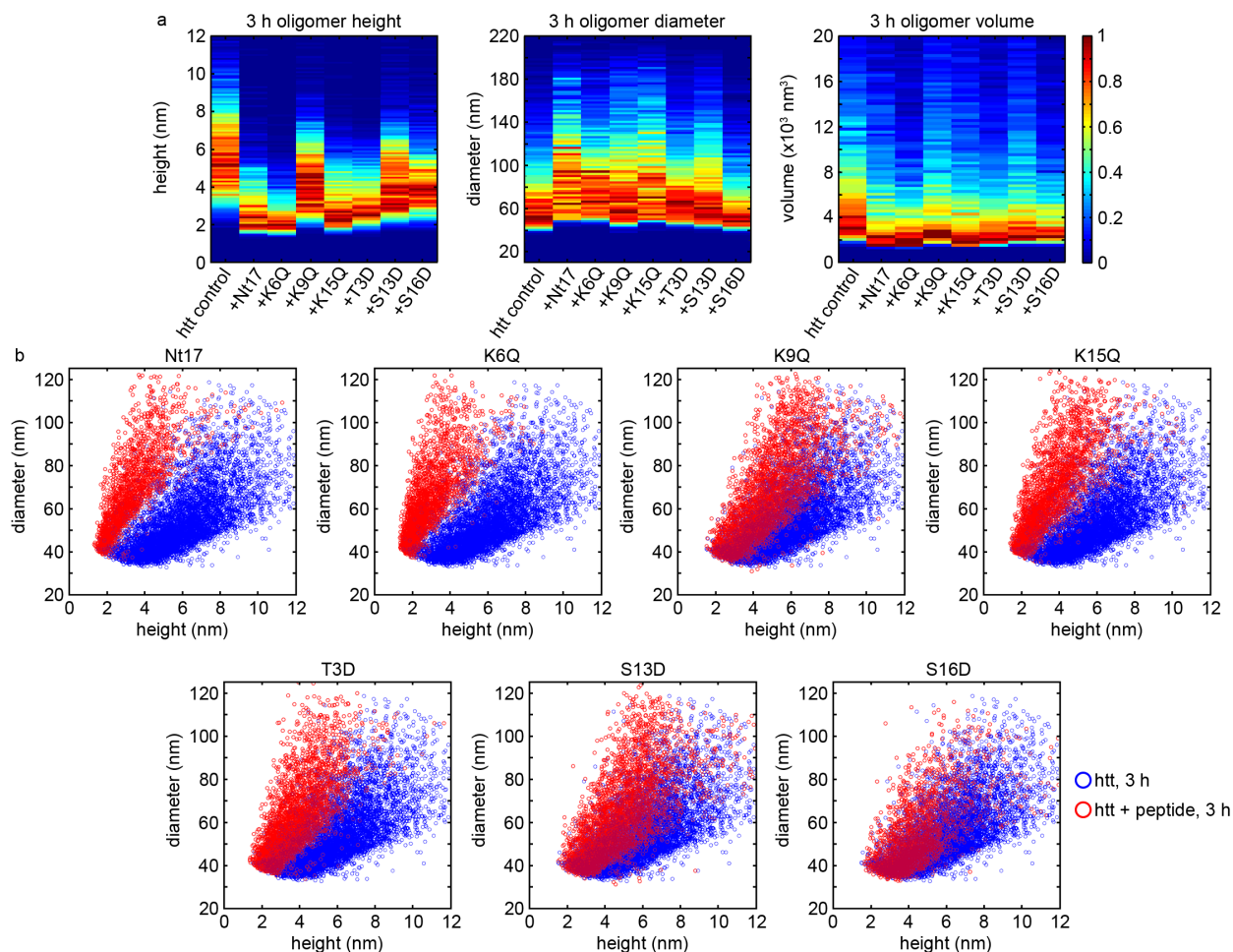


Figure 3.3. AFM analysis of observed htt-exon1(46Q) oligomeric aggregates in the absence and presence of each Nt17 peptide. (a) Histograms of oligomer heights, diameters, and volumes for each condition. (b) Correlation plots of diameters and heights of each oligomer at 3 h for htt-exon1(46Q) versus htt-exon1(46Q) with each Nt17 peptide.

Oligomer morphology was evaluated by comparing diameters, heights, and volumes of Nt17 peptide-containing oligomers to the pure htt-exon1(46Q) oligomers at 3 h. Overall, peptide-containing oligomers shifted to smaller heights, slightly larger diameters, and smaller volumes (Figure 3.2a). The pure htt-exon1(46Q) oligomers had a mode height of approximately 5 nm, diameter of 50 nm, and volume of $3.0 \times 10^3 \text{ nm}^3$ while peptide-containing oligomers ranged from 2-4 nm in height, 50-60 nm in diameter, and $2.0 \times 10^3 \text{ nm}^3$ to $3.0 \times 10^3 \text{ nm}^3$ in volume. Based on volume measurements, peptide-containing oligomers were smaller. In addition, peptide-

containing oligomers were typically shorter (height) but were more spread out (diameters). This suggests that the peptide-containing oligomers were more easily compressed, e.g. less rigid, in comparison to pure htt-exon1(46Q) oligomers. The smaller overall size and reduced aggregate rigidity is most likely due to the reduction in polyQ and proline-rich domains contained in full-length htt-exon1, as peptide containing oligomers flatten out onto the mica surface. Looking more closely at oligomer diameter versus height of peptide-containing oligomers compared to pure htt-exon1(46Q) oligomers at 3 h, trends suggesting different peptide incorporation efficiencies emerge (Figure 3.2b). The most pronounced shift occurred with wild-type Nt17 peptide-containing oligomers, as the peptide-containing oligomers show virtually no overlap with the pure htt-exon1(46Q) containing oligomers. An intermediate shift occurred with oligomers containing Nt17 peptides with mutations mimicking acetylation (K6Q, K9Q, and K15Q), where slightly more overlap with the pure htt-exon1(46Q) oligomers overall. The smallest shifts occurred with oligomers containing Nt17 peptides with mutations mimicking phosphorylation (T3D, S13D, and S16D), where overall there was the most overlap with the pure htt-exon1(46Q) oligomers. The peptide-containing oligomers that have less overlap with the pure htt-exon1(46Q) oligomers indicate the peptide has been more efficiently incorporated, and these trends match well with those observed in the ThT aggregation assay. For example, of the three phosphorylation mimicking peptides, T3D displayed the least amount of overlap, and it was the most effective in reducing fibril formation of these three peptides.

With respect to htt, Nt17 domains associate to form the α -helix rich core structure of oligomers,^{18,17} bringing polyQ domains into close proximity to promote nucleation.^{13,19–21} Nt17 peptides inhibit htt fibril formation by incorporating into the α -helix rich oligomer intermediates, increasing the spacing between polyQ domains.²¹ This enhanced spacing reduces the efficiency

of nucleation. The relative efficiency of the mutant Nt17 peptides to inhibit fibril formation suggests altered ability to incorporate into oligomers. That is, wild type Nt17 peptides readily incorporate into oligomers. Acetylation mimicking mutations reduce the ability to incorporate into oligomers, and Nt17 peptides with phosphorylation mimicking mutations are the least efficiently incorporated into oligomers. Phosphorylation^{12,44,57} and acetylation¹¹ within Nt17 of intact htt-exon1 proteins reduce fibril formation, with phosphorylation having a larger inhibitory effect. This suggests that these post-translational modifications reduce aggregation in full-length htt-exon1 by destabilizing oligomer intermediates and reducing the efficiency of nucleation.

The notion that the effectiveness of Nt17 peptides to impeded fibril formation corresponding to their relative incorporation into oligomer intermediates is further supported by altered oligomer morphologies observed by AFM. Reduction of the polyQ and proline-rich domains reduce the protein mass incorporated into oligomers, resulting in small, less rigid oligomers. The largest shift in morphology is observed with free wild-type Nt17, with more efficient incorporation causing a larger reduction in polyQ density that shifts toward smaller oligomers. The peptides mimicking acetylation have an intermediate incorporation and the phosphorylation mimics are least efficiently incorporated; all peptides generally shift to smaller oligomer sizes, but relative to wild-type the shift is less pronounced for acetylation mimics and least pronounced for phosphorylation mimics. Once incorporated, mutations within Nt17 likely impact oligomer stability and the ability of oligomers to undergo nucleation. The incorporation of free Nt17 peptide reduces the polyQ domain density in oligomers, decreasing the local concentration to prevent nucleation and inhibit subsequent fibril formation. With more efficient peptide incorporation, nucleation is more effectively inhibited.

3.4.2 Modifications Within Nt17 Alters Complex Formation Between Peptide and Lipids.

Nt17 facilitates htt-exon1(46Q) interactions with lipid and can modify aggregation on membranes.¹⁰ Nt17 peptide has a similar interaction mechanism with membranes as htt-exon1(46Q),³¹ and the mechanism is not significantly altered by the addition of glutamines.⁵⁸ Therefore, synthetic Nt17 peptide with and without modifications was used to investigate complex formation and determine the degree of membrane interaction between Nt17 and lipids using cVSSI-MS. Each Nt17 peptide (10 μ M) was incubated with POPC/POPS (75/25% w/w) in a 1:10 peptide:lipid molar ratio for 5 h prior to analysis with cVSSI-MS. Experiments were performed in triplicate using positive ion mode. Identified isotopic distributions of each complex were deconvoluted using automated Matlab scripts that determine the individual contributions of each possible configuration of a complex by using theoretical spectra to generate the best fit of the raw data over 1.0×10^6 simulations. The root mean squared deviation (RMSD) between the simulated best fit and the raw data was calculated. For each identified complex, the integrated peak area was calculated by integrating the ion signal for each isotopic distribution of the given complex. Complexes are represented in [M+L] format, where M represents Nt17 peptide and L represents lipid, and the integrated peak areas for each complex were normalized to that of the singly-charged POPC lipid monomer ($[L+H]^+$ at m/z 760.59), to correct for plume generation and performance since it was the most abundant peak present across all sample conditions, then represented as a percentage of all peptide-containing ions.

Peptide/lipid complexation was observed to some degree with all peptides studied. Overall, wild-type Nt17 yielded a greater variety of peptide/lipid complexes that were generally more abundant relative to those of the K6Q, K9Q, and K15Q acetylation mimics and the T3D, S13D, and S16D phosphorylation mimics (Figure 3.4a). Overall, all peptide complexes followed

the same observed trend as wild-type peptide with relative complex abundances of $M > 2M > 3M > 4M$ and increased lipid content further reduced complex abundance such that $L > 2L > 3L$. However, the exact lipid contributions for complexes formed by different peptides were more variable. Incubation of wild-type Nt17 peptide with PC/PS lipid yielded eight unique complexes, the most out of all peptides studied, containing upwards of 4M and 3L (Figure 3.4b, Table 3.1). After incubation of the K6Q mutant three complexes were identified that contained up to 2M and 2L (Figure 3.4c, Table 3.2). The K9Q mutant yielded four complexes after incubation that contained up to 3M and 2L (Figure 3.4d, Table 3.3). Incubation of the K15Q mutant yielded two complexes that contained M and up to 2L (Figure 3.4e, Table 3.4). After the incubation of the T3D mutant, four complexes were identified that contained up to 4M and L (Figure 3.5f, Table 3.5). The S13D mutant yielded five complexes after incubation that contained up to 3M and 2L (Figure 3.4g, Table 3.6). Incubation of the S16D mutant yielded seven complexes that contained up to 4M and 2L (Figure 3.4h, Table 3.7).

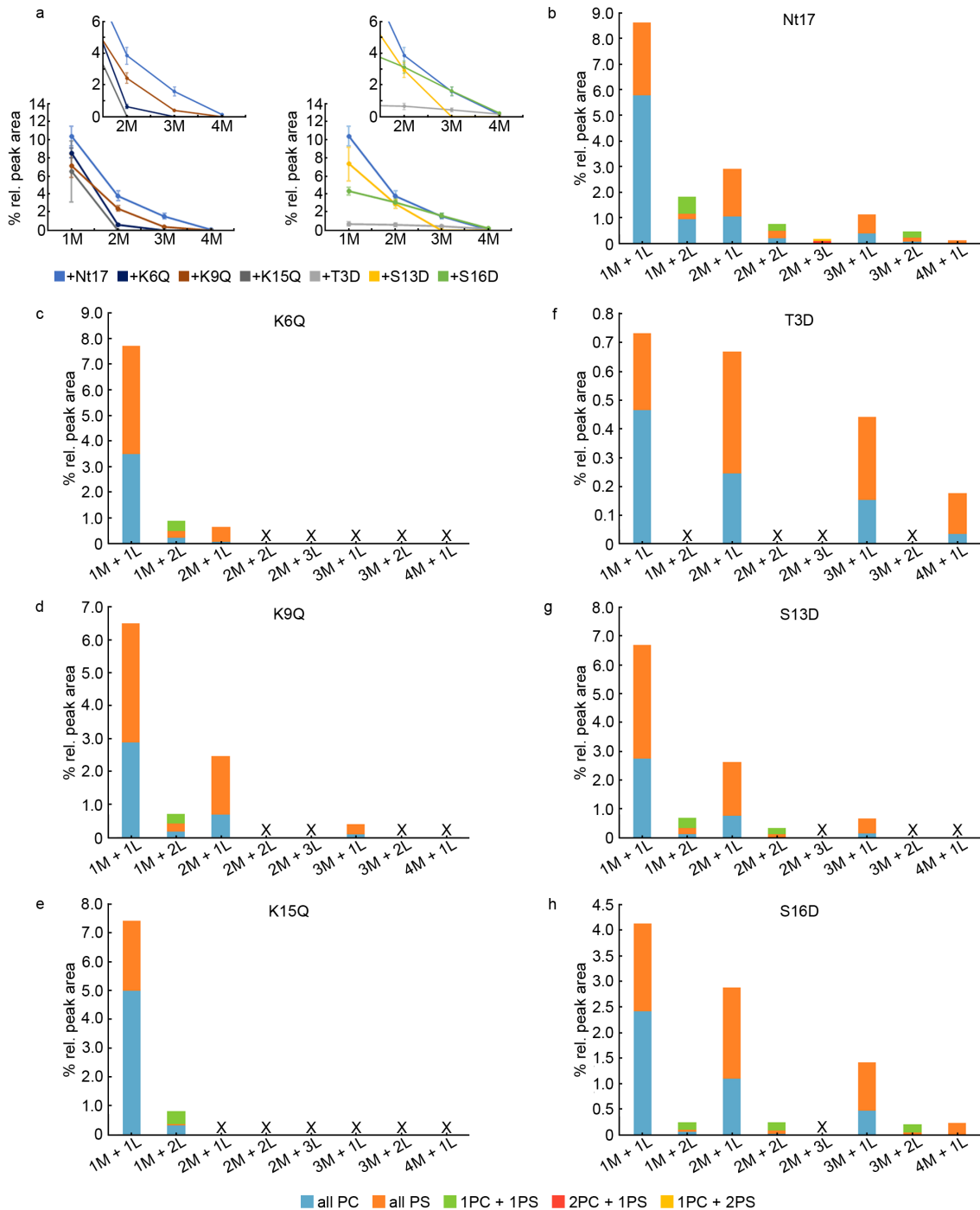


Figure 3.4. Analysis of Nt17/lipid complexation in the presence of POPC/POPS (75/25% w/w) vesicles using cVSSI-MS. Peptide is denoted as M and lipid as L. The Nt17 peptide concentration was 10 μ M and the peptide:lipid ratio was 1:10. (a) The total percent relative peak areas for 1M, 2M, 3M, and 4M complexes identified for each peptide after 5 h incubation with lipid. (b-h) The percent relative peak areas for each identified complex of a given peptide with specified lipid iteration contributions. X indicates that the corresponding complex was not identified for the given condition.

Table 3.1. Identified ions of wild-type Nt17 peptide incubated with POPC/POPS lipid vesicles with their respective possible iterations, contribution of each iteration, RMSD from iteration determinations, percent relative peak areas, and SEM from triplicate spectra.

Ion^a	Iterations	Avg. Iteration Contribution	Avg. RMSD	Avg. % Relative Peak Area	SEM
1M+1L	1M+1PC	0.670	0.0758	5.796	0.578
	1M+1PS	0.331		2.846	0.215
1M+2L	1M+2PC	0.514	0.0169	0.935	0.169
	1M+2PS	0.127		0.230	0.038
	1M+1PC+1PS	0.358		0.646	0.103
2M+1L	2M+1PC	0.357	0.0786	1.042	0.139
	2M+1PS	0.643		1.871	0.215
2M+2L	2M+2PC	0.249	0.0465	0.196	0.050
	2M+2PS	0.398		0.301	0.046
	2M+1PC+1PS	0.353		0.267	0.048
2M+3L	2M+3PC	0.042	0.0739	0.009	0.005
	2M+3PS	0.022		0.005	0.005
	2M+2PC+1PS	0.526		0.086	0.013
	2M+1PC+2PS	0.210		0.080	0.029
3M+1L	3M+1PC	0.328	0.0573	0.377	0.077
	3M+1PS	0.672		0.759	0.121
3M+2L	3M+2PC	0.136	0.0545	0.076	0.040
	3M+2PS	0.284		0.150	0.063
	3M+1PC+1PS	0.581		0.244	0.021
4M+1L	4M+1PC	0.010	0.1178	0.001	0.001
	4M+1PS	0.990		0.125	0.021

^a The following monoisotopic masses were used to assign peaks: 1973.03 for Nt17 peptide, 759.58 for POPC lipid, and 760.51 for POPS lipid.

Table 3.2. Identified ions of K6Q mutant Nt17 peptide incubated with POPC/POPS lipid vesicles with their respective possible iterations, contribution of each iteration, RMSD from iteration determinations, percent relative peak areas, and SEM from triplicate spectra.

Ion^a	Iterations	Avg. Iteration Contribution	Avg. RMSD	Avg. % Relative Peak Area	SEM
1M+1L	1M+1PC	0.455	0.1321	3.490	0.106
	1M+1PS	0.545		4.214	0.381
1M+2L	1M+2PC	0.235	0.0515	0.208	0.015
	1M+2PS	0.297		0.272	0.069
	1M+1PC+1PS	0.468		0.413	0.004
2M+1L	2M+1PC	0.085	0.0904	0.054	0.026
	2M+1PS	0.915		0.592	0.135

^a The following monoisotopic masses were used to assign peaks: 1973.00 for K6Q mutant Nt17 peptide, 759.58 for POPC lipid, and 760.51 for POPS lipid.

Table 3.3. Identified ions of K9Q mutant Nt17 peptide incubated with POPC/POPS lipid vesicles with their respective possible iterations, contribution of each iteration, RMSD from iteration determinations, percent relative peak areas, and SEM from triplicate spectra.

Ion^a	Iterations	Avg. Iteration Contribution	Avg. RMSD	Avg. % Relative Peak Area	SEM
1M+1L	1M+1PC	0.449	0.1333	2.883	0.387
	1M+1PS	0.551		3.606	0.642
1M+2L	1M+2PC	0.223	0.0589	0.170	0.071
	1M+2PS	0.258		0.242	0.119
	1M+1PC+1PS	0.519		0.285	0.074
2M+1L	2M+1PC	0.282	0.0742	0.689	0.100
	2M+1PS	0.718		1.764	0.251
3M+1L	3M+1PC	0.197	0.0757	0.076	0.022
	3M+1PS	0.803		0.326	0.046

^a The following monoisotopic masses were used to assign peaks: 1973.00 for K9Q mutant Nt17 peptide, 759.58 for POPC lipid, and 760.51 for POPS lipid.

Table 3.4. Identified ions of K15Q mutant Nt17 peptide incubated with POPC/POPS lipid vesicles with their respective possible iterations, contribution of each iteration, RMSD from iteration determinations, average percent relative peak areas, and SEM from triplicate spectra.

Ion^a	Iterations	Avg. Iteration Contribution	Avg. RMSD	Avg. % Relative Peak Area	SEM
1M+1L	1M+1PC	0.594	0.1000	3.450	1.809
	1M+1PS	0.406		2.311	1.156
1M+2L	1M+2PC	0.412	0.1598	0.317	0.174
	1M+2PS	0.073		0.038	0.038
	1M+1PC+1PS	0.515		0.442	0.301

^a The following monoisotopic masses were used to assign peaks: 1973.00 for K15Q mutant Nt17 peptide, 759.58 for POPC lipid, and 760.51 for POPS lipid.

Table 3.5. Identified ions of T3D mutant Nt17 peptide incubated with POPC/POPS lipid vesicles with their respective possible iterations, contribution of each iteration, RMSD from iteration determinations, average percent relative peak areas, and SEM from triplicate spectra.

Ion^a	Iterations	Avg. Iteration Contribution	Avg. RMSD	Avg. % Relative Peak Area	SEM
1M+1L	1M+1PC	0.639	0.0821	0.466	0.147
	1M+1PS	0.361		0.266	0.084
2M+1L	2M+1PC	0.365	0.0688	0.247	0.076
	2M+1PS	0.635		0.422	0.122
3M+1L	3M+1PC	0.341	0.0581	0.155	0.051
	3M+1PS	0.659		0.287	0.077
4M+1L	4M+1PC	0.185	0.0843	0.035	0.018
	4M+1PS	0.815		0.143	0.038

^a The following monoisotopic masses were used to assign peaks: 1987.02 for T3D mutant Nt17 peptide, 759.58 for POPC lipid, and 760.51 for POPS lipid.

Table 3.6. Identified ions of S13D mutant Nt17 peptide incubated with POPC/POPS lipid vesicles with their respective possible iterations, contribution of each iteration, RMSD from iteration determinations, average percent relative peak areas, and SEM from triplicate spectra.

Ion^a	Iterations	Avg. Iteration Contribution	Avg. RMSD	Avg. % Relative Peak Area	SEM
1M+1L	1M+1PC	0.425	0.1276	2.748	0.355
	1M+1PS	0.575		3.955	1.118
1M+2L	1M+2PC	0.152	0.0495	0.117	0.082
	1M+2PS	0.294		0.221	0.145
	1M+1PC+1PS	0.554		0.343	0.174
2M+1L	2M+1PC	0.300	0.0871	0.765	0.002
	2M+1PS	0.700		1.852	0.322
2M+2L	2M+2PC	0.044	0.0569	0.009	0.006
	2M+2PS	0.273		0.116	0.081
	2M+1PC+1PS	0.683		0.203	0.072
3M+1L	3M+1PC	0.242	0.0372	0.154	0.012
	3M+1PS	0.758		0.499	0.074

^a The following monoisotopic masses were used to assign peaks: 2001.03 for S13D mutant Nt17 peptide, 759.58 for POPC lipid, and 760.51 for POPS lipid.

Table 3.7. Identified ions of S16D mutant Nt17 peptide incubated with POPC/POPS lipid vesicles with their respective possible iterations, contribution of each iteration, RMSD from iteration determinations, average percent relative peak areas, and SEM from triplicate spectra.

Ion ^a	Iterations	Avg. Iteration Contribution	Avg. RMSD	Avg. % Relative Peak Area	SEM
1M+1L	1M+1PC	0.585	0.1198	2.413	0.232
	1M+1PS	0.415		1.710	0.156
1M+2L	1M+2PC	0.209	0.0610	0.055	0.025
	1M+2PS	0.158		0.043	0.019
	1M+1PC+1PS	0.633		0.146	0.037
2M+1L	2M+1PC	0.380	0.0815	1.097	0.134
	2M+1PS	0.620		1.783	0.203
2M+2L	2M+2PC	0.074	0.0565	0.023	0.019
	2M+2PS	0.206		0.060	0.026
	2M+1PC+1PS	0.720		0.167	0.019
3M+1L	3M+1PC	0.328	0.0467	0.476	0.104
	3M+1PS	0.672		0.938	0.101
3M+2L	3M+2PC	0.015	0.0967	0.002	0.001
	3M+2PS	0.201		0.044	0.016
	3M+1PC+1PS	0.784		0.163	0.049
4M+1L	4M+1PC	0.025	0.1226	0.007	0.005
	4M+1PS	0.975		0.226	0.041

^a The following monoisotopic masses were used to assign peaks: 2001.03 for S16D mutant Nt17 peptide, 759.58 for POPC lipid, and 760.51 for POPS lipid.

Considering htt demonstrates a preference for anionic lipids⁴¹ and the variation in contribution for different complex configurations, further analysis of complex lipid compositions was performed where the percentage of POPS per complex was evaluated (Figure 3.5). Analysis revealed that higher order complexes that contain more peptides tend to favor the incorporation of anionic POPS over zwitterionic POPC. For wild-type Nt17, the average POPS composition of the [M+L] complex was 33.05%, [2M+L] was 64.33%, [3M+L] was 67.24%, and [4M+L] was 99.01% (Figure 3.5a). The average POPS composition for the K6Q mutant complexes [M+L] and [2M+L] were 54.5% and 91.52% respectively (Figure 3.5b). For the K9Q mutant, average POPS composition for [M+L] was 55.14%, [2M+L] was 71.77%, and [3M+L] was 80.26%

(Figure 3.5c). The average POPS composition for the K15Q mutant complexes [M+L] and [M+2L] were 29.44% and 19.22% respectively (Figure 3.5d). For the T3D mutant the average POPS composition was 36.13% for [M+L], 63.46% for [2M+L], 65.94% for [3M+L], and 81.50% for [4M+L] (Figure 3.5e). The S13D mutant had average POPS compositions of 57.54% for [M+L], 69.98% for [2M+L], and 75.75% for [3M+L] (Figure 3.5f). The average POPS composition for the S16D mutant complexes [M+L], [2M+L], [3M+L], and [4M+L] were 41.50%, 61.97%, 67.16%, and 97.48% respectively (Figure 3.5g). Despite the clear trend of higher order complexes containing more peptide correlating to increased POPS composition, an increase in the number of lipids incorporated into a complex did not produce a clear trend.

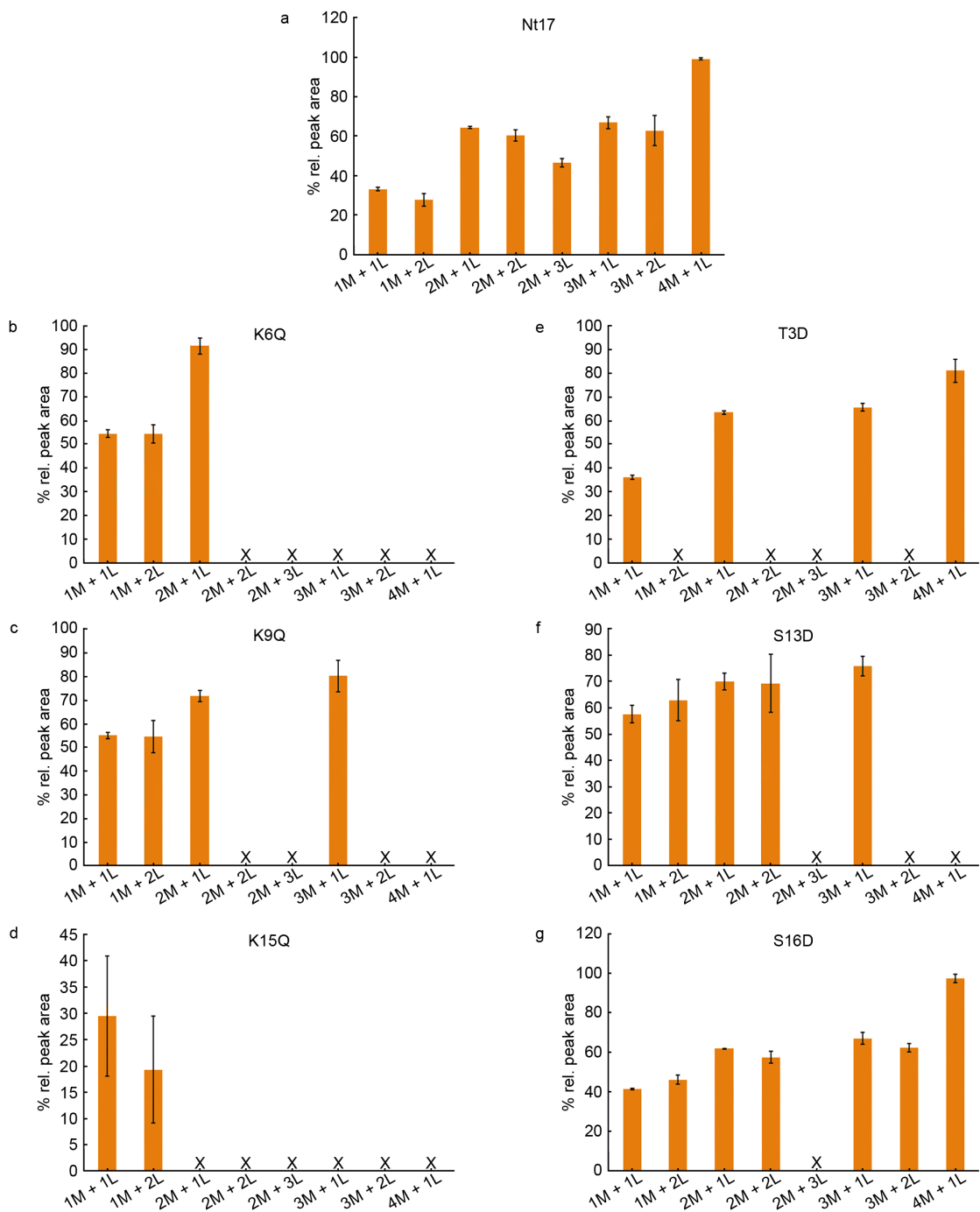


Figure 3.5. The percent POPS composition for each identified complex of a peptide. X indicates that the corresponding complex was not identified for the given condition. Error bars represent SEM.

For each peptide, the relative peak areas of complexes containing M, 2M, 3M, and 4M peptide were calculated and the percentage of those complexes that contained lipid was determined (Figure 3.6). For wild-type Nt17 the 4M species only existed as lipid bound (100%), while 3M, 2M, and M complexes were 39.9%, 27.8%, and 12.8% lipid bound, respectively (Figure 3.6a). For K6Q, only M (8.7%) and 2M (20.7%) complexes contained lipid. 3M complexes were observed, and though none were lipid bound, the 3M complexes were of lower relative peak area than those of the M and 2M (Figure 3.6b). In the case of K9Q, 8.4% of M, 19.1% of 2M, and 24.6% of 3M complexes were lipid bound (Figure 3.6c). K15Q only formed M complexes, of which 6.6% were lipid bound (Figure 3.6d). T3D 4M complexes were always lipid bound (100%) followed by 3M (4.4%), 2M (2.9%), and M (1.1%) complexes (Figure 3.6e). For S13D the 2M complexes were more often lipid bound than M complexes, at 16.9% and 9.2% respectively, and much like K6Q the 3M complexes only existed without lipid but were of lower relative peak area than the M and 2M complexes (Figure 3.6f). For S16D M, 2M, 3M, and 4M complexes were observed and 6.6%, 11.8%, 21.4%, and 100% of those complexes, respectively, were lipid bound (Figure 3.6g). Generally, as peptides formed multimeric species their probability of being lipid bound increased, suggesting that oligomerization enhances lipid association.

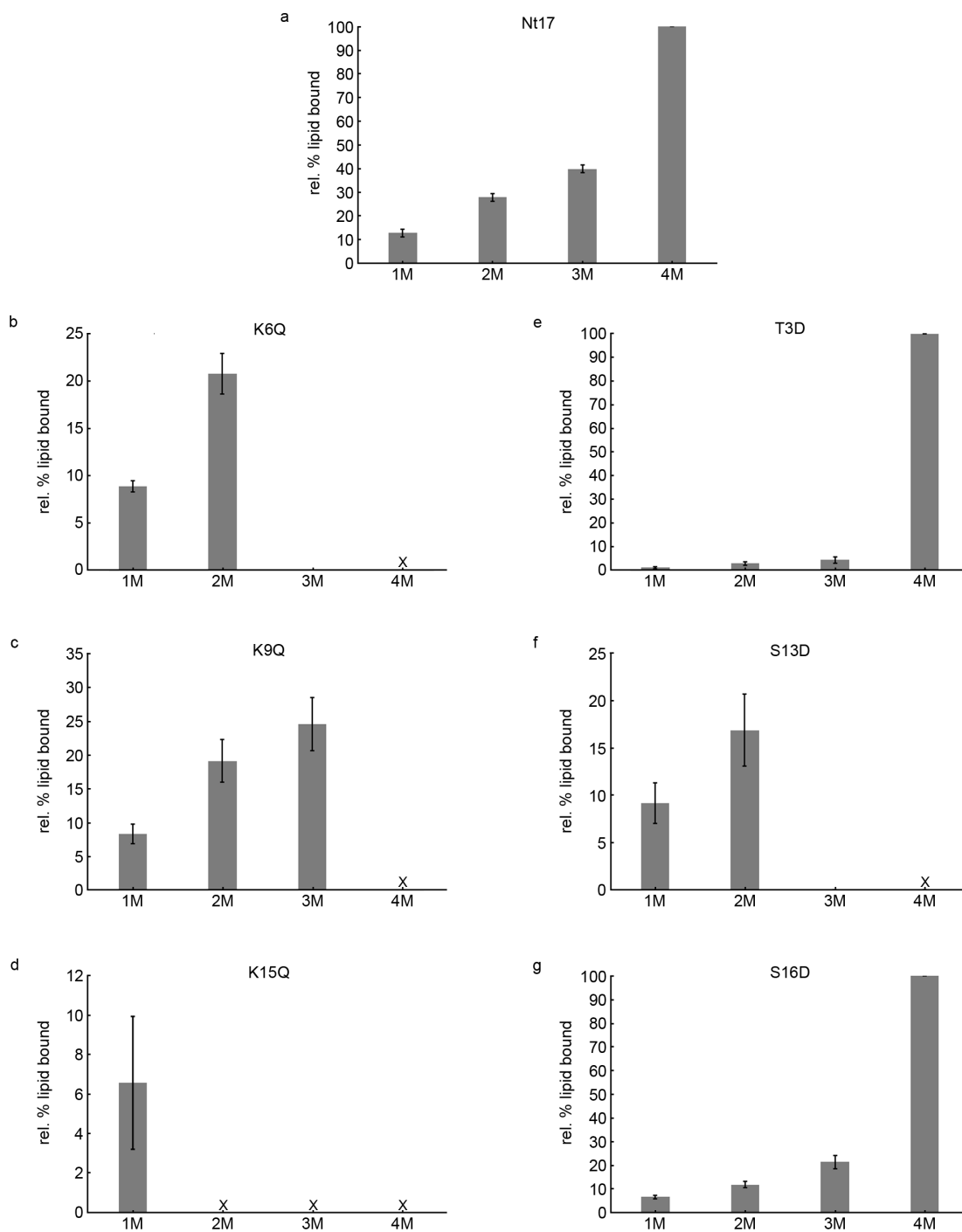


Figure 3.6. The relative percent of the total monomeric (1M), dimeric (2M), trimeric (3M), and tetrameric (4M) species that are lipid bound for each peptide. Error bars represent SEM. X indicates that species containing that number of peptides were not identified for a given peptide. If no X is indicated and no bar is present, all species identified for that number of peptides did not contain lipid.

Nt17 facilitates lipid interactions via a transition to an amphipathic α -helix,^{16,22} a transition that still occurs even with mutations mimicking acetylation and phosphorylation. Previous studies have demonstrated that acetylation does not alter α -helical structure with respect to lipid binding¹¹ and the phosphomimic mutations also do not alter secondary peptide structure.^{43,45} The interaction between Nt17 and lipid bilayers is summed up in four general steps: approach, reorganization, anchoring, and insertion.⁵⁸ Generally the approach step is driven by charged residues within Nt17; when Nt17 is exposed to a POPE membrane early interactions occur between the membrane and S13, K15, or S16.⁵⁸ Once at the membrane surface, the structure and orientation of Nt17 is stabilized by salt bridges formed between the membrane and peptide residues K6, K9, and E12 and hydrogen bonding between the membrane and peptide involving residues T3 and S13.⁵⁸ Another important consideration is the role of lipid composition in Nt17/lipid interactions, as changes to lipid composition can impact Nt17 approach and overall orientation at the membrane surface⁴⁰ in addition to the degree of insertion.⁵⁹ For pure POPC membranes, Nt17 favors a C-terminal approach where S13, K15, and S16 are close to the membrane surface while T3, K6, and K9 broadly sample orientations ranging from parallel to antiparallel with the membrane surface.⁴⁰ POPC/POPS vesicles demonstrate stronger interactions with Nt17 compared to pure POPC vesicles, and increasing POPS content increases Nt17 affinity for the membrane, demonstrating a major electrostatic contribution to peptide/membrane interactions where F11 inserts into the membrane to anchor the peptide.⁵⁹ With these considerations, it is likely that the mutations in this study alter the approach of the peptide and stabilizing interactions at the membrane surface including electrostatics, salt-bridge formation, and hydrogen bonding.

3.4.3 Oligomer/Lipid Interactions are Modified by the Incorporation of Modified Nt17

Peptides. Considering the ThT assays and AFM experiments indicate that oligomerization and subsequent nucleation is altered in addition to Nt17/lipid complexation, and with oligomeric species being the most lipid active⁶⁰ further characterization of oligomeric interactions with respect to lipid binding was necessary. To determine the impact incorporating free Nt17 peptides into oligomeric structures had on their ability to bind lipids, a colorimetric/fluorescent membrane binding assay with lipid/PDA vesicles was used. The lipid systems utilized in these experiments were TBLE and POPC/POPS (75/25% w/w). When exposed to proteins, the fluorescence of each system directly correlates to the extent of protein/lipid interaction, and the fluorescent signals for all conditions were normalized to the htt-exon1(46Q) control and averaged across all runs (Figure 3.7).

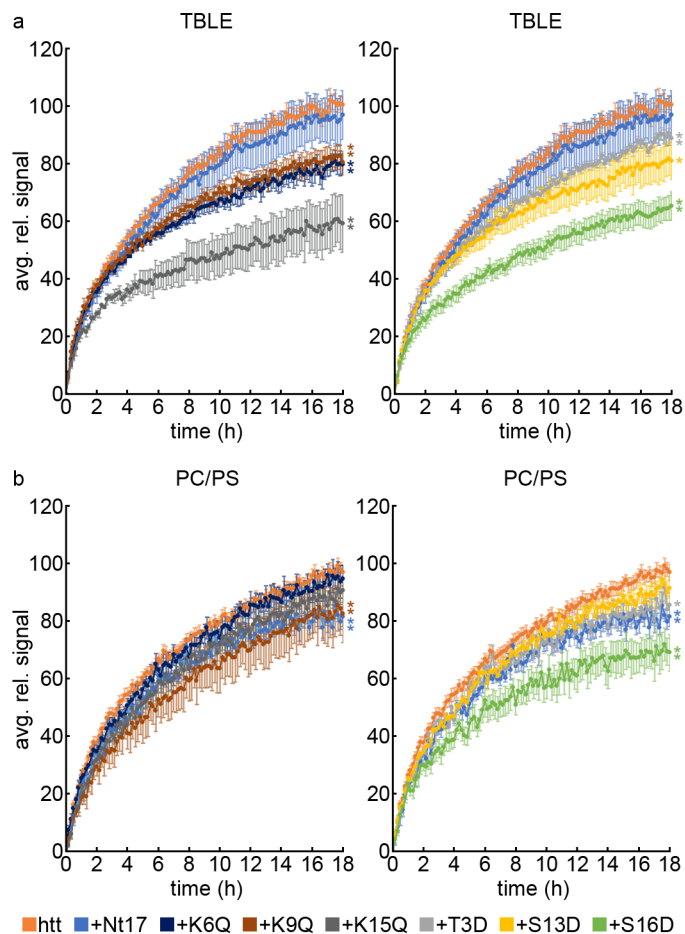


Figure 3.7. PDA/lipid binding assays for htt-exon1(46Q) incubated alone or with each Nt17 peptide in the presence of different lipid systems. Oligomers were incubated in the presence of (a) TBLE or (b) PC/PS. Htt-exon1(46Q) concentration was 10 μ M, and the protein:peptide ratio was 1:1. All conditions were calculated and averaged across all runs then normalized as a percentage to the htt-exon1(46Q) control. Error bars represent SEM. Using a Student's t-test, * represents a p-value of <0.05 and ** represents a p-value of <0.01 relative to the htt-exon1(46Q) control.

The incubation of htt-exon1(46Q) oligomers with free Nt17 peptides generally reduced interactions with TBLE relative to oligomers composed purely of htt-exon1(46Q) (Figure 3.7a). Oligomers containing free, wild-type Nt17 peptides demonstrated virtually no change in lipid interactions. However, oligomers containing peptides mimicking acetylation showed significant reductions in lipid binding ($p < 0.01$ for all three peptides). Specifically, the K15Q mutant had the greatest impact, with approximately a 40% reduction in signal relative to the htt-exon1(46Q)

control. The K6Q and K9Q mutants each demonstrated approximately a 20% reduction in signal relative to the htt-exon1(46Q) control. Oligomers containing peptides mimicking phosphorylation also showed significant reductions in lipid binding ($p < 0.01$ for T3D and S16D, $p < 0.05$ for S13D). Oligomers containing S16D mutant peptides had the largest impact, with approximately a 35% reduction in signal. Though less significant statistically, oligomers containing S13D peptides demonstrated approximately a 20% reduction in signal. Oligomers containing T3D peptides had the lowest impact, with an approximately 10% reduction in signal.

In the case of the PC/PS lipid system, generally the impacts of incorporating free Nt17 peptides were less than those observed with TBLE (Figure 3.7b). Oligomers containing free, wild-type Nt17 peptides showed a significant reduction in signal ($p < 0.01$) of approximately 15%. For oligomers containing peptides mimicking acetylation, only the K9Q peptide showed a significant reduction in signal ($p < 0.01$) by approximately 15%. The K6Q and K15Q peptide-containing oligomers showed no significant changes in lipid interactions relative to the htt-exon1(46Q) control. For oligomers containing peptides mimicking phosphorylation, only those containing S16D and T3D peptides showed significant reductions in lipid binding ($p < 0.01$ and $p < 0.05$ respectively). Oligomers containing S16D peptides showed approximately a 30% reduction in signal, while those containing T3D peptides had less of an impact with approximately a 10% reduction in signal relative to the htt-exon1(46Q) control.

It has been demonstrated that certain residues are crucial to stabilizing multimeric structures once Nt17 transitions to an α -helical structure. Specifically, the potential electrostatic interaction between K15 and E11 can help stabilize the dimer-dimer interface in a tetrameric structure.¹³ The removal of positive charges by carbethoxylation favors monomeric conformations of Nt17 as monomeric conformations become more abundant with increasing

modification while multimeric species are destabilized and decrease in abundance as detected by ion-mobility spectrometry-mass spectrometry (IMS-MS).¹⁶ Molecular dynamics studies indicated that K6 is likely involved in the stabilization of dimeric species through interactions with E12 and S16¹⁶ while K9 is implicated in intramolecular salt bridges with E5 and/or E12.^{11,41} With both S13 and S16 being solvent exposed, modification to these residues could be involved in the packing of tetrameric structures into higher order species necessary for oligomer stabilization to facilitate fibril formation.¹² Oligomer stability as a function of introducing mutations mimicking acetylation and phosphorylation could be another dominant factor in altered oligomer/lipid interactions as shown in PDA assays. Generally, there appears to be larger consequences for changes made to the C-terminus, as modification of K15 had the largest impact among the acetylation mimics while the S16 mutant had the largest impact among phosphorylation mutants.

3.5 References

- (1) Macdonald, M. A Novel Gene Containing a Trinucleotide Repeat That Is Expanded and Unstable on Huntington's Disease Chromosomes. *Cell* **1993**, 72 (6), 971–983. [https://doi.org/10.1016/0092-8674\(93\)90585-E](https://doi.org/10.1016/0092-8674(93)90585-E).
- (2) Snell, R. G.; MacMillan, J. C.; Cheadle, J. P.; Fenton, I.; Lazarou, L. P.; Davies, P.; MacDonald, M. E.; Gusella, J. F.; Harper, P. S.; Shaw, D. J. Relationship between Trinucleotide Repeat Expansion and Phenotypic Variation in Huntington's Disease. *Nat. Genet.* **1993**, 4 (4), 393–397. <https://doi.org/10.1038/ng0893-393>.
- (3) Penney, J. B.; Vonsattel, J.-P.; Macdonald, M. E.; Gusella, J. F.; Myers, R. H. CAG Repeat Number Governs the Development Rate of Pathology in Huntington's Disease. *Ann. Neurol.* **1997**, 41 (5), 689–692. <https://doi.org/10.1002/ana.410410521>.
- (4) Scherzinger, E.; Lurz, R.; Turmaine, M.; Mangiarini, L.; Hollenbach, B.; Hasenbank, R.; Bates, G. P.; Davies, S. W.; Lehrach, H.; Wanker, E. E. Huntingtin-Encoded Polyglutamine Expansions Form Amyloid-like Protein Aggregates In Vitro and In Vivo. *Cell* **1997**, 90 (3), 549–558. [https://doi.org/10.1016/S0092-8674\(00\)80514-0](https://doi.org/10.1016/S0092-8674(00)80514-0).
- (5) Scherzinger, E.; Sittler, A.; Schweiger, K.; Heiser, V.; Lurz, R.; Hasenbank, R.; Bates, G. P.; Lehrach, H.; Wanker, E. E. Self-Assembly of Polyglutamine-Containing Huntingtin Fragments into Amyloid-like Fibrils: Implications for Huntington's Disease Pathology. *Proc. Natl. Acad. Sci.* **1999**, 96 (8), 4604–4609. <https://doi.org/10.1073/pnas.96.8.4604>.

- (6) Chen, S.; Berthelie, V.; Hamilton, J. B.; O’Nuallai, B.; Wetzel, R. Amyloid-like Features of Polyglutamine Aggregates and Their Assembly Kinetics †. *Biochemistry* **2002**, *41* (23), 7391–7399. <https://doi.org/10.1021/bi011772q>.
- (7) Adegbuyiro, A.; Sedighi, F.; Pilkington, A. W.; Groover, S.; Legleiter, J. Proteins Containing Expanded Polyglutamine Tracts and Neurodegenerative Disease. *Biochemistry* **2017**, *56* (9), 1199–1217. <https://doi.org/10.1021/acs.biochem.6b00936>.
- (8) Nagarajan, A.; Jawahery, S.; Matysiak, S. The Effects of Flanking Sequences in the Interaction of Polyglutamine Peptides with a Membrane Bilayer. *J. Phys. Chem. B* **2014**, *118* (24), 6368–6379. <https://doi.org/10.1021/jp407900c>.
- (9) Arndt, J. R.; Chaibva, M.; Legleiter, J. The Emerging Role of the First 17 Amino Acids of Huntingtin in Huntington’s Disease. *Biomol. Concepts* **2015**, *6* (1). <https://doi.org/10.1515/bmc-2015-0001>.
- (10) Burke, K. A.; Kauffman, K. J.; Umbaugh, C. S.; Frey, S. L.; Legleiter, J. The Interaction of Polyglutamine Peptides with Lipid Membranes Is Regulated by Flanking Sequences Associated with Huntingtin. *J. Biol. Chem.* **2013**, *288* (21), 14993–15005. <https://doi.org/10.1074/jbc.M112.446237>.
- (11) Chaibva, M.; Jawahery, S.; Pilkington, A. W.; Arndt, J. R.; Sarver, O.; Valentine, S.; Matysiak, S.; Legleiter, J. Acetylation within the First 17 Residues of Huntingtin Exon 1 Alters Aggregation and Lipid Binding. *Biophys. J.* **2016**, *111* (2), 349–362. <https://doi.org/10.1016/j.bpj.2016.06.018>.
- (12) Mishra, R.; Hoop, C. L.; Kodali, R.; Sahoo, B.; van der Wel, P. C. A.; Wetzel, R. Serine Phosphorylation Suppresses Huntingtin Amyloid Accumulation by Altering Protein Aggregation Properties. *J. Mol. Biol.* **2012**, *424* (1–2), 1–14. <https://doi.org/10.1016/j.jmb.2012.09.011>.
- (13) Kotler, S. A.; Tugarinov, V.; Schmidt, T.; Ceccon, A.; Libich, D. S.; Ghirlando, R.; Schwieters, C. D.; Clore, G. M. Probing Initial Transient Oligomerization Events Facilitating Huntingtin Fibril Nucleation at Atomic Resolution by Relaxation-Based NMR. *Proc. Natl. Acad. Sci.* **2019**, *116* (9), 3562–3571. <https://doi.org/10.1073/pnas.1821216116>.
- (14) Vitalis, A.; Wang, X.; Pappu, R. V. Quantitative Characterization of Intrinsic Disorder in Polyglutamine: Insights from Analysis Based on Polymer Theories. *Biophys. J.* **2007**, *93* (6), 1923–1937. <https://doi.org/10.1529/biophysj.107.110080>.
- (15) Wang, X.; Vitalis, A.; Wyczalkowski, M. A.; Pappu, R. V. Characterizing the Conformational Ensemble of Monomeric Polyglutamine. *Proteins Struct. Funct. Bioinforma.* **2005**, *63* (2), 297–311. <https://doi.org/10.1002/prot.20761>.
- (16) Arndt, J. R.; Kondalaji, S. G.; Maurer, M. M.; Parker, A.; Legleiter, J.; Valentine, S. J. Huntingtin N-Terminal Monomeric and Multimeric Structures Destabilized by Covalent Modification of Heteroatomic Residues. *Biochemistry* **2015**, *54* (28), 4285–4296. <https://doi.org/10.1021/acs.biochem.5b00478>.
- (17) Jayaraman, M.; Kodali, R.; Sahoo, B.; Thakur, A. K.; Mayasundari, A.; Mishra, R.; Peterson, C. B.; Wetzel, R. Slow Amyloid Nucleation via α -Helix-Rich Oligomeric Intermediates in Short Polyglutamine-Containing Huntingtin Fragments. *J. Mol. Biol.* **2012**, *415* (5), 881–899. <https://doi.org/10.1016/j.jmb.2011.12.010>.
- (18) Sivanandam, V. N.; Jayaraman, M.; Hoop, C. L.; Kodali, R.; Wetzel, R.; van der Wel, P. C. A. The Aggregation-Enhancing Huntingtin N-Terminus Is Helical in Amyloid Fibrils. *J. Am. Chem. Soc.* **2011**, *133* (12), 4558–4566. <https://doi.org/10.1021/ja110715f>.

- (19) Williamson, T. E.; Vitalis, A.; Crick, S. L.; Pappu, R. V. Modulation of Polyglutamine Conformations and Dimer Formation by the N-Terminus of Huntingtin. *J. Mol. Biol.* **2010**, *396* (5), 1295–1309. <https://doi.org/10.1016/j.jmb.2009.12.017>.
- (20) Thakur, A. K.; Jayaraman, M.; Mishra, R.; Thakur, M.; Chellgren, V. M.; L Byeon, I.-J.; Anjum, D. H.; Kodali, R.; Creamer, T. P.; Conway, J. F.; M Gronenborn, A.; Wetzel, R. Polyglutamine Disruption of the Huntingtin Exon 1 N Terminus Triggers a Complex Aggregation Mechanism. *Nat. Struct. Mol. Biol.* **2009**, *16* (4), 380–389. <https://doi.org/10.1038/nsmb.1570>.
- (21) Mishra, R.; Jayaraman, M.; Roland, B. P.; Landrum, E.; Fullam, T.; Kodali, R.; Thakur, A. K.; Arduini, I.; Wetzel, R. Inhibiting the Nucleation of Amyloid Structure in a Huntingtin Fragment by Targeting α -Helix-Rich Oligomeric Intermediates. *J. Mol. Biol.* **2012**, *415* (5), 900–917. <https://doi.org/10.1016/j.jmb.2011.12.011>.
- (22) Burke, K. A.; Hensal, K. M.; Umbaugh, C. S.; Chaibva, M.; Legleiter, J. Huntingtin Disrupts Lipid Bilayers in a PolyQ-Length Dependent Manner. *Biochim. Biophys. Acta BBA - Biomembr.* **2013**, *1828* (8), 1953–1961. <https://doi.org/10.1016/j.bbamem.2013.04.025>.
- (23) Li, S.-H.; Li, X.-J. Huntingtin–Protein Interactions and the Pathogenesis of Huntington’s Disease. *Trends Genet.* **2004**, *20* (3), 146–154. <https://doi.org/10.1016/j.tig.2004.01.008>.
- (24) Cattaneo, E.; Zuccato, C.; Tartari, M. Normal Huntingtin Function: An Alternative Approach to Huntington’s Disease. *Nat. Rev. Neurosci.* **2005**, *6* (12), 919–930. <https://doi.org/10.1038/nrn1806>.
- (25) De Rooij, K. Subcellular Localization of the Huntington’s Disease Gene Product in Cell Lines by Immunofluorescence and Biochemical Subcellular Fractionation. *Hum. Mol. Genet.* **1996**, *5* (8), 1093–1099. <https://doi.org/10.1093/hmg/5.8.1093>.
- (26) Xia, J. Huntingtin Contains a Highly Conserved Nuclear Export Signal. *Hum. Mol. Genet.* **2003**, *12* (>12), 1393–1403. <https://doi.org/10.1093/hmg/ddg156>.
- (27) Atwal, R. S.; Xia, J.; Pinchev, D.; Taylor, J.; Epand, R. M.; Truant, R. Huntingtin Has a Membrane Association Signal That Can Modulate Huntingtin Aggregation, Nuclear Entry and Toxicity. *Hum. Mol. Genet.* **2007**, *16* (21), 2600–2615. <https://doi.org/10.1093/hmg/ddm217>.
- (28) Gu, M.; Gash, M. T.; Mann, V. M.; Javoy-Agid, F.; Cooper, J. M.; Schapira, A. H. V. Mitochondrial Defect in Huntington’s Disease Caudate Nucleus. *Ann. Neurol.* **1996**, *39* (3), 385–389. <https://doi.org/10.1002/ana.410390317>.
- (29) Panov, A. V.; Gutekunst, C.-A.; Leavitt, B. R.; Hayden, M. R.; Burke, J. R.; Strittmatter, W. J.; Greenamyre, J. T. Early Mitochondrial Calcium Defects in Huntington’s Disease Are a Direct Effect of Polyglutamines. *Nat. Neurosci.* **2002**, *5* (8), 731–736. <https://doi.org/10.1038/nm884>.
- (30) Choo, Y. S. Mutant Huntingtin Directly Increases Susceptibility of Mitochondria to the Calcium-Induced Permeability Transition and Cytochrome c Release. *Hum. Mol. Genet.* **2004**, *13* (14), 1407–1420. <https://doi.org/10.1093/hmg/ddh162>.
- (31) Chang, D. T. W.; Rintoul, G. L.; Pandipati, S.; Reynolds, I. J. Mutant Huntingtin Aggregates Impair Mitochondrial Movement and Trafficking in Cortical Neurons. *Neurobiol. Dis.* **2006**, *22* (2), 388–400. <https://doi.org/10.1016/j.nbd.2005.12.007>.
- (32) Orr, A. L.; Li, S.; Wang, C.-E.; Li, H.; Wang, J.; Rong, J.; Xu, X.; Mastroberardino, P. G.; Greenamyre, J. T.; Li, X.-J. N-Terminal Mutant Huntingtin Associates with Mitochondria and Impairs Mitochondrial Trafficking. *J. Neurosci.* **2008**, *28* (11), 2783–2792. <https://doi.org/10.1523/JNEUROSCI.0106-08.2008>.

- (33) Kegel, K. B.; Sapp, E.; Yoder, J.; Cuiffo, B.; Sobin, L.; Kim, Y. J.; Qin, Z.-H.; Hayden, M. R.; Aronin, N.; Scott, D. L.; Isenberg, G.; Goldmann, W. H.; DiFiglia, M. Huntingtin Associates with Acidic Phospholipids at the Plasma Membrane. *J. Biol. Chem.* **2005**, *280* (43), 36464–36473. <https://doi.org/10.1074/jbc.M503672200>.
- (34) Bäuerlein, F. J. B.; Saha, I.; Mishra, A.; Kalemánov, M.; Martínez-Sánchez, A.; Klein, R.; Dudanova, I.; Hipp, M. S.; Hartl, F. U.; Baumeister, W.; Fernández-Busnadiego, R. In Situ Architecture and Cellular Interactions of PolyQ Inclusions. *Cell* **2017**, *171* (1), 179–187.e10. <https://doi.org/10.1016/j.cell.2017.08.009>.
- (35) Riguet, N.; Mahul-Mellier, A.-L.; Maharjan, N.; Burtscher, J.; Croisier, M.; Knott, G.; Hastings, J.; Patin, A.; Reiterer, V.; Farhan, H.; Nasarov, S.; Lashuel, H. A. Nuclear and Cytoplasmic Huntingtin Inclusions Exhibit Distinct Biochemical Composition, Interactome and Ultrastructural Properties. *Nat. Commun.* **2021**, *12* (1), 6579. <https://doi.org/10.1038/s41467-021-26684-z>.
- (36) Gasset-Rosa, F.; Chillon-Marinas, C.; Goginashvili, A.; Atwal, R. S.; Artates, J. W.; Tabet, R.; Wheeler, V. C.; Bang, A. G.; Cleveland, D. W.; Lagier-Tourenne, C. Polyglutamine-Expanded Huntingtin Exacerbates Age-Related Disruption of Nuclear Integrity and Nucleocytoplasmic Transport. *Neuron* **2017**, *94* (1), 48–57.e4. <https://doi.org/10.1016/j.neuron.2017.03.027>.
- (37) Beasley, M.; Stonebraker, A. R.; Hasan, I.; Kapp, K. L.; Liang, B. J.; Agarwal, G.; Groover, S.; Sedighi, F.; Legleiter, J. Lipid Membranes Influence the Ability of Small Molecules To Inhibit Huntingtin Fibrillization. *Biochemistry* **2019**, *58* (43), 4361–4373. <https://doi.org/10.1021/acs.biochem.9b00739>.
- (38) Levy, G. R.; Shen, K.; Gavrilov, Y.; Smith, P. E. S.; Levy, Y.; Chan, R.; Frydman, J.; Frydman, L. Huntingtin's N-Terminus Rearrangements in the Presence of Membranes: A Joint Spectroscopic and Computational Perspective. *ACS Chem. Neurosci.* **2019**, *10* (1), 472–481. <https://doi.org/10.1021/acchemneuro.8b00353>.
- (39) Pandey, N. K.; Isas, J. M.; Rawat, A.; Lee, R. V.; Langen, J.; Pandey, P.; Langen, R. The 17-Residue-Long N Terminus in Huntingtin Controls Stepwise Aggregation in Solution and on Membranes via Different Mechanisms. *J. Biol. Chem.* **2018**, *293* (7), 2597–2605. <https://doi.org/10.1074/jbc.M117.813667>.
- (40) Beasley, M.; Frazee, N.; Groover, S.; Valentine, S. J.; Mertz, B.; Legleiter, J. Physicochemical Properties Altered by the Tail Group of Lipid Membranes Influence Huntingtin Aggregation and Lipid Binding. *J. Phys. Chem. B* **2022**, *126* (16), 3067–3081. <https://doi.org/10.1021/acs.jpcc.1c10254>.
- (41) Côté, S.; Binette, V.; Salnikov, E. S.; Bechinger, B.; Mousseau, N. Probing the Huntingtin 1-17 Membrane Anchor on a Phospholipid Bilayer by Using All-Atom Simulations. *Biophys. J.* **2015**, *108* (5), 1187–1198. <https://doi.org/10.1016/j.bpj.2015.02.001>.
- (42) Chaibva, M.; Gao, X.; Jain, P.; Campbell, W. A.; Frey, S. L.; Legleiter, J. Sphingomyelin and GM1 Influence Huntingtin Binding to, Disruption of, and Aggregation on Lipid Membranes. *ACS Omega* **2018**, *3* (1), 273–285. <https://doi.org/10.1021/acsomega.7b01472>.
- (43) Chiki, A.; DeGuire, S. M.; Ruggeri, F. S.; Sanfelice, D.; Ansaloni, A.; Wang, Z.-M.; Cendrowska, U.; Burai, R.; Vieweg, S.; Pastore, A.; Dietler, G.; Lashuel, H. A. Mutant Exon1 Huntingtin Aggregation Is Regulated by T3 Phosphorylation-Induced Structural Changes and Crosstalk between T3 Phosphorylation and Acetylation at K6. *Angew. Chem. Int. Ed.* **2017**, *56* (19), 5202–5207. <https://doi.org/10.1002/anie.201611750>.

- (44) Aiken, C. T.; Steffan, J. S.; Guerrero, C. M.; Khashwji, H.; Lukacsovich, T.; Simmons, D.; Purcell, J. M.; Menhaji, K.; Zhu, Y.-Z.; Green, K.; LaFerla, F.; Huang, L.; Thompson, L. M.; Marsh, J. L. Phosphorylation of Threonine 3: IMPLICATIONS FOR HUNTINGTIN AGGREGATION AND NEUROTOXICITY. *J. Biol. Chem.* **2009**, *284* (43), 29427–29436. <https://doi.org/10.1074/jbc.M109.013193>.
- (45) DeGuire, S. M.; Ruggeri, F. S.; Fares, M.-B.; Chiki, A.; Cendrowska, U.; Dietler, G.; Lashuel, H. A. N-Terminal Huntingtin (Htt) Phosphorylation Is a Molecular Switch Regulating Htt Aggregation, Helical Conformation, Internalization, and Nuclear Targeting. *J. Biol. Chem.* **2018**, *293* (48), 18540–18558. <https://doi.org/10.1074/jbc.RA118.004621>.
- (46) Kalchman, M. A.; Graham, R. K.; Xia, G.; Koide, H. B.; Hodgson, J. G.; Graham, K. C.; Goldberg, Y. P.; Gietz, R. D.; Pickart, C. M.; Hayden, M. R. Huntingtin Is Ubiquitinated and Interacts with a Specific Ubiquitin-Conjugating Enzyme. *J. Biol. Chem.* **1996**, *271* (32), 19385–19394. <https://doi.org/10.1074/jbc.271.32.19385>.
- (47) Steffan, J. S. SUMO Modification of Huntingtin and Huntington's Disease Pathology. *Science* **2004**, *304* (5667), 100–104. <https://doi.org/10.1126/science.1092194>.
- (48) Sedighi, F.; Adegbuyiro, A.; Legleiter, J. SUMOylation Prevents Huntingtin Fibrillization and Localization onto Lipid Membranes. *ACS Chem. Neurosci.* **2020**, *11* (3), 328–343. <https://doi.org/10.1021/acchemneuro.9b00509>.
- (49) Wang, Y.; Lin, F.; Qin, Z.-H. The Role of Post-Translational Modifications of Huntingtin in the Pathogenesis of Huntington's Disease. *Neurosci. Bull.* **2010**, *26* (2), 153–162. <https://doi.org/10.1007/s12264-010-1118-6>.
- (50) Burra, G.; Thakur, A. K. Inhibition of Polyglutamine Aggregation by SIMILAR Huntingtin N-Terminal Sequences: Prospective Molecules for Preclinical Evaluation in Huntington's Disease: BURRA et Al. *Biopolymers* **2017**, *108* (4), e23021. <https://doi.org/10.1002/bip.23021>.
- (51) Chen, S.; Berthelie, V.; Yang, W.; Wetzel, R. Polyglutamine Aggregation Behavior in Vitro Supports a Recruitment Mechanism of Cytotoxicity. *J. Mol. Biol.* **2001**, *311* (1), 173–182. <https://doi.org/10.1006/jmbi.2001.4850>.
- (52) Muchowski, P. J.; Schaffar, G.; Sittler, A.; Wanker, E. E.; Hayer-Hartl, M. K.; Hartl, F. U. Hsp70 and Hsp40 Chaperones Can Inhibit Self-Assembly of Polyglutamine Proteins into Amyloid-like Fibrils. *Proc. Natl. Acad. Sci.* **2000**, *97* (14), 7841–7846. <https://doi.org/10.1073/pnas.140202897>.
- (53) Zheng, F.; Wu, Z.; Chen, Y. A Quantitative Method for the Measurement of Membrane Affinity by Polydiacetylene-Based Colorimetric Assay. *Anal. Biochem.* **2012**, *420* (2), 171–176. <https://doi.org/10.1016/j.ab.2011.09.026>.
- (54) Burke, K. A.; Legleiter, J. Atomic Force Microscopy Assays for Evaluating Polyglutamine Aggregation in Solution and on Surfaces. In *Tandem Repeats in Genes, Proteins, and Disease*; Hatters, D. M., Hannan, A. J., Eds.; Methods in Molecular Biology; Humana Press: Totowa, NJ, 2013; Vol. 1017, pp 21–40. https://doi.org/10.1007/978-1-62703-438-8_2.
- (55) Ranganathan, N.; Li, C.; Suder, T.; Karanji, A. K.; Li, X.; He, Z.; Valentine, S. J.; Li, P. Capillary Vibrating Sharp-Edge Spray Ionization (CVSSI) for Voltage-Free Liquid Chromatography-Mass Spectrometry. *J. Am. Soc. Mass Spectrom.* **2019**, *30* (5), 824–831. <https://doi.org/10.1007/s13361-019-02147-0>.
- (56) Li, C.; Attanayake, K.; Valentine, S. J.; Li, P. Facile Improvement of Negative Ion Mode Electrospray Ionization Using Capillary Vibrating Sharp-Edge Spray Ionization. *Anal. Chem.* **2020**, *92* (3), 2492–2502. <https://doi.org/10.1021/acs.analchem.9b03983>.

- (57) Gu, X.; Greiner, E. R.; Mishra, R.; Kodali, R.; Osmand, A.; Finkbeiner, S.; Steffan, J. S.; Thompson, L. M.; Wetzel, R.; Yang, X. W. Serines 13 and 16 Are Critical Determinants of Full-Length Human Mutant Huntingtin Induced Disease Pathogenesis in HD Mice. *Neuron* **2009**, *64* (6), 828–840. <https://doi.org/10.1016/j.neuron.2009.11.020>.
- (58) Côté, S.; Wei, G.; Mousseau, N. Atomistic Mechanisms of Huntingtin N-Terminal Fragment Insertion on a Phospholipid Bilayer Revealed by Molecular Dynamics Simulations: Htt^{NT} Q_N Insertion on a Phospholipid Bilayer. *Proteins Struct. Funct. Bioinforma.* **2014**, *82* (7), 1409–1427. <https://doi.org/10.1002/prot.24509>.
- (59) Michalek, M.; Aisenbrey, C.; Bechinger, B. Investigation of Membrane Penetration Depth and Interactions of the Amino-Terminal Domain of Huntingtin: Refined Analysis by Tryptophan Fluorescence Measurement. *Eur. Biophys. J.* **2014**, *43* (8–9), 347–360. <https://doi.org/10.1007/s00249-014-0966-9>.
- (60) Sedighi, F.; Skeens, A.; Adegbuyiro, A.; Bard, J.; Siriwardhana, C.; Donley, E.; Geldenhuys, W. J.; Legleiter, J. Oligomerization Enhances Huntingtin Membrane Activity but Is Suppressed by Covalent Crosslinking. *bioRxiv* **2023**, 2023.03.01.530665. <https://doi.org/10.1101/2023.03.01.530665>.
- (61) Burke, K. A.; Yates, E. A.; Legleiter, J. Biophysical Insights into How Surfaces, Including Lipid Membranes, Modulate Protein Aggregation Related to Neurodegeneration. *Front. Neurol.* **2013**, *4*. <https://doi.org/10.3389/fneur.2013.00017>.
- (62) Aisenbrey, C.; Borowik, T.; Byström, R.; Bokvist, M.; Lindström, F.; Misiak, H.; Sani, M.-A.; Gröbner, G. How Is Protein Aggregation in Amyloidogenic Diseases Modulated by Biological Membranes? *Eur. Biophys. J.* **2008**, *37* (3), 247–255. <https://doi.org/10.1007/s00249-007-0237-0>.
- (63) Gorbenko, G. P.; Kinnunen, P. K. J. The Role of Lipid–Protein Interactions in Amyloid-Type Protein Fibril Formation. *Chem. Phys. Lipids* **2006**, *141* (1–2), 72–82. <https://doi.org/10.1016/j.chemphyslip.2006.02.006>.

4. Future Directions and Concluding Remarks

4.1 Introduction

In Chapter 2, the effects of cholesterol content on htt aggregation, lipid binding, and complexation were explored. Additionally, a variety of lipid systems with different physiochemical properties were used to further probe such interactions. These results highlight the complexities associated with htt/lipid interactions and more specifically the intricacies of these interactions as lipid compositions are varied. The specific impacts of cholesterol on aggregation, lipid binding, and complexation in the presence of specific lipid systems are unique, and a change in lipid composition while maintaining a constant amount of cholesterol altered the three processes explored due to changes in lipid physiochemical properties. Considering the complexities of lipid interactions observed in Chapter 2, it was also of interest to explore the effects of point-mutations, ultimately resulting in changes to the net charge of the Nt17 domain, on the same types of interactions. The addition of free, monomeric Nt17 peptides to monomeric htt protein had significant impacts on fibrilization with changes in oligomer morphologies also being observed. Interestingly, the impacts of incorporating the free peptides into oligomers had less pronounced effects on lipid binding while suggesting that C-terminal modifications specifically have a larger impact on lipid interactions. Mutations within Nt17 also altered the ability of the peptides to complex with lipids. Collectively, these results indicate changes in interactions between htt proteins and htt with lipids, specifically with respect to oligomeric species, when mutations are introduced within the Nt17 domain. This further highlights complexities surrounding htt interactions. The results from Chapter 2 and Chapter 3 together underscore the intricacies associated with the poorly understood toxic mechanism of HD and

demonstrate the need to explore general interactions of htt within the cellular environment to better understand the overall toxic mechanism and elucidate novel therapeutic approaches.

A variety of techniques have been employed in an effort to identify the specific toxic mechanism of HD, better diagnostic options, and novel therapeutic routes. However, the toxic mechanism of HD is poorly understood largely due to the complexities associated with pathogenic htt interactions, as highlighted in Chapters 2 and 3. Furthermore, diagnostic and disease monitoring approaches are limited, and treatments only exist for the symptoms of HD rather than the disease itself. Htt has been demonstrated to have significant interactions with a variety of cellular and subcellular components which subsequently cause changes to these environments. Identifying changes to protein expression or lipid production as a function of pathogenic htt expression could serve to elucidate additional parts of the toxic mechanism, identify potential biomarker panels for diagnostics and disease monitoring, and reveal new therapeutic targets and/or approaches. Proteomics and lipidomics are already well established methods in the study of neurodegenerative diseases, with proteomic and lipidomic methods having identified changes in protein and lipid profiles in AD¹⁻⁵ and PD.⁴⁻⁷ In the case of HD specifically, current biomarkers rely on imaging techniques and clinical manifestations with very few biomarkers of potential having been identified in samples such as blood, plasma, and CSF.⁸

Preliminary proteomic and lipidomic studies are best served in model organisms prior to moving on to studies with human samples. As such, one model organism that would be ideal for preliminary studies is *Caenorhabditis elegans* (*C. elegans*). This model is experimentally advantageous due to their ability to breed in large numbers and their short generation times,⁹ which allow for efficient experimental timelines. Furthermore, there is 83% homology with the human genome and only 11% of the genome is nematode specific.¹⁰ Most human disease genes

and pathways are present, and *C. elegans* models have already been established in the study of AD,^{2,11} PD,^{9,12,13} and HD.^{14,15} Modeling neurodegenerative diseases in *C. elegans* is especially advantageous given key biological elements of neurons present in humans are conserved, and phenotypes corresponding to disease states are present since non-native human proteins that are expressed in transgenic models are functionally active.¹⁶ One model expressing htt are *C. elegans* strains EAK102 (htt15Q) and EAK103 (htt128Q) which correspond to nonpathogenic and pathogenic strains respectively. This specific model expresses htt in the body wall muscle cells of the *C. elegans*,¹⁴ which could make the model especially useful in the search for markers of generic cell damage outside of the central nervous system (CNS), which are of particular interest as they would allow for disease detection and monitoring using samples such as blood and plasma as opposed to samples of CSF that require more invasive processes to acquire.

4.2 Research in Progress: Proteomics of *C. elegans* HD Model

Htt has been identified to have various functions, one of which is transcriptional regulation.¹⁷ Transcriptional regulation is crucial for cells to respond to intracellular and extracellular signals. When transcription is dysregulated, the amount of mRNA being produced is altered which subsequently impacts the expression of corresponding proteins. Transcriptional dysregulation has been observed in cases of pathogenic htt expression, with mRNA production usually being downregulated though there are instances of upregulation as well.¹⁸ Proteomics is a method in which proteins within a given sample can be both identified and quantified. Proteomic studies utilizing *C. elegans* have been established, and differences in protein expression due to a variety of factors have been observed.^{2,10,13,19–26} As such, the combination of proteomic methods with the previously described *C. elegans* model of HD would provide the opportunity to look for changes in protein expression in the pathogenic strain compared to the nonpathogenic strain. Any

proteins identified as having different levels of expression can provide information crucial to understanding the toxic mechanisms of HD while also identifying potential biomarkers that could be used for diagnostics and disease monitoring.

To identify changes in protein expression in pathogenic versus nonpathogenic strains of *C. elegans* expressing htt, synchronized populations of *C. elegans* need to be established, a method commonly used in various -omics studies.^{21,25-27} The process of synchronization allows for the collection of large populations of worms, while also ensuring that all worms intended for use under specific sample conditions are at the same stage of life which is crucial for time-dependent studies. Synchronized populations can be obtained by collecting eggs from worms grown on nematode growth media (NGM) plates, then transferring all collected eggs to fresh NGM plates for growth.

Once synchronized populations are obtained, survival assays and thrashing rate assays are necessary to validate the model by evaluating lifespan and behavioral dysfunction respectively. For the survival assay, synchronized populations of *C. elegans* need to be incubated on NGM plates that contain 5-fluorodeoxyuridine (FUDR) to prevent self-fertilization and the production of progeny. Over the course of 30 consecutive days, the locomotion of the worms will be scored, with worms that show no movement being scored as deceased. Over the 30 consecutive days, the fraction of living versus deceased worms can be calculated and plotted to generate survival curves. For the thrashing rate assay, the total number of thrashes, defined as each time a worm changes its aspect ratio, can be counted over 30 seconds. Changes to the thrashing rate can be determined by repeating the process over the course of days. The survival curves and thrashing rate assays can then be used to determine ideal experimental timepoints for proteomic sample

collection. One target population would be early in the lifespan, before any deviation in the fraction of worms alive between pathogenic and nonpathogenic strains, and before significant deviations in behavioral dysfunction between strains. The second target population would be later in the lifespan, once the fraction of worms alive starts to deviate between the pathogenic and nonpathogenic strains, and after behavioral dysfunction has progressed in the pathogenic strain. Worms from these timepoints, collected for each strain, allow for direct, age-matched comparisons between the pathogenic and nonpathogenic strains, while also allowing for the evaluation of impacts over time within an individual strain for a more complete picture of fluctuations in protein abundances across strains and as a function of time/disease progression.

Large populations of worms, from at least two different batches of growth, for each timepoint and strain must be collected to average out any random fluctuations in protein production across populations. Populations can be collected by washing cultured worms, treated with FUDR to keep all worms the same age by preventing progeny production, off the NGM plates with buffer, followed by thorough washes with deionized water (dH₂O) to remove any residual bacteria. The wash can be removed after pelleting the worms via centrifugation, after which the worm populations can be snap frozen using liquid nitrogen (LN₂) and stored at -80 °C until needed. To prepare for proteomic analysis, the proteins must be extracted and digested. Proteins can be extracted via sonication in extraction buffer, then separated from worm debris by centrifugation. Bulk protein concentration can be determined via Bradford assay, after which the protein solution can be reduced and alkylated prior to being enzymatically digested. The protein digest can then be analyzed using reversed-phase liquid chromatography (RPLC-MS), where utilization of tandem mass spectrometry (MS/MS) mode can further facilitate peptide and overall protein identification. Identified proteins can then be compared across samples, and the

calculation of the exponentially modified protein abundance index (emPAI) can provide an estimation of the absolute amount of each identified protein within the samples for a quantitative comparison.^{28,29}

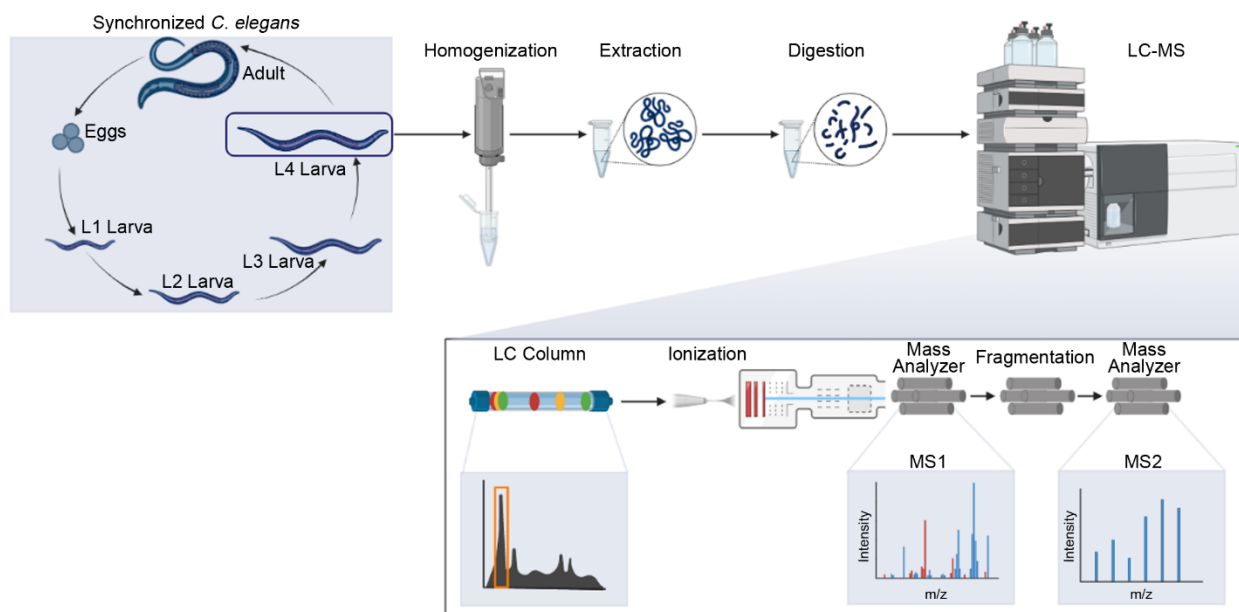


Figure 4.1. A generic proteomics experimental workflow.³⁰ From synchronized populations of *C. elegans* worms in the L4 stage are collected for samples. The worms are homogenized in buffer and the proteins extracted in bulk solution. Proteins are then denatured, reduced, and alkylated prior to being digested. The protein digest can then be analyzed using LC-MS where peptides are separated using a C18 column, then ionized and identified using the MS/MS mode.

A preliminary proteomic method was successfully established utilizing *C. elegans* strains EAK102 (htt15Q) and EAK103 (htt128Q) obtained from the Caenorhabditis Genetics Center (Figure 4.1). The worms were grown as described previously, then age synchronized populations were obtained using established methods.³¹ Survival assays and thrashing rate assays suggested that the ideal timepoints for these studies would be day 2 and day 7. At the appropriate times, at least 4,000 worms from each strain were collected over at least two different batches of growth. Once the populations were obtained, they were washed, suspended in dH₂O, and stored at -80 °C

until needed. To prepare the populations for proteomic analysis, the samples were thawed and all batches for corresponding strains/timepoints were combined. Excess water was removed, and samples were resuspended in 100 mM ammonium bicarbonate buffer containing 6 M urea (pH 7.8) and ethylenediaminetetraacetic acid (EDTA) free protease inhibitor was added. Once suspended, samples were probe sonicated for three cycles of 10-15 sec and were stored on ice between cycles. This released proteins into bulk solution where they were denatured by the high urea concentration. A high-speed centrifugation pelleted out any worm debris, and the protein-containing supernatant was removed for use. A Bradford assay using bovine serum albumin (BSA) standards was performed to obtain a calibration curve, which was then used to determine the bulk protein concentration of each sample (the estimated average molecular weight of proteins was 50,000 g/mol). 500 µg of protein for each sample was then transferred to a fresh microcentrifuge tube. The protein samples were then reduced using dithiothreitol (DTT) in a 40:1 molar ratio of DTT:protein, alkylated using iodoacetamide (IA) in an 80:1 molar ratio of IA:protein. The reduction and alkylation steps make the hydrophobic cores of the proteins more accessible to trypsin for digestion. These reactions were quenched with L-cysteine in a 40:1 molar ratio of L-cysteine:protein. Each sample was then diluted such that the final concentration of urea in the sample was less than 2 M to allow for proper trypsin function and protein digestion. Trypsin was added to each sample in a 1:20 w/w ratio of trypsin:protein and allowed to digest for 24 hours.

Once the digestion was complete, the samples were analyzed using RPLC-MS with a water/formic acid to acetonitrile/formic acid gradient elution. MS/MS mode was also utilized during the runs. The first run of the samples indicated the presence of very little peptide loaded onto the column. As such, each sample was lyophilized overnight then reconstituted with LC-MS

grade water at half of the original volume. The now concentrated samples were run and peptides were observed, however there were also highly-charged species present. These highly charged species were indicative of partially-digested and undigested proteins, suggesting the digestion was not as efficient as desired. Some preliminary proteins were identified, generally with a medium confidence level, based on the peptide ion fragmentation patterns observed in MS/MS mode and the calculation of preliminary emPAI scores suggest there are observable differences in protein expression between age-matched samples of the different strains as well as over time within each strain.

Overall, a successful proteomic method has been established and preliminary results were obtained. Moving forward with this project, some minor adjustments can be made to improve sample preparation and subsequently the quality of the results. For the next preparation, starting with 1,000 μg of protein will provide a more sufficient concentration of protein, especially when factoring in losses due to reaction steps not being 100% efficient, which could improve the quality of data obtained from RPLC-MS operated in MS/MS mode. Additionally, increasing the ratio of trypsin to 1:10 trypsin:protein and extending the digestion time could improve digestion efficiency and yield more peptide/protein assignments and subsequently improve protein identification, increase the confidence of assignments, and improve emPAI scores. Additionally, the use of nano-electrospray ionization (nESI) will be available in the future, which could further improve studies. With nESI, capillaries with an opening 1-10 μm are located very close to the MS orifice and are loaded with only 1-5 μL of sample solution which is infused at significantly reduced flow rates. Thus nESI would require significantly less sample while increasing the MS and MS/MS signals by 2-3 times that of regular electrospray, with detection limits as low as 10^{-8}

mol/L.³² These benefits can translate into the efficient identification of hundreds to thousands of proteins.

4.3 Lipidomics: An Approach to Lipid Dysregulation

Lipid homeostasis is critical to both cellular structure and function, and as such alterations in lipid production can have serious downstream implications. One crucial membrane component is cholesterol, which regulates membrane fluidity and permeability while also influencing the overall organization of the membrane. In HD, it has been identified that cholesterol homeostasis is dysregulated.³³⁻³⁷ Beyond just HD, lipid homeostasis is also disrupted in AD^{38,39} and PD,⁴⁰ demonstrating a common theme among neurodegenerative diseases. Lipidomics methods have been used to monitor the lipidome and identify differences in lipid production in a variety of *C. elegans* studies.^{26,27,41} Using lipidomic methods in conjunction with a *C. elegans* model for HD can identify differences in lipid production resulting from pathogenic htt expression when compared to a non-pathogenic control. Understanding which aspects of lipid homeostasis are altered can provide insight into potentially toxic mechanisms in addition to serving as potential biomarkers that can be used for disease monitoring.

Generic lipidomic workups start with sample processing, with the most crucial step being the sample collection itself. Biological samples must be immediately processed or flash frozen, with short storage times, as this is necessary to prevent enzymatic and chemical processes that can ultimately metabolize lipids present. For example, in plasma samples left at room temperature there is an artificial increase in lysophosphatidylcholine (LPC)⁴² and lysophosphatidic acid (LPA)⁴³ components. After collection it is crucial that the sample is homogenized in cases where lipids must be extracted from cells/tissues, which would be required in the case of processing *C. elegans* populations. Homogenization ensures all aspects of the

cells/tissues are accessible to the chosen extraction solvents to obtain the most accurate lipid profiles. After homogenization, the next step is the extraction of the lipids. The extraction step(s) reduce sample complexity by removing any non-lipid components and enriching lipids to improve signal during analysis. A common form of extraction in lipidomic sample processing is liquid-liquid extraction, for which multiple established protocols exist.⁴⁴⁻⁴⁶ Single step extractions are faster and more robust than multi-phase extractions, but they often have more non-lipid components present after extraction. Another extraction technique is solid-phase extraction (SPE), which can yield highly enriched samples that have very few contaminants. SPE, however, can be very labor intensive and the extraction process becomes increasingly more complex when larger numbers of lipid classes must be analyzed or large numbers of sample cohorts are required for biomarker discovery efforts. Once processed, the most common chromatographic separation method in lipidomics is RPLC, which can separate lipids based on their nonpolar fatty acyl chains. Coupling of RPLC with MS can allow for targeted and non-targeted approaches depending on the scope of the study. Targeted approaches can utilize selected reaction monitoring (SRM) or multiple reaction monitoring (MRM) modes where user selected precursor ions are selected for fragmentation in the mass spectrometer. Non-targeted approaches can utilize data dependent acquisition mode (DDA), where more abundant precursors are selected for fragmentation, or data independent acquisition (DIA) mode, where all precursors are selected for fragmentation and precursor and fragment ions are linked via chromatographic profiles. These methods provide different levels of coverage and assignments to fit the desired scope of the study.

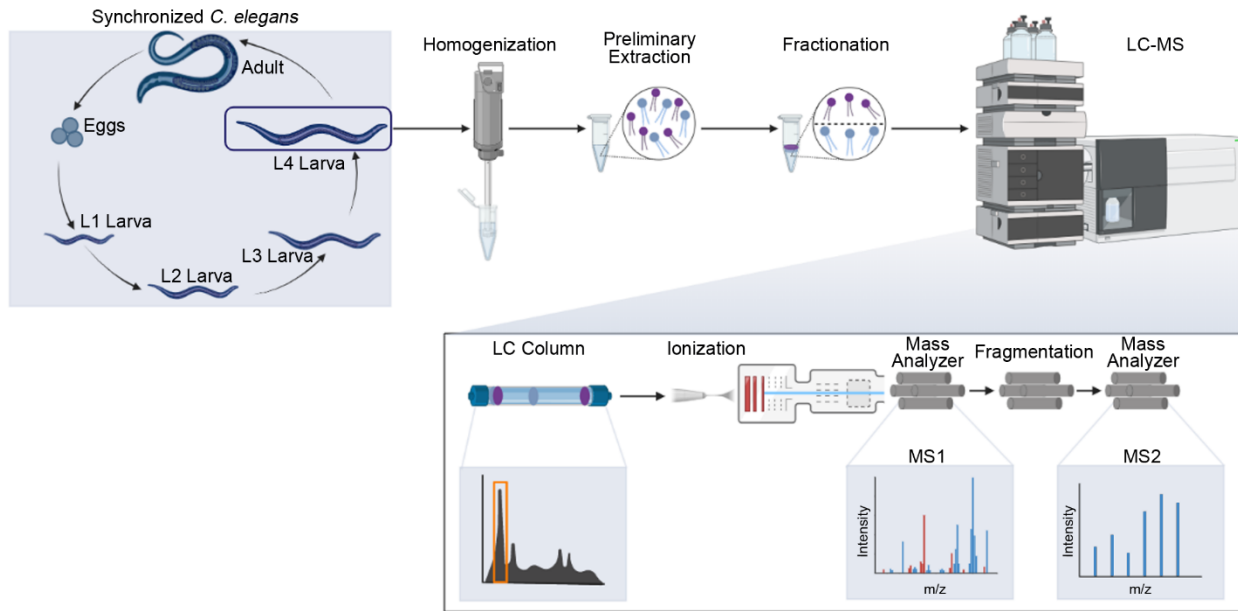


Figure 4.2. A generic lipidomics experimental workflow.³⁰ Synchronized populations of *C. elegans* worms in the L4 stage are collected for samples. The worms are homogenized in solvent and the lipids extracted. Lipids can then be fractionated to allow for easier analysis. The lipid fractions can then be analyzed using LC-MS where lipids are separated using a column, then ionized and identified using MS/MS methods.

A preliminary, and thus more robust, lipidomic method can be utilized to establish a basis for more specific and intensive lipidomic analysis once lipids or lipid classes of interest are identified (Figure 4.2). First, synchronized worm populations of the EAK102 (htt15Q) and EAK103 (htt128Q) must be established and the timepoints for sample collection determined using survival assays and thrashing rate assays as described previously. Once sample populations are collected, they must be homogenized for efficient lipid extraction, which can be accomplished using mechanical methods, such as mortar and pestle, or by using a probe sonicator. Lipids can then be extracted using a single or multi-phase extraction, with a multi-phase extraction being preferable to limit potential contamination by non-lipid components. This process would have to be repeated multiple times to maximize extraction efficiency. The extract would be centrifuged to pellet out any worm debris, while saving the supernatant for use. The

lipid extract can then be analyzed using RPLC-MS, where operation in MS/MS mode could aid in both lipid identification and structural elucidation.

The preliminary lipidomic method would elucidate specific lipids and classes of interest, after which a more specific approach can be employed for better characterization of the different components. Better characterization would be more efficient with fractionation of the extract into more manageable fractions, which can be accomplished with SPE as it would allow for more efficient and specific lipid analysis given there are fewer lipids/lipid classes per sample. While LC-MS is well suited to phospholipids, neutral lipids, and sphingolipids, when the lipid extract is fractionated gas chromatography-mass spectrometry (GC-MS) becomes another useful method for analysis, as it is better suited to identify individual lipid classes. More specifically, GC-MS is better for the identification of free fatty acids (FFAs) and steroids which can be made volatile through silylation derivatization, while the other higher molecular weight and less volatile or non-volatile lipid classes are still better suited to LC-MS.⁴⁷ Again, much like with the LC-MS method, MS/MS mode can be utilized with GC-MS for more efficient identification and structural elucidation.

4.5 Conclusions

HD is a fatal neurodegenerative disease caused by an expanded polyQ domain within htt, which causes the formation of toxic aggregate species. Though many therapeutic strategies have focused on targeting htt aggregation,⁴⁸⁻⁵³ a treatment or cure for HD is still elusive. The results presented in this dissertation underscore the complexities associated with htt interactions both in the presence of and directly with lipid membranes. Overall membrane composition and mutations to the Nt17 domain of htt are modulating factors with respect to htt aggregation,

aggregate morphology, lipid binding, and htt/lipid complexation which present additional considerations with respect to therapeutic approaches to HD.

In Chapter 2, the effect of cholesterol content on various pure lipid systems of differing physiochemical properties on htt aggregation, aggregate morphologies, lipid binding, and htt/lipid complexation were examined. Lipid systems of pure POPC, DOPC, and POPG were used, and various levels of exogenous cholesterol were added to each system. ThT assays revealed that increased cholesterol content promoted aggregation for the DOPC system, while inhibiting aggregation in the POPC and POPG systems. PDA assays showed that an increasing cholesterol content resulted in a decrease in htt lipid binding for POPC and increased lipid binding for DOPC and POPG. Differences in htt/lipid complexation with each lipid system were also observed with increased cholesterol content. Overall, these results highlight the intricacies of htt interactions in the presence of lipids and directly with lipids as a function of overall lipid composition.

In Chapter 3, the impact of charge on early htt interactions was explored. Free Nt17 peptides, that were wild-type or mimicked acetylation or phosphorylation at specific amino acid residues, were used to identify the impacts that putative post-translational modifications had on aggregation, aggregate morphologies, lipid binding, and htt/lipid complexation in the presence of POPC/POPS and TBLE lipid systems. The addition of all free Nt17 peptides inhibited fibril formation as shown in ThT assays, with wild-type being most effective followed by acetylation mimics then phosphorylation mimics. The incorporation of free Nt17 peptides into oligomeric structures resulted in a shift in aggregate morphology as observed with AFM, with wild-type producing the largest deviation followed by acetylation mimics then phosphorylation mimics. The ability of the peptides to interact with PC/PS lipids also changed as a function of mutation

type/location as observed with cVSSI, but overall mutant peptides interacted with the lipid system less than that of wild-type. Despite changes in complexation, all peptides preferentially interacted with anionic PS lipid while larger complexes that contained more peptide were more often lipid bound. Peptide-containing oligomers generally interacted less with both PC/PS vesicles and TBLE vesicles compared to pure htt-exon1 oligomers as demonstrated by PDA lipid binding assays. Collectively, this data suggests complex early interactions starting at the monomeric level that then translate into altered interactions at the oligomeric level, and that these interactions are influenced by factors including peptide charge and the environment.

Overall, the results presented here demonstrate the intricacies of htt interactions, especially with respect to those with and/or in the presence of various lipid systems. Together, these results underscore the intricacies critical to the toxic mechanism of HD. Further studies focusing on more general interactions of htt within the cellular environment and the general impacts on cellular processes with respect to the proteome and lipidome can further elucidate critical aspects of the toxic mechanism to which the aforementioned intricacies of htt interactions play a role. Identification of specific proteins and lipids that are altered as a function of mutant htt expression can present novel therapeutic targets and approaches, while also providing the opportunity to identify potential biomarkers beneficial to both diagnostics and disease monitoring.

4.6 References

- (1) Butterfield, D. A.; Boyd-Kimball, D.; Castegna, A. Proteomics in Alzheimer's Disease: Insights into Potential Mechanisms of Neurodegeneration: Proteomics in Alzheimer's Disease. *J. Neurochem.* **2003**, *86* (6), 1313–1327. <https://doi.org/10.1046/j.1471-4159.2003.01948.x>.
- (2) Boyd-Kimball, D.; Poon, H. F.; Lynn, B. C.; Cai, J.; Pierce Jr., W. M.; Klein, J. B.; Ferguson, J.; Link, C. D.; Butterfield, D. A. Proteomic Identification of Proteins Specifically Oxidized in *Caenorhabditis Elegans* Expressing Human A β (1–42): Implications for Alzheimer's Disease. *Neurobiol. Aging* **2006**, *27* (9), 1239–1249. <https://doi.org/10.1016/j.neurobiolaging.2005.07.001>.

- (3) Castaño, E. M.; Roher, A. E.; Esh, C. L.; Kokjohn, T. A.; Beach, T. Comparative Proteomics of Cerebrospinal Fluid in Neuropathologically-Confirmed Alzheimer's Disease and Non-Demented Elderly Subjects. *Neurol. Res.* **2006**, *28* (2), 155–163. <https://doi.org/10.1179/016164106X98035>.
- (4) Sowell, R. A.; Owen, J. B.; Allan Butterfield, D. Proteomics in Animal Models of Alzheimer's and Parkinson's Diseases. *Ageing Res. Rev.* **2009**, *8* (1), 1–17. <https://doi.org/10.1016/j.arr.2008.07.003>.
- (5) Castellanos, D. B.; Martín-Jiménez, C. A.; Rojas-Rodríguez, F.; Barreto, G. E.; González, J. Brain Lipidomics as a Rising Field in Neurodegenerative Contexts: Perspectives with Machine Learning Approaches. *Front. Neuroendocrinol.* **2021**, *61*, 100899. <https://doi.org/10.1016/j.yfrne.2021.100899>.
- (6) Rotunno, M. S.; Lane, M.; Zhang, W.; Wolf, P.; Oliva, P.; Viel, C.; Wills, A.-M.; Alcalay, R. N.; Scherzer, C. R.; Shihabuddin, L. S.; Zhang, K.; Sardi, S. P. Cerebrospinal Fluid Proteomics Implicates the Granin Family in Parkinson's Disease. *Sci. Rep.* **2020**, *10* (1), 2479. <https://doi.org/10.1038/s41598-020-59414-4>.
- (7) Dong, W.; Qiu, C.; Gong, D.; Jiang, X.; Liu, W.; Liu, W.; Zhang, L.; Zhang, W. Proteomics and Bioinformatics Approaches for the Identification of Plasma Biomarkers to Detect Parkinson's Disease. *Exp. Ther. Med.* **2019**. <https://doi.org/10.3892/etm.2019.7888>.
- (8) Killoran, A. Biomarkers for Huntington's Disease: A Brief Overview. *J. Rare Dis. Res. Treat.* **2016**, *1* (2), 46–50. <https://doi.org/10.29245/2572-9411/2016/2.1029>.
- (9) Surguchov, A. Invertebrate Models Untangle the Mechanism of Neurodegeneration in Parkinson's Disease. *Cells* **2021**, *10* (2), 407. <https://doi.org/10.3390/cells10020407>.
- (10) Lai, C.-H.; Chou, C.-Y.; Ch'ang, L.-Y.; Liu, C.-S.; Lin, W. Identification of Novel Human Genes Evolutionarily Conserved in *Caenorhabditis Elegans* by Comparative Proteomics. *Genome Res.* **2000**, *10* (5), 703–713. <https://doi.org/10.1101/gr.10.5.703>.
- (11) Brandt, R.; Gergou, A.; Wacker, I.; Fath, T.; Hutter, H. A *Caenorhabditis Elegans* Model of Tau Hyperphosphorylation: Induction of Developmental Defects by Transgenic Overexpression of Alzheimer's Disease-like Modified Tau. *Neurobiol. Aging* **2009**, *30* (1), 22–33. <https://doi.org/10.1016/j.neurobiolaging.2007.05.011>.
- (12) Cao, P.; Yuan, Y.; Pehek, E. A.; Moise, A. R.; Huang, Y.; Palczewski, K.; Feng, Z. Alpha-Synuclein Disrupted Dopamine Homeostasis Leads to Dopaminergic Neuron Degeneration in *Caenorhabditis Elegans*. *PLoS ONE* **2010**, *5* (2), e9312. <https://doi.org/10.1371/journal.pone.0009312>.
- (13) Ichibangase, T.; Saimaru, H.; Takamura, N.; Kuwahara, T.; Koyama, A.; Iwatsubo, T.; Imai, K. Proteomics Of *Caenorhabditis Elegans* Over-Expressing Human α -Synuclein Analyzed by Fluorogenic Derivatization–Liquid Chromatography/Tandem Mass Spectrometry: Identification of Actin and Several Ribosomal Proteins as Negative Markers at Early Parkinson's Disease Stages. *Biomed. Chromatogr.* **2008**, *22* (3), 232–234. <https://doi.org/10.1002/bmc.931>.
- (14) Lee, A. L.; Ung, H. M.; Sands, L. P.; Kikis, E. A. A New *Caenorhabditis Elegans* Model of Human Huntingtin 513 Aggregation and Toxicity in Body Wall Muscles. *PLOS ONE* **2017**, *12* (3), e0173644. <https://doi.org/10.1371/journal.pone.0173644>.
- (15) Machiela, E.; Dues, D. J.; Senchuk, M. M.; Van Raamsdonk, J. M. Oxidative Stress Is Increased in *C. Elegans* Models of Huntington's Disease but Does Not Contribute to Polyglutamine Toxicity Phenotypes. *Neurobiol. Dis.* **2016**, *96*, 1–11. <https://doi.org/10.1016/j.nbd.2016.08.008>.

- (16) Wolozin, B.; Gabel, C.; Ferree, A.; Guillily, M.; Ebata, A. Watching Worms Whither. In *Progress in Molecular Biology and Translational Science*; Elsevier, 2011; Vol. 100, pp 499–514. <https://doi.org/10.1016/B978-0-12-384878-9.00015-7>.
- (17) Cattaneo, E.; Zuccato, C.; Tartari, M. Normal Huntingtin Function: An Alternative Approach to Huntington's Disease. *Nat. Rev. Neurosci.* **2005**, *6* (12), 919–930. <https://doi.org/10.1038/nrn1806>.
- (18) Cha, J.-H. J. Transcriptional Dysregulation in Huntington's Disease. *Trends Neurosci.* **2000**, *23* (9), 387–392. [https://doi.org/10.1016/S0166-2236\(00\)01609-X](https://doi.org/10.1016/S0166-2236(00)01609-X).
- (19) Audhya, A.; Desai, A. Proteomics in *Caenorhabditis Elegans*. *Brief. Funct. Genomic. Proteomic.* **2008**, *7* (3), 205–210. <https://doi.org/10.1093/bfgp/eln014>.
- (20) Kaji, H.; Tsuji, T.; Mawuenyega, K. G.; Wakamiya, A.; Taoka, M.; Isobe, T. Profiling Of *Caenorhabditis Elegans* Proteins Using Two-Dimensional Gel Electrophoresis and Matrix Assisted Laser Desorption/Ionization-Time of Flight-Mass Spectrometry. *Electrophoresis* **2000**, *21* (9), 1755–1765. [https://doi.org/10.1002/\(SICI\)1522-2683\(20000501\)21:9<1755::AID-ELPS1755>3.0.CO;2-S](https://doi.org/10.1002/(SICI)1522-2683(20000501)21:9<1755::AID-ELPS1755>3.0.CO;2-S).
- (21) Larance, M.; Pourkarimi, E.; Wang, B.; Brenes Murillo, A.; Kent, R.; Lamond, A. I.; Gartner, A. Global Proteomics Analysis of the Response to Starvation in *C. Elegans**. *Mol. Cell. Proteomics* **2015**, *14* (7), 1989–2001. <https://doi.org/10.1074/mcp.M114.044289>.
- (22) Mawuenyega, K. G.; Kaji, H.; Yamauchi, Y.; Shinkawa, T.; Saito, H.; Taoka, M.; Takahashi, N.; Isobe, T. Large-Scale Identification of *Caenorhabditis e Legans* Proteins by Multidimensional Liquid Chromatography–Tandem Mass Spectrometry. *J. Proteome Res.* **2003**, *2* (1), 23–35. <https://doi.org/10.1021/pr025551y>.
- (23) Merrihew, G. E.; Davis, C.; Ewing, B.; Williams, G.; Käll, L.; Frewen, B. E.; Noble, W. S.; Green, P.; Thomas, J. H.; MacCoss, M. J. Use of Shotgun Proteomics for the Identification, Confirmation, and Correction of *C. Elegans* Gene Annotations. *Genome Res.* **2008**, *18* (10), 1660–1669. <https://doi.org/10.1101/gr.077644.108>.
- (24) Narayan, V.; Ly, T.; Pourkarimi, E.; Murillo, A. B.; Gartner, A.; Lamond, A. I.; Kenyon, C. Deep Proteome Analysis Identifies Age-Related Processes in *C. Elegans*. *Cell Syst.* **2016**, *3* (2), 144–159. <https://doi.org/10.1016/j.cels.2016.06.011>.
- (25) Simonsen, K. T.; Møller-Jensen, J.; Kristensen, A. R.; Andersen, J. S.; Riddle, D. L.; Kallipolitis, B. H. Quantitative Proteomics Identifies Ferritin in the Innate Immune Response of *C. Elegans*. *Virulence* **2011**, *2* (2), 120–130. <https://doi.org/10.4161/viru.2.2.15270>.
- (26) Wan, Q.-L.; Shi, X.; Liu, J.; Ding, A.-J.; Pu, Y.-Z.; Li, Z.; Wu, G.-S.; Luo, H.-R. Metabolomic Signature Associated with Reproduction-Regulated Aging in *Caenorhabditis Elegans*. *Aging* **2017**, *9* (2), 447–474. <https://doi.org/10.18632/aging.101170>.
- (27) Wan, Q.-L.; Yang, Z.-L.; Zhou, X.-G.; Ding, A.-J.; Pu, Y.-Z.; Luo, H.-R.; Wu, G.-S. The Effects of Age and Reproduction on the Lipidome of *Caenorhabditis Elegans*. *Oxid. Med. Cell. Longev.* **2019**, *2019*, 1–14. <https://doi.org/10.1155/2019/5768953>.
- (28) Ishihama, Y.; Oda, Y.; Tabata, T.; Sato, T.; Nagasu, T.; Rappsilber, J.; Mann, M. Exponentially Modified Protein Abundance Index (EmPAI) for Estimation of Absolute Protein Amount in Proteomics by the Number of Sequenced Peptides per Protein. *Mol. Cell. Proteomics* **2005**, *4* (9), 1265–1272. <https://doi.org/10.1074/mcp.M500061-MCP200>.
- (29) Kudlicki, A. The Optimal Exponent Base for EmPAI Is 6.5. *PLoS ONE* **2012**, *7* (3), e32339. <https://doi.org/10.1371/journal.pone.0032339>.
- (30) Created with BioRender.Com.

- (31) Corsi, A. K. A Transparent Window into Biology: A Primer on *Caenorhabditis Elegans*. *WormBook* **2015**, 1–31. <https://doi.org/10.1895/wormbook.1.177.1>.
- (32) Karas, M.; Bahr, U.; Dülcks, T. Nano-Electrospray Ionization Mass Spectrometry: Addressing Analytical Problems beyond Routine. *Fresenius J. Anal. Chem.* **2000**, *366* (6–7), 669–676. <https://doi.org/10.1007/s002160051561>.
- (33) Valenza, M. Dysfunction of the Cholesterol Biosynthetic Pathway in Huntington’s Disease. *J. Neurosci.* **2005**, *25* (43), 9932–9939. <https://doi.org/10.1523/JNEUROSCI.3355-05.2005>.
- (34) Trushina, E.; Singh, R. D.; Dyer, R. B.; Cao, S.; Shah, V. H.; Parton, R. G.; Pagano, R. E.; McMurray, C. T. Mutant Huntingtin Inhibits Clathrin-Independent Endocytosis and Causes Accumulation of Cholesterol in Vitro and in Vivo. *Hum. Mol. Genet.* **2006**, *15* (24), 3578–3591. <https://doi.org/10.1093/hmg/ddl434>.
- (35) Korade, Z.; Kenworthy, A. K. Lipid Rafts, Cholesterol, and the Brain. *Neuropharmacology* **2008**, *55* (8), 1265–1273. <https://doi.org/10.1016/j.neuropharm.2008.02.019>.
- (36) Valenza, M.; Leoni, V.; Karasinska, J. M.; Petricca, L.; Fan, J.; Carroll, J.; Pouladi, M. A.; Fossale, E.; Nguyen, H. P.; Riess, O.; MacDonald, M.; Wellington, C.; DiDonato, S.; Hayden, M.; Cattaneo, E. Cholesterol Defect Is Marked across Multiple Rodent Models of Huntington’s Disease and Is Manifest in Astrocytes. *J. Neurosci.* **2010**, *30* (32), 10844–10850. <https://doi.org/10.1523/JNEUROSCI.0917-10.2010>.
- (37) Vance, J. E. Dysregulation of Cholesterol Balance in the Brain: Contribution to Neurodegenerative Diseases. *Dis. Model. Mech.* **2012**, *5* (6), 746–755. <https://doi.org/10.1242/dmm.010124>.
- (38) Di Paolo, G.; Kim, T.-W. Linking Lipids to Alzheimer’s Disease: Cholesterol and Beyond. *Nat. Rev. Neurosci.* **2011**, *12* (5), 284–296. <https://doi.org/10.1038/nrn3012>.
- (39) Wong, M. W.; Braid, N.; Poljak, A.; Pickford, R.; Thambisetty, M.; Sachdev, P. S. Dysregulation of Lipids in Alzheimer’s Disease and Their Role as Potential Biomarkers. *Alzheimers Dement.* **2017**, *13* (7), 810–827. <https://doi.org/10.1016/j.jalz.2017.01.008>.
- (40) Alecu, I.; Bennett, S. A. L. Dysregulated Lipid Metabolism and Its Role in α -Synucleinopathy in Parkinson’s Disease. *Front. Neurosci.* **2019**, *13*, 328. <https://doi.org/10.3389/fnins.2019.00328>.
- (41) Witting, M.; Schmitt-Kopplin, P. The *Caenorhabditis Elegans* Lipidome. *Arch. Biochem. Biophys.* **2016**, *589*, 27–37. <https://doi.org/10.1016/j.abb.2015.06.003>.
- (42) Liebisch, G.; Drobnik, W.; Lieser, B.; Schmitz, G. High-Throughput Quantification of Lysophosphatidylcholine by Electrospray Ionization Tandem Mass Spectrometry. *Clin. Chem.* **2002**, *48* (12), 2217–2224. <https://doi.org/10.1093/clinchem/48.12.2217>.
- (43) Scherer, M.; Schmitz, G.; Liebisch, G. High-Throughput Analysis of Sphingosine 1-Phosphate, Sphinganine 1-Phosphate, and Lysophosphatidic Acid in Plasma Samples by Liquid Chromatography–Tandem Mass Spectrometry. *Clin. Chem.* **2009**, *55* (6), 1218–1222. <https://doi.org/10.1373/clinchem.2008.113779>.
- (44) Bligh, E. G.; Dyer, W. J. A RAPID METHOD OF TOTAL LIPID EXTRACTION AND PURIFICATION. *Can. J. Biochem. Physiol.* **1959**, *37* (8), 911–917. <https://doi.org/10.1139/o59-099>.
- (45) Lebaron, F. N.; Folch, J. THE EFFECT OF PH AND SALT CONCENTRATION ON AQUEOUS EXTRACTION OF BRAIN PROTEINS AND LIPOPROTEINS. *J. Neurochem.* **1959**, *4* (1), 1–8. <https://doi.org/10.1111/j.1471-4159.1959.tb13168.x>.

- (46) Matyash, V.; Liebisch, G.; Kurzchalia, T. V.; Shevchenko, A.; Schwudke, D. Lipid Extraction by Methyl-Tert-Butyl Ether for High-Throughput Lipidomics. *J. Lipid Res.* **2008**, *49* (5), 1137–1146. <https://doi.org/10.1194/jlr.D700041-JLR200>.
- (47) Wu, Z.; Shon, J. C.; Liu, K.-H. Mass Spectrometry-Based Lipidomics and Its Application to Biomedical Research. *J. Lifestyle Med.* **2014**, *4* (1), 17–33. <https://doi.org/10.15280/jlm.2014.4.1.17>.
- (48) Nagai, Y.; Tucker, T.; Ren, H.; Kenan, D. J.; Henderson, B. S.; Keene, J. D.; Strittmatter, W. J.; Burke, J. R. Inhibition of Polyglutamine Protein Aggregation and Cell Death by Novel Peptides Identified by Phage Display Screening. *J. Biol. Chem.* **2000**, *275* (14), 10437–10442. <https://doi.org/10.1074/jbc.275.14.10437>.
- (49) Lecerf, J.-M.; Shirley, T. L.; Zhu, Q.; Kazantsev, A.; Amersdorfer, P.; Housman, D. E.; Messer, A.; Huston, J. S. Human Single-Chain Fv Intrabodies Counteract *in Situ* Huntingtin Aggregation in Cellular Models of Huntington's Disease. *Proc. Natl. Acad. Sci.* **2001**, *98* (8), 4764–4769. <https://doi.org/10.1073/pnas.071058398>.
- (50) Colby, D. W.; Chu, Y.; Cassady, J. P.; Duennwald, M.; Zazulak, H.; Webster, J. M.; Messer, A.; Lindquist, S.; Ingram, V. M.; Wittrup, K. D. Potent Inhibition of Huntingtin Aggregation and Cytotoxicity by a Disulfide Bond-Free Single-Domain Intracellular Antibody. *Proc. Natl. Acad. Sci.* **2004**, *101* (51), 17616–17621. <https://doi.org/10.1073/pnas.0408134101>.
- (51) Ehrnhoefer, D. E.; Duennwald, M.; Markovic, P.; Wacker, J. L.; Engemann, S.; Roark, M.; Legleiter, J.; Marsh, J. L.; Thompson, L. M.; Lindquist, S.; Muchowski, P. J.; Wanker, E. E. Green Tea (–)-Epigallocatechin-Gallate Modulates Early Events in Huntingtin Misfolding and Reduces Toxicity in Huntington's Disease Models. *Hum. Mol. Genet.* **2006**, *15* (18), 2743–2751. <https://doi.org/10.1093/hmg/ddl210>.
- (52) Bonanomi, M.; Natalello, A.; Visentin, C.; Pastori, V.; Penco, A.; Cornelli, G.; Colombo, G.; Malabarba, M. G.; Doglia, S. M.; Relini, A.; Regonesi, M. E.; Tortora, P. Epigallocatechin-3-Gallate and Tetracycline Differently Affect Ataxin-3 Fibrillogenesis and Reduce Toxicity in Spinocerebellar Ataxia Type 3 Model. *Hum. Mol. Genet.* **2014**, *23* (24), 6542–6552. <https://doi.org/10.1093/hmg/ddu373>.
- (53) Chaudhary, R. K.; Patel, K. A.; Patel, M. K.; Joshi, R. H.; Roy, I. Inhibition of Aggregation of Mutant Huntingtin by Nucleic Acid Aptamers In Vitro and in a Yeast Model of Huntington's Disease. *Mol. Ther.* **2015**, *23* (12), 1912–1926. <https://doi.org/10.1038/mt.2015.157>.